ISSN 1028-8546

Azərbaycan Milli Elmlər Akademiyası
Fizika-Riyaziyyat və Texnika Elmləri Bölməsi
Fizika İnstitutu

3

Fizika

Cild
XII
2006

Bakı ✵ Elm

ISSN 1028-8546

Azərbaycan Milli Elmlər Akademiyası
Fizika-Riyaziyyat və Texnika Elmləri Bölməsi
Fizika İnstitutu

3

Fizika

Cild

XII

2006

Bakı ✵ Elm

2006 Cild XII, 3
Elmi jurnal

ISSN 1028-8546
2006, Vol. XII, 3

Fizika

Azərbaycan Milli Elmlər Akademiyası
Fizika-Riyaziyyat və Texnika Elmləri Bölməsi
Fizika İnstitutu
Azerbaijan National Academy of Sciences
Department of Physical, Mathematical and Technical Sciences
Institute of Physics

Jurnal 1995-ci ildən nəşr edilir
Journal was published from 1995

Təsisçi: Azərbaycan Milli Elmlər Akademiyası, Fizika İnstitutu
Organizer: Institute of Physics, Azerbaijan National Academy of Sciences

Jurnal Fizika İnstitutunun aşağıdakı əməkdaşları tərəfindən yığılıb nəşrə hazırlanmış və çap olunmuşdur:

E.A. Axundova,
N.İ. Acalova,
S.İ. Əliyeva,
N.A. Axundova
E.Ə. Tərlanova
Baş texniki redaktoru: T.R. Mehdiyev

Journal is preformed for publishing by the following collaborators of the Institute of Physics:

E.A. Akhundova
N.I. Ajalova
S.I. Aliyeva
N.A. Akhundova
E.A. Tarlanova
Technical editor-in-chief: T.R. Mehdiyev

Redaksiyanın ünvanı:
Bakı. Az. 1143, H. Cavid prospekti, 33,
Az. MEA Fizika İnstitutu
Tel.: (99412) 39-51-63, 39-32-23;
Faks: (994 12) 39-59-61
E-mail: joph@physics.ab.az
joph@rambler.ru

Publishing Office
Baku. Az. 1143, H. Javid av, 33,
Az. NAS Institute of Physics
Tel.: (99412) 39-51-63, 39-32-23;
Fax: (994 12) 39-59-61
E-mail: joph@physics.ab.az
joph@rambler.ru

Çapa təqdim olunmuşdur:
It is authorized for printing: 06.12.06

THE NONLINEAR PROPERTIES OF OPTICAL FIBERS WITH STRUCTURED MEMBRANE

T.R. MEHDIYEV, N.R. BABAYEVA
Institute of Physics of NAS of Azerbaijan
Az-1143 Baku, H.Javid av., 33

The calculative and experimental data for microstructured fibers, carried out on the base of quartz, layered materials of A_3B_6 and $LiNbO_3$ type are given.

The experimental and theoretical works in the area of cable transmission of light energy had been begun in 60-ties of XX century. The practical realization and introduction of these works became possible from the moment of creation of stable optical connection lines, the main role in which the fiber-optical cables on the base quartz and glass, light sources – optical quantum generators, optical parametric regenerator amplifiers of optical signals, optical holographic diffractional lattices, CCD-receiving matrixes, optoelectronic devices of decoding were played. The maximally possible parameter values, corresponding with theoretical estimations and models, treated in refs of Kogelnik (1958), Kayzer (1974), Rassel's group (1996), Stegeman's group (1986) and others have been already achieved for the traditional direction of technology development of optical cables in last decades. It is need to note, that the list of single-mode optical fibers by G652 is given in second number of "light-wave", 2003 journal.

The high technology, simplicity and the main, wide accessible materials for the carrying out – glass, quartz, causes to MS (microstructured), and especially PhC (photonocrystallic)-fibers, as the development analysis of this direction shows. The optical fiber with record small damping (0,151 db/km on wave length 1568 nm, losses on Rayleigh scattering are 0,128 db/km, summary losses on the absorption are 0,018 db/km, losses on perfect fibers are 0,004 db/km, common losses aren't than 0,16 db/km) has been created in "Sumitomo" company. The fiber had been prepared with core from pure quartz of high degree of homogeneity, surrounded by two membranes from quartz, doped by fluorine. The theoretical estimations show, that use of this fiber in communication system allows us to increase the distance between the transponders till 330km.

Usually, MS-fibers present themselves the quartz or glass microstructure with periodical or aperiodic situated air apertures. Such structure allows to rule the dispersion of waveguide modes because of the nonlinear properties of material membrane, changes of membrane structure, and also localization value of electromagnetic radiation in their core, connected as with radiation power, diffusive on the fiber, so with difference of indexes of refraction of core and cladding as the refs [1-8] show. The waveguide modes in such fibers form because of the phenomena of internal reflectance on the boundary between quartz or glass core and MS-membrane, the effective index of refraction of which is lower, cladding index of refraction because of the presence of air apertures, and also interference of reflected and scattered waves [9-10]. The important result of periodicity of situation of air apertures is the appearance of photon forbidden bands. The ruling of degree of radiation localization in fiber core and parts of radiation power, diffusive in it, is achieved because of the change of gas concentration in membrane [11-13].

The calculative and experimental data for microstructured fibers, carried out on the base of quartz, layered materials of A_3B_6 type, for example GaSe and $LiNbO_3$ are given in the given message.

The quartz MS-fibers were prepared on standard method, by the way of drawing at high temperature from mold, taken from hollow tubes. In the case of $LiNbO_3$ monocrystals the aperture system with periodical structure was drifted on. The crystal structure of Gas, GaSe, InSe crystals present itself the consecution of loosely coupled layers; the gap between the layers is 3-4Å [14]. These layered materials are related to photon crystals. Many investigations, for example refs [15-17] are dedicated to the investigation of optical properties, and also band structure. The $LiNbO_3$ is well known nonlinear crystal [18-19].

Taking under the consideration, that interaction length in mode of hard focusing is limited by length of stop mark region, in case of Gaussian beam the values of specific enlargement factor of efficiency of nonlinear-optical processes in fiber, are defined by well known expression [20] $\frac{I_f l_{eff}^f}{I_t l_{eff}^t} \approx \frac{\lambda}{\pi\, w_0^2\, \alpha}$, where α is loss factor (αl>>1), l is fiber length; l_{eff} is effective interaction length; w_0 is radius of stop mark of focused beam; λ is radiation wave length; f and t are indexes, taking under the consideration the conditions for fiber and hard focusing, $I_{eff}^t \approx \frac{\pi\, w_0^2}{\lambda}$. $\xi = \frac{I_f l_{eff}^f}{I_t l_{eff}^t} \approx \frac{\lambda\eta}{\pi a^2 \alpha}$ is obtained, taking under the consideration the radiation distribution between core and membrane fiber for factor of waveguide efficiency increase of nonlinear process without taking under the consideration of radius a of fiber core, and also imaging $I \cdot l_{eff}$ in the $I_f l_{eff}^f = \int_0^l dz \frac{P\eta}{\pi a^2} \exp(-\alpha z)$ form, where η is radiation part, localized in core (αl>>1). The radiation part, localized in core of MS fiber was defined according to [7,21], when after the simplifications it is followed:

$$\eta = \frac{\Xi_{core}}{\Xi_{core} + \Xi_{clad}}$$

$$\Xi_{core} = \frac{\beta}{J_1^2(u)}\left\{a_1 a_3\left[J_0^2(u)+J_1^2(u)\right]+a_2 a_4\left[J_2^2(u)+J_1(u)J_3(u)\right]\right\}$$

$$\Xi_{clad} = \frac{\beta}{K_1^2(w)}\frac{u^2}{w^2}\left\{a_1 a_5\left[K_0^2(w)-K_1^2(w)\right]+a_2 a_6\left[K_2^2(w)+K_1(w)K_3(w)\right]\right\}:$$

Here

$$a_1 = \frac{f_2-1}{2};\ a_2 = a_1+1;\ a_3 = \frac{f_1-1}{2};$$
$$a_4 = a_3+1;\ a_5 = a_3+\Delta;\ a_6 = a_4-\Delta;$$

$$f_1 = \frac{(uw)^2}{v^2}\left[b_1+(1-2\Delta)b_2\right];\ f_2 = \frac{V^2}{(uw)^2(b_1+b_2)};$$
$$b_1 = \frac{1}{2u}\left(\frac{J_0(u)}{J_1(u)}-\frac{J_2(u)}{J_1(u)}\right);\ b_2 = \frac{1}{2w}\left(\frac{K_0(w)}{K_1(w)}+\frac{K_2(w)}{K_1(w)}\right);$$

$$\Delta = \frac{1}{2}\left(1-\frac{n_{clad}^2}{n_{core}^2}\right);\ v = kan_{core}\cdot\sqrt{2\Delta};\ k = \frac{2\pi}{\lambda};$$

$$\beta = \frac{n_{core}}{\sqrt{1-\left(\frac{u}{akn_{core}}\right)^2}};\ w = \sqrt{v^2-u^2};\qquad ;$$

v is waveguide parameter; β is constant of mode distribution; w is mode parameter in membrane; $J_n(u)$ is Bessel function of genre one; $K_n(u)$ is modified Bessel function of genre two; u is mode parameter in fiber core [28].

The dependence ξ on a, calculated on ratio data is given on the fig.1. Let's consider the limit cases of a and λ ratio, when $v>>1$ and $v<<1$. Choosing the expression for character angle beam width from [21] and presenting the waveguide parameter as the ratio of θ_c sliding critical angle to θ_d character angle beam width, we obtain the following formula for case of Gaussian profile of radiation intensity by w_0 width:

$$v = \frac{2\theta_c}{\theta_d};\ \theta_c \approx \sqrt{2\Delta};\ \theta_d \approx \frac{\lambda}{\pi n_{core} a}.$$

It is seen from here, that waveguide parameter v can be considered in the capacity of the balance measure of influence of diffraction effects and waveguide limit of light beam because gradient of profile of refractive index. At $v>>1$ we have the case of big waveguide radiuses, for which the diffraction effects are insignificant, and significant part of radiation power is concentrated in core and is defined from $\eta \approx 1-\frac{u^2}{v^3}$ expression. At $v<<1$ the fiber radius is small, diffraction plays the significant role and significant part of radiation power spreads in fiber membrane. In this case:

$$\eta \approx 1{,}261\frac{v^2+2}{v^4}exp\left(-\frac{4}{v^2}\right).$$

The given expressions for η are proved experimentally and describe the ξ behavior. From the fig.1a it is followed, that value of optimal radius of core of quartz fiber lies in range 0,24-0,26 mcm, for GaSe – 0,015-0,025 mcm, for $LiNbO_3$ – 0,1-0,13 mcm. The maximum is achieved at radius of fiber core, which is equal to 1,5 mcm for weakly directing quartz fibers with Δ parameter near $5\cdot10^{-3}$ for $\lambda\approx$1mcm. In practices, maximal parameters are achieved for pulled and MS-fibers with high factors of membrane filling by air [22, 23].

The refractive index of core is less, than refractive index of membrane in hollow waveguides. That's why, the constants of mode distribution have imaginary components, differing from zero and pass of light in these waveguides accompanies by radiation losses. The attenuation coefficient of radiation intensity is defined by the expression [24] for EH_{mm} hollow waveguide with n_{core} near 1.

$$\alpha = \left(\frac{u_{mm}}{2\pi}\right)^2\frac{\lambda^2}{a^3}\frac{n^2+1}{\sqrt{n^2-1}},$$

Where $n=n_{clod}$ and from when it is followed, that attenuation coefficient of main mode of hollow waveguide with quartz membrane and internal radius 7 mcm for λ=1mcm exceeds 6,5 cm^{1}. Such fiber isn't useable for practical application. The loss decrease is decreased by the creation of photon-crystal membrane. The decrease of optical loss coefficient, relatively to losses in hollow waveguide with entire membrane, in this case is characterized by the ratio of logarithms of refractive indexes from wall of hollow waveguide core and periodical structure. The increase of layer number of periodical structure leads to the decrease of loss factor $\frac{\alpha_{PBG}}{\alpha_h} \propto a\exp\left(-2|\chi|Nd\right)$, where χ is coupling factor of direct and opposite waves in periodical structure; d is modulation period of refractive index in membrane in center of photon forbidden band.

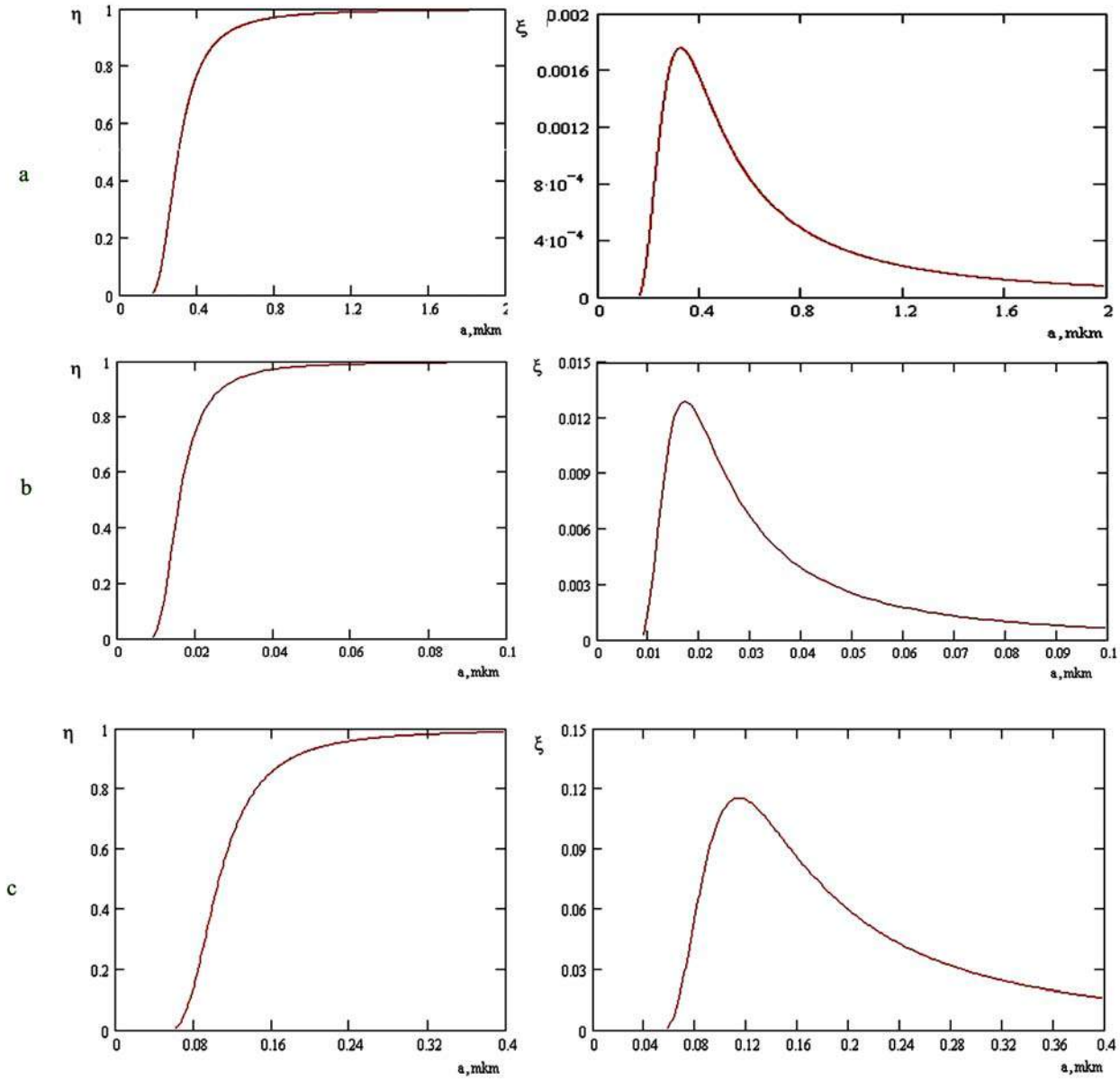

Fig.1. The dependence of factors of ξ-waveguide increase of efficiency of nonlinear-optical processes and η-part of radiation, localized in the center, on *a* radius of fiber core, carried out from: a. quartz, λ=1 mcm; b. GaSe, λ=0,2 mcm; c. $LiNbO_3$, λ=0,8 mcm.

The influence estimation of waveguide losses in hollow waveguide with entire or PhC-membrane, having the l length for the stationary FCSc, in the neglect of effects of rating depletion gives the following:

$$I_s(l) = I_s(0)\exp(gI_0 I_{eff} - \alpha_s l); \quad l_{eff} = \frac{1}{\alpha_p}\left[1 - \exp(-\alpha_p l\right],$$

where g is coefficient of FCSc-amplification; I_0 is initial intensity of rating signal; α_p and α_s are loss factors on the rating frequency and Stokes signal. The increase of Stokes signal is carried out only at the condition $gI_0 > \alpha_s$ (for gI_0=0,3 cm^{-3} fig.2), in opposite case the waveguide losses lead to the damping of Stokes signal. The value of Stokes signal linearly depends on fiber length, if $\alpha_p l$, $\alpha_s l$, $gI_0 l$ <<1. In case $\alpha_p l$>>1, the waveguide modes lead to rating weakening and intensity of Stokes signal exponentially decreases as l function. Taking under the consideration the limits, we obtain the following for the optimal fiber length and maximal coefficient of FCSc-amplification in hollow waveguide:

$$l_{opt}^{SRS} = \frac{1}{\alpha_p}\ln\frac{gI_0}{\alpha_s}; \quad G = \frac{gI_0}{\alpha_p} - \frac{\alpha_s}{\alpha_p}\left(1 + \ln\frac{gI_0}{\alpha_s}\right).$$

In case $gI_0 >> \alpha_s$, α_p the maximal increase of integral coefficient of FCSc-amplification in mode of hard focusing has the form, obtained earlier.

The length of nonlinear-optical interaction limit is limited by effects of group lateness, which lead to the "scattering" of rating pulses and Stokes signal on character length $l_w = \frac{\tau}{\left|\upsilon_p^{-1} - \upsilon_s^{-1}\right|}$, where υ_p and υ_s are group velocities of rating and Stokes pulses, correspondingly, τ is rating pulse duration. The dispersion of group velocity leads to the

smearing of short pulses on character length $l_d = \frac{\tau^2}{|\beta_2|}$. The influence of tuning of group velocities and dispersion of group velocity in waveguide mode FCSc can be decreased by the way of the selection of waveguide and gas parameters with taking under the consideration the waveguide component dispersion. It is need to note, that mode number "*k*" in pure gas isn't the propagation constant $k=n\omega/c$ for the own mode of hollow waveguide.

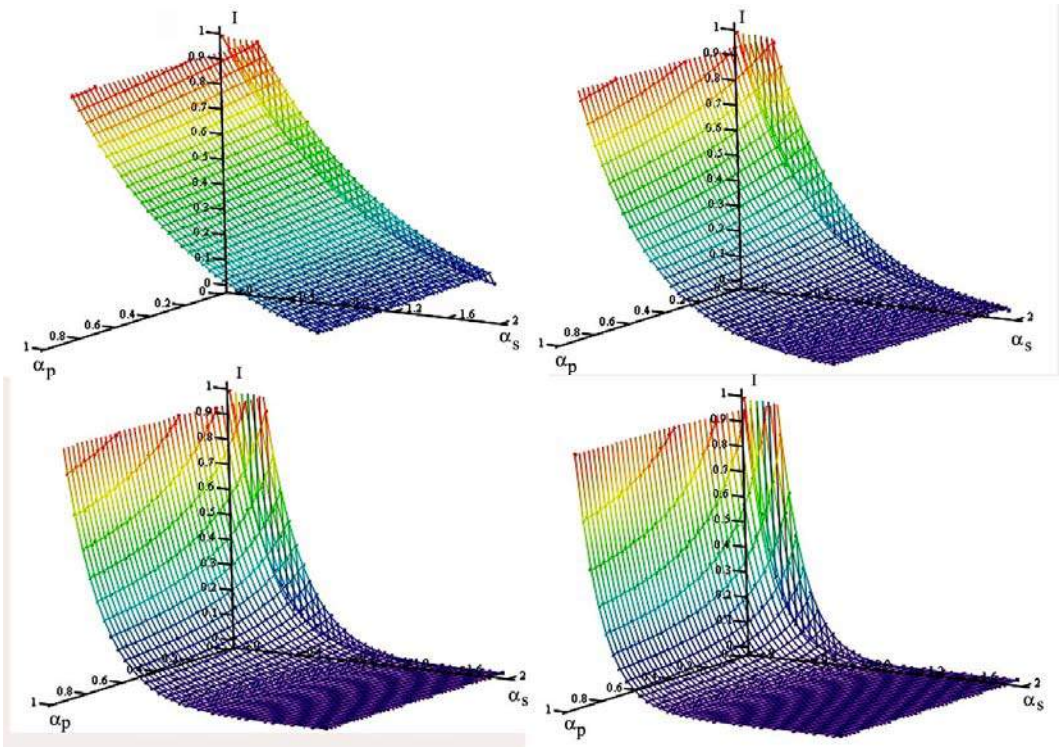

Fig.2. The dependence of FCS signal on fiber length 1 and loss coefficients on radiation frequency of rating and Stokes signal. The duration of rating pulses is 100 fs, energy is 0,01-1 mcJ, 1=1,2,4,6 cm.

The last is defined by the expression $K^{pq} = (k^2 - h_{pq}^2)^{\frac{1}{2}}$, where the value h_{pq} is obtained from the characteristic equation for own mode of waveguide. As the results show, the carrying out of the condition gI_0=0,3см$^{-3}$ can be achieved for the molecular hydrogen or nitrogen. This point of view is proved by results of ref [30]. The analysis of fig.3 shows, that the entire compensation of material and waveguide components of dispersion of group velocity can be achieved for the hollow waveguide with internal radius 50 mcm, filled by molecular hydrogen, on wave length 530 nm. The wave length for zero dispersion point can be obtained from the expression for the propagation constants of waveguide mode $k_2 = \upsilon_0^{-2}\left(\frac{\lambda}{2\pi n}\right)^3\left(\frac{u_m}{a}\right)^2$, where $\upsilon_0 = \frac{c}{n}\left(1+\frac{\omega}{n}\cdot\frac{\partial n}{\partial\omega}\Big|_{\omega_i}\right)^{-1}$.

It is followed from here, that wave length of zero dispersion point of group velocity can be reconstructed, changing the internal radius of waveguide, or choosing the type of waveguide mode, or choosing the gas and changing of its pressure in waveguide.

The hydrogen distribution in interplane crystal spaces is the peculiarity of GaSe, intercalated by hydrogen, as it was mentioned in ref [29].

In case of photon crystal $LiNbO_3$, the conclusions, obtained for quartz fiber coincide with experiments, if the change of refractive index doesn't take place under the influence of exciting radiation.

In last both cases intercalation process doesn't present big troubles technologically.

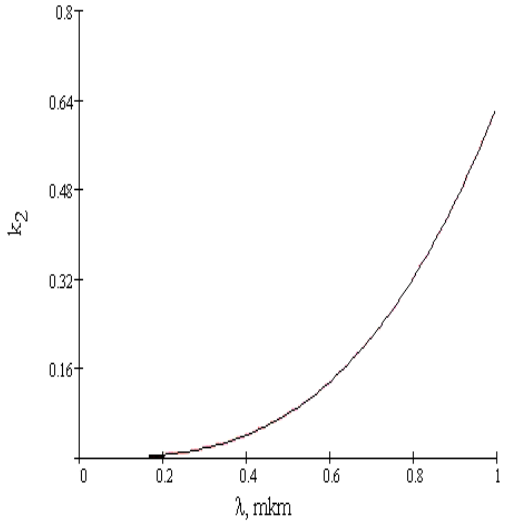

Fig.3. The spectral dependencies for the zero dispersion point of group velocity in hollow quartz waveguide, filled by molecular hydrogen. The internal radius of waveguide, train width and canal radius are 50 mcm, gas pressure is 0,5 arm, wave length is 530 mcm.

[1] *J.C. Knight, et al*. Opt. Lett., 1996, 21, 1547.
[2] *J.C. Knight, et al.* Science, 1998, 282, 1476.
[3] *C.M. Bowden, A.M. Zheltikov*. "Nonlinear optics of photonic crystals: feature issue", J. Opt. Soc. Am., 2002, B19, 9.
[4] *A.B. Fedotov i dr.*, Pisma JETF, 2000, 71, 407.
[5] *M.V. Alfimov i dr.*, Pisma JETF, 2000, 71, 714.
[6] *A.M. Jeltikov i dr.*, Pisma JETF, 2001, 120, 570.
[7] *A.M. Jeltikov*. UFN, 2000, 170, 1203.
[8] *B. Egleton et al.* Opt. Express, 2001, 9, 698.
[9] *J.C. Knight et al*., IEEE Photon Technol. Lett., 2000, 12, 807.
[10] *N.G.R. Broderick et al*., Opt. Lett., 1999, 24, 1335.
[11] *A.B. Fedotov et al.* Appl. Phys., 2001, B73, 181.
[12] *T.A. Birks, W.J. Wadsworth, P.St. Russell*, J. Opt. Lett., 2000, 25, 1425.
[13] *D.A. Akimov et al.*, Appl. Phys., 2002, B74, 307.
[14] *A. Kuhn, A. Chevy, R. Chevalier*. Phys. Stat. Sol (a), 1975, 31, pp.469-475.
[15] *V.V. Sobolev*. Bands and exitons of gallium, indium and tallium chalgenides, Kishinev, Shiintsa, 1982.
[16] *T.R. Mekhtiev*. «Energeticheskie spektri politipov selenida qalliya», dokt. dissertatsiya, Baku, 1992.
[17] *E.A. Vinogradov, G.N. Zhizhin, I.N. Melnik, S.I. Subbotin, V.V. Panfilov, K.R. Allakhverdiyev,S.S. Babayev, V.F. Zhidaz* Phys. Stat. Sol.(b), 1980, v.99, n.1, pp.215-283.
[18] *P. Gunter, J.P. Huignard*. "Photorefractive Materials and Their Applications II", Springer-Verlag Heidalberg, New York, 1989.
[19] *R. Mouras; P. Bourson; M.D. Fontana; G. Boulon*. Optics Communications, 1 October 2001, vol. 197,no. 4, pp. 439-444(6).
[20] *G.P. Agravai*. "Nonlinear Fiber Optics", 1989, Boston, Academic Press .
[21] *A.W. Snyder, J.D. Lowe*. "Optical Waveguide Theory, 1983, London, Chapman and Hall.
[22] *A.B. Fedotov et al.* Appl. Phys., 2001, B73, 181.
[23] *A.B. Fedotov et al*. J. Opt. Soc. Am.,2002, B19, 2156.
[24] *M.J. Adams*. "An introduction to Optical Waveguides", 1981, Chichester, Wiley.
[25] *R.F. Cregan et al*. Science, 1999, 285, 1537.
[26] *J. Broeng et al.* Opt. Lett., 2000, 25, 96.
[27] *M.D. Leveson, J.J. Song*. "Coherent Nonlinear Optics: Recent Advances", Topics in Current Physics, Vl.21, 1980, Berlin, Springer-Verlag, p.293.
[28] *A.W. Snyder, J.D. Lowe*. "Optical Waveguide Theory", London, 1983, p190.
[29] *T.R..Mehdiyev*. Fizika (Azerbaijan), 1996, v.2, N.1, p. 60-62.
[30] *A.M. Jeltikov*. UFN, 2004, t. 174, №1.

T.P. Mehdiyev, N.R. Babayeva

STRUKTURLAŞDIRILMIŞ SƏTHLİ OPTİK FİBERLƏRİN QEYRİ-XƏTTİ XÜSUSİYYƏTLƏRİ

Kvars, A_3B_6 qrup laylı materialların və $LiNbO_3$ əsasında yerinə yetirilmiş mikrostrukturlaşdırılmış fiberlər üçün hesabi və eksperimental göstəricilər verilmişdir.

Т.Р. Мехтиев, Н.Р. Бабаева

НЕЛИНЕЙНЫЕ СВОЙСТВА ОПТИЧЕСКИХ ВОЛОКОН СО СТРУКТУРИРОВАННОЙ ОБОЛОЧКОЙ

Приведены расчетные и экспериментальные данные для микроструктурированных волокон, выполненных на основе кварца, слоистых материалов группы A_3B_6 и $LiNbO_3$.

Received: 15.09.06

ELECTROLUMINESCENCE OF LAYERED MONOCRYSTALS Of A_3B_6<RE>

A.S. ABDINOV, R.F. BABAEVA, A.T. BAGIROVA, R.M. RZAEV
Baku State University,
Az 1148, Z. Khalilov str., 23, Baku, Azerbaijan Republic

The brightness characteristics and spectral distribution of an electroluminescence, and also its dependence on the temperature, prehistory and initial dark resistivity of a sample, on the frequency and duration of a pulse field in specially not alloyed and alloyed by rare-earth elements as gadolinium, holmium and dysprosium with various percentage $N_{РЗЭ}\approx10^{-5}\div10^{-1}$ at. %) in layered monocrystals of InSe and GaSe are investigated at various temperatures (from 77 K) in a wide range of constant, sine wave and pulse electric fields of applied intensity. It is established, that at $T\leq100$K brightness of electroluminescence (B_γ) does not depend almost on the temperature, and further with increasing of T sharply decreases (exponentially). At $T\approx200$K and 160K the luminescence absolutely disappears in crystals *p*-GaSe and *n*-InSe - there is a temperature suppression of an electroluminescence. With increasing of N_{RE} brightness of a luminescence firstly (at $N_{RE}\leq10^{-4}$ at. %) decreases a little, and further increases (in crystals not alloyed specially). Thus non-monotone dependence B_γ on prehistory of a sample varies also. It is established, that the structure of spectral distribution of B_γ does not depend almost on the N_{RE}. With change N_{RE} brightness of separate strips of radiation only varies. Change of the chemical nature of the entered impurity in investigated crystals does not influence an electroluminescence.

It is shown, that the most stable values of electroluminescent parameters are provided in crystals with $N_{RE}\approx10^{-2}\div10^{-1}$ at. % .

It is supposed, that dependence of an electroluminescence on the doping level by rare-earth elements is caused by change of interlaminar connections depending on the N_{RE} in investigated crystals.

The electroluminescence in layered crystals of A_3B_6 is found out enough for a long time [1, 2]. However by present time some interesting its aspects (dependence of brightness on the temperature, initial dark resistivity and prehistory of sample, and also dependence of radiation spectrum on the direction concerning a «C» axis of crystal) are not investigated almost. Influence of alloying by rare-earth elements (*RE*) as gadolinium (Gd), holmium (Ho) and dysprozium (*Dy*) on an electroluminescence of crystals GaSe and InSe which considerably changes their photoelectric and photoluminescent properties [3–5] is not investigated also.

The present work is devoted to complex investigation of the above-stated questions.

Investigated samples with thickness of $0.100\leq d\leq1.000$ mm and cross-section size of $(2\div3)\text{x}(4\div6)\text{mm}^2$ were cut off from large monocrystals of InSe and GaSe, grown by a method of slow cooling at a constant gradient of temperature along ingot [6]. Current contacts have been created by soldering metals as In, Ga, Sn, or drawing of silver paste in open air on fresh-chipped surfaces of samples. Measurements were carried out in the temperature range of ($77\leq T\leq300$K) under action of an electric voltage of various types (sinusoidal-variable and rectangular-impact) with a various voltage, frequency and duration (up to 350V, $5\cdot10^4$Hz и 10 μs respectively. The spectral distributions of an electroluminescence and photoconductivity, dependence of brightness of electroluminescence (B_γ) and photocurrent (I_{ph}) on the temperature, the dark volt -ampere characteristic and the volt - brightness characteristic of an electroluminescence, and also dependence of brightness of an electroluminescence on frequency and duration of a stimulating electric voltage were removed on the same sample under various conditions. Samples with various percentage of entered impurity $N_{RE}\approx0$; 10^{-5}; 10^{-4}; $5\cdot10^{-4}$; 10^{-3}; $5\cdot10^{-3}$; 10^{-2}; 10^{-1} at. % were used.

It is established as a result of the measurements carried out by us, that electroluminescence (*EL*) as in specially not alloyed, in alloyed by Gd, Ho and Dy with $N_{РЗЭ}\approx10^{-5}\div10^{-1}$ at.% crystals *p*-GaSe and *n*-InSe is raised at rather low temperatures ($T_l\leq200$K for $T_l\leq160$K for GaSe and InSe, respectively) under action of an electric current of the various type (unidirectional pulse and sinusoidal-variable) with intensity, the greater some E_z. The value of E_z under other identical conditions depends on temperature (T), initial dark resistivity (ρ_{TO}) and prehistory of a sample, and also on the doping level (N_{RE}).

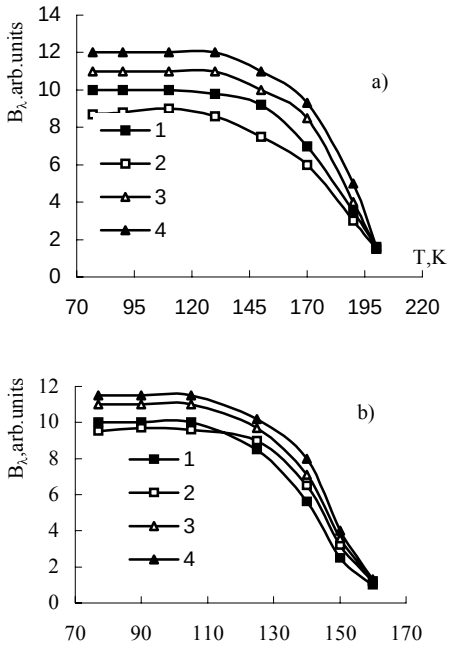

Fig. 1. Temperature dependence of brightness of an electroluminescence in not alloyed specially (1), and also alloyed by *RE* (2, 3) crystals *p*-GaSe (a) and n-InSe (b). N_{RE}, at.% : (a) 1 - 0; 2 - 10^{-5}; 3 - 10^{-2}, (b) 1 - 0; 2 - 10^{-4}; 3 - 10^{-1}

The value of E_z increases with increasing of ρ_{TO} and T and with increasing of N_{RE}- varies non-monotone. In particular, the value of E_z with increasing of N_{RE} firstly (at $N_{RE}\leq10^{-4}$at.%) increases a little, and then (at $10^{-4}<N_{RE}\leq10^{-1}$at.%) decreasing comes nearer to value having places in not alloyed specially

low-ohmic crystals (~$5\cdot10^2$ and 10^2V/cm at 77 K for *p*-GaSe and *n*-InSe, accordingly). With increasing of N_{RE} dependence of parameters and characteristics of an electroluminescence on ρ_{TO} and prehistory of a sample, firstly ($N_{RE}\leq10^{-4}$ at.%) amplifies a little, and brightness of luminescence (B_ℓ) - is weakened concerning initial. Further (at $10^{-4}<N_{RE}\leq10^{-1}$at.%) with increasing of N_{RE} besides a degree of stability of electroluminescent characteristics and the parameters, appreciable image increases also B_ℓ. The electroluminescent radiation in crystals *p*-GaSe<*RE*> and *n*-InSe<RE> with $N_{RE}\approx10^{-2}\div10^{-1}$at.% is characterized with the greatest brightness, and also the highest degree of stability and reproducibility of parameters and characteristics.

The electroluminescence with the least E_z and the greatest B_ℓ is observed at 77K in specially not alloyed crystals. With the further increase of temperature firstly (at $T\leq100$K) brightness of a luminescence does not vary (fig. 1, curve 1), and further exponentially decreases sharply and at $T\approx200$K and $T\approx160$K for *p*-GaSe and *n*-InSe accordingly there is a temperature suppression of electroluminescent radiation.

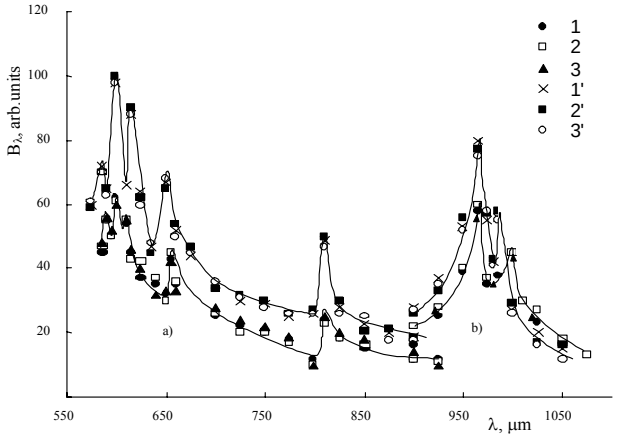

Fig.2. Spectral distribution of brightness of an electroluminescence in crystals *p*-GaSe<RE> (a) and *n*-InSe<RE> (b) at the various chemical nature of the entered impurity.N_{RE}, at.% : 1, 2, 3 - 10^{-4}; 1^1, 2^1, 3^1 - 10^{-1}.*RE*: 1, 1^1 - Gd; 2, 2^1 - Ho; 3, 3^1 - Dy.

In both groups of crystals at rather small N_{RE} with increasing of temperature B_ℓ all over again (up to 100 K) increases concerning having a place at 77K, and further a little as well as in a case of specially not alloyed crystals decreases exponentially (fig.2, curve 2).

It is established, that spectral distribution of brightness of electroluminescent radiation in *p*-GaSe has more complex structure, than in *n*-InSe. In particular, on *EL* spectrum of crystals *p*-GaSe besides the bright basic, a number of weaker maximums is observed also. Besides in both materials the *EL* spectrum at excitation along layers almost on ~0.1eV is displaced aside longer waves concerning a spectrum corresponding to a case of excitation to perpendicularly natural layers. However at increase of N_{RE} this displacement gradually decreases and at $10^{-2}\div10^{-1}$ at.% sometimes becomes not appreciable. For both semiconductors the structure of $B_\ell(\lambda)$ curves does not depend almost on the doping. With increasing of N_{RE} only on *EL* spectrum of crystals *p*-GaSe additional strips of radiation are shown by more clearer - their contrast increases. It is necessary to note, that at all us the considered conditions electroluminescent properties of investigated crystals appeared dependent only from percentage of the entered impurity, and their dependence on the chemical nature of an impurity is not found out almost (fig.2).

Also it is established, that as in crystals not alloyed specially, in *p*-GaSe<*RE*> and *n*-InSe<*RE*> too dependence of B_ℓ(U) has sedate, and dependence B_ℓ(I) - linear character. The energy determined on the basic maximum of the electroluminescence spectrum, allows telling, that process of radiation thus is caused by recombination of injected no basic current carriers through the slow r-centers of recombination [7].

It is shown, that the range of temperature *EL* suppression in samples investigated by us well coincides with a range of temperature clearing own photoconductivity, and also with a temperature range of supervision of negative photoconductivity and *IR* clearing of intrinsic photoconductivity. If at excitation modes of an electroluminescence simultaneously to illuminate a sample also with light, creating negative photoconductivity, or *IR* clearing of intrinsic photoconductivity then *EL* radiations it is not observed. With change N_{RE} though non-monotone, but weak displacement of red border of *EL* nevertheless is observed, that most likely, can is caused by influence of doping on the energetic depth (ε_r) of bedding of the *r*-centers. These results too testify that the electroluminescence in investigated crystals is directly caused by recombination of no basic carriers of a current through the *r*-centers of slow recombination.

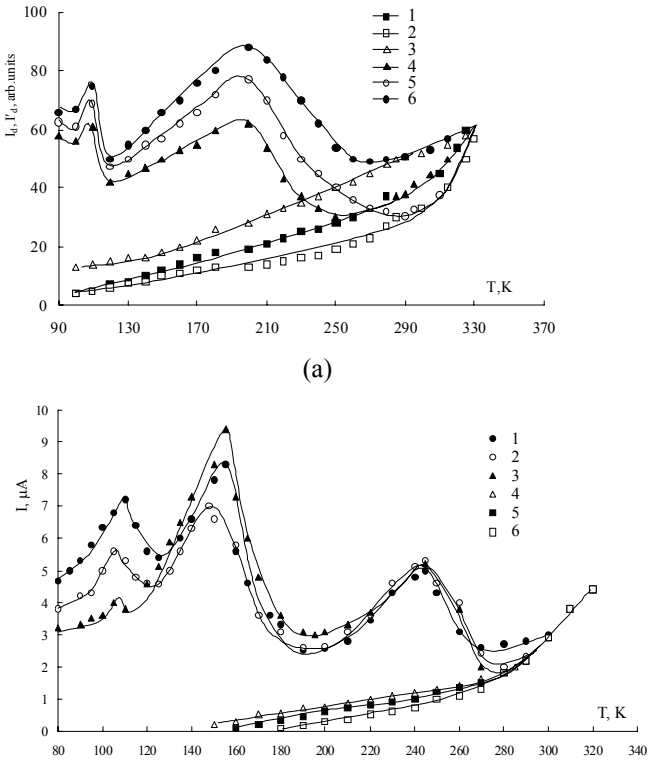

Fig. 3. Temperature dependence of dark (1-3) and quasidark (4-6) conductivity in crystals *p*-GaSe<*RE*> (a) and *n*-InSe<RE> (b). N_{RE}, at.% : 1, 4- 0; 2, 5 - 10^{-4}; 3, 6 - 10^{-1}.

The uniform positions of dependences of *EL* on the ρ_{TO}, prehistory of a sample, temperatures, and doping level is possible to explain in view of partial disorder of crystals GaSe and InSe [7]. Apparently, thus existing recombination barriers interfere the recombination of no basic carriers through located in high-resistance inclusions of the slow r-centers of recombination.

Within the framework of this model, dependence of an electroluminescence on the RE doping level can speak dependence of a degree of disorder of investigated samples on the N_{RE} [3-5].

As to displacement of spectral distribution B_ℓ aside longer waves of a spectrum at excitation in a direction of natural layers, most likely, it is caused with presence of potential barrier $\Delta\varphi_c \approx 0.1$eV between next natural layers [8]. It is supposed, that at *RE* doping because of growth of number covalent connections of *RE* ions taking place in the next layers, the general share ionic-covalent connections concerning weak molecular between natural layers [9] increases also. Therefore with increasing N_{RE} the value of $\Delta\varphi_c$ and the found out displacement of spectral distribution decreases is weakened.

The thermostimulated conductivity measurement carried out by us (fig.3) testify that entered *RE* impurity enter into investigated crystals as levels of sticking for the basic carriers instead of as the *r*-centers of slow recombination. As to influence of these impurity on energetic depth of the *r*-centers it is possible to assume, that it is appears by change of donor-acceptor interaction pairs that sometimes appears appreciable in investigated semiconductors.

[1] *G.A.Ahundov.*Optics and spectroscopy. 1965,18. pp.743.

[2] *G.A.Ahundov, A.Sh. Abdinov, N.M.Mehtiev, A.G.Kyazim-zade.* Optics and spectroscopy. 1975, 38, pp. 952.

[3] *A.Sh.Abdinov,R.F.Babaeva, M.A.Dzhafarov, Yu.G.Nurullaev, R.M.Rzaev.* Inorganic materials. 1999, 34. pp. 271.

[4] *A.Sh.Abdinov, R.F.Babaeva, R.M.Rzaev, G.H.Eyvazova.* Problems of power. 2001, 1. pp. 66.

[5] *A.Sh.Abdinov, R.F.Babayev*. Applied physics. 2004, 5. pp. 74.

[6] *A.M.Guseinov, T.I.Sadykhov*. In cll. "Electric properties of semiconductors and plasmas of the gas category ". Baku. BSU. 1984, pp. 42.

[7] *A.Sh.Abdinov, V.E.Mamedov, E.Y.Salaev*. Trans. of AHAS. Physical and mathematical cer. N. 4., 1981, pp. 85.

[8] *G.A.Ahundov,A.Sh.Abdinov,A.Г.Kyazim-zade, N.M.Mehtiev.* Microelectronics. 4., 1975, pp. 465.

[9] *Z.S.Medvedeva.* Chalcogenids elements of III subgroups of periodic system. M. "Science". 1968. - 214 p.

Ə.Ş. Abdinov, R.F. Babayeva, A.T. Bağırova, R.M. Rzayev

LAYLI A_3B_6<NTE> MONOKRİSTALLARINDA ELEKTROLÜMİNESSENSİYA

Qadolinium, holmium və disprozium tipli, nadir torpaq elementləri ilə aşqarlanmış indium və qallium selen monokristallarında elektrolüminessensiya tədqiq edilmişdir. Müəyyənləşdirilmişdir ki, $T \leq 100$K olduqda şüalanmanın parlaqlığı (B_ℓ) temperaturdan asılı deyil, sonra isə temperaturun artması ilə eksponensial qanunla azalır. T≈200K və 160K-də uyğun olaraq *p*-GaSe □ə *n*-InSe kristallarında elektrolüminessensiyanın temperatur sönməsi baş verir. N_{NTE}-nin artması ilə əvvəlcə ($N_{NTE} \leq 10^{-4}$ at. % olduqda) işıqlanmanın parlaqlığı bir qədər azalır, sonra isə artır. N_{NTE}-nin dəyişməsi ilə ayrı-ayrı şüalanma zolaqlarının parlaqlığı da dəyişir. Daxil edilən aşqarın kimyəvi təbiətinin dəyişməsi isə ektrolüminessensiyaya təsir göstərmir. $N_{NTE} \approx 10^{-2} \div 10^{-1}$ at. % olduqda elektrolüminessensiya parametrləri ən stabil qiymətlərini alır.

А.Ш. Абдинов, Р.Ф. Бабаева, А.Т. Багирова, Р.М. Рзаев

ЭЛЕКТРОЛЮМИНЕСЦЕНЦИЯ СЛОИСТЫХ МОНОКРИСТАЛЛОВ A_3B_6<РЗЭ>

Исследована электролюминесценция в легированных редкоземельными элементами типа гадолиния, гольмия и диспрозия, кристаллах моноселенида индия и галлия. Установлено, что при $T \leq 100$K яркость электролюминесценции (B_ℓ) почти не зависит от температуры, а далее с ростом T уменьшается. При $T \approx 200$K и 160K в кристаллах селенида индия и галлия соответственно, свечение совсем исчезает - происходит температурное тушение электролюминесценции. С ростом $N_{РЗЭ}$ яркость свечения сначала (при $N_{РЗЭ} \leq 10^{-4}$ ат.%) несколько уменьшается, а далее увеличивается относительно исходного. С изменением $N_{РЗЭ}$ меняется также яркость отдельных полос излучения. Изменение химической природы введенной примеси на электролюминесценцию в изучаемых кристаллах не влияет. При $N_{РЗЭ} \approx 10^{-2} \div 10^{-1}$ ат. % обеспечиваются самые стабильные значения электролюминесцентных параметров.

Received: 16.09.06

KOH və NAOH-ın DURU SULU MƏHLULLARININ DİELEKTRİK XASSƏLƏRİ

E.Ə. MƏSİMOV, H.Ş. HƏSƏNOV, H.F. ABBASOV, B.G. PAŞAYEV
Bakı Dövlət Universiteti,
Az 1148, Azərbaycan, Bakı, Z. Xəlilov küç, 23

KOH və NaOH-ın sulu məhlulunun kiçik konsentrasiyalar oblastında dielektrik xassələri tədqiq edilmişdir. Alınan nəticələr göstərir ki, baxılan temperatur və konsentrasiya intervalında həm KOH, həm də NaOH suyun strukturuna dağıdıcı təsir göstərir. Koul-Koul diaqramlarından relaksasiya müddətləri və Skanavi modeli əsasında su klasterlərinin ölçüləri təyin edilmişdir.

Məlumdur ki, bioloji obyektlərin funksional fəaliyyəti onların ayrılmaz tərkib hissəsi olan suyun termodinamik halından və ya strukturundan çox ciddi şəkildə asılıdır. Məhlulun strukturu haqqında ən informativ metodlardan biri dielektrik ölçmə (dielektrik spektroskopiya) metodudur.

Bioloji obyektlərin, məsələn, bioloji membranların, toxumaların və s. dielektrik xassələrini tədqiq etməklə Svan [1] bu növ maddələrdə, əsasən, 3 növ dispersiya - α, β, γ dispersiyaları müşahidə etmişdir.

α - dispersiya ionların diffuziyası ilə bağlı olub, ion-diffuziya və ya ion-miqrasiya polyarizasiyası ilə əlaqədardır [2]. Şvarts α-dispersiyanı bioloji obyektin tərkibindəki məhluldakı suspenziya hissəciklərinə ikiqat elektrik layı nəzəriyyəsini tətbiq etməklə izah etmişdir [3]. Məhlulu elektrik sahəsinə gətirdikdə suspenziya hissəciklərindəki ionların yerdəyişməsi polyarizasiya yaradır və sahə götürüldükdən sonra ionların ilkin suspenziyadaxili paylanması diffuziya yolu ilə τ relaksasiya müddətində bərpa olunur. α -dispersiya çox kiçik tezliklərdə ($10\div0^3$ Hs) müşahidə olunur.

β - dispersiya fiziki xassələri (keçiriciliyi və dielektrik nüfuzluluğu) fərqlənən iki mühitin sərhəddində müşahidə edilən Maksvell-Vaqner polyarizasiyası ilə bağlıdır [2]. β - dispersiya $10^3\div10^6$Hs tezliklərdə müşahidə edilir. Hər iki α ilə β - dispersiya dielektrik nüfuzluluğunun yüksək qiyməti ilə ($10^5\div10^8$) digər növ dispersiyalardan kəskin fərqlənir.

γ - dispersiya bioloji obyektlərin tərkibindəki «bağlı» su molekulları ilə əlaqədardır və $10^7\div10^8$Hs tezliklərdə müşahidə edilir. $10^6\div10^7$Hs tezlik intervalında bioloji obyektlərdə sabit dipol momentinə malik böyük zülal molekullarının varlığı ilə əlaqədar daha bir dispersiya - δ dispersiya müşahidə olunur [4].

Kiçik dipolların orientasiyası ilə bağlı polyarizasiya daha yüksək tezliklərdə (10^9Hs) baş verir, elektronların relaksasiyası isə daha yüksək tezliklərdə - 10^{12}Hs-də özünü biruzə verir. Hər iki relaksasiya yüksək sürətlidir: kiçik dipolların relaksasiya müddəti nanosaniyə, elektronların relaksasiya müddəti pikosaniyə tərtibindədir.

İşdə K^+ və Na^+ ionlarının bioloji obyektlərin, konkret olaraq biomembranların fəaliyyətində çox böyük rol oynadığını nəzərə alaraq [5] KOH və NaOH-ın duru sulu məhlulunun səs tezliklərində dielektrik xassələri tədqiq edilmişdir.

Ölçmələr, əsasən otaq temperaturunda (20÷30°S) körpü üsulu ilə xüsusi düzəldilmiş yuvacıqda aparılmışdır. Yuvacıq üzərinə qızıl çəkilmiş, arasına tədqiq olunan məhlul doldurulmuş köynəkləri olan müstəvi kondensatordan ibarət olub, nümunənin elektrik tutumunu (C) və keçirijiliyini (σ) 20÷200000Hs tezlik intervalında ölçməyə imkan verir.

Nümunəyə bir-birilə parallel birləşdirilmiş ideal kondensator və ideal rezistor sistemi kimi baxsaq ona dəyişən elektrik sahəsi verdikdə $\left(E = E_o\,\ell^{i\omega t}\right)$ sistemdən axan cərəyana sırf «keçiricilik» və «induksiya» cərəyanlarının cəmi kimi baxmaq olar:

$$j = j_s + j_i = \lambda E + \frac{dD}{dt} = \lambda E + \frac{d\left(\varepsilon_o E + P\right)}{dt} =$$
$$= \left(\lambda + i\omega\varepsilon_o\varepsilon_\infty + \frac{\varepsilon_s - \varepsilon_\infty}{1 + i\omega\tau} i\omega\varepsilon_o\right)E = \qquad (1)$$
$$= \frac{1}{S}\cdot\frac{dq}{dt} = \frac{CdU}{Sdt} = \varepsilon_o\varepsilon\frac{dE}{dt} = \varepsilon_o\varepsilon i\omega E$$

Müqayisə göstərir ki, dielektrik nüfuzluluğu kompleks kəmiyyətdir:

$$\varepsilon = \frac{\lambda}{i\varepsilon_o\omega} + \varepsilon_\infty + \frac{\varepsilon_s - \varepsilon_\infty}{1 + i\omega\tau} = \varepsilon' - i\varepsilon'' \qquad (2)$$

$$\varepsilon' = \varepsilon_\infty + \frac{\varepsilon_s - \varepsilon_\infty}{1 + \omega^2\tau^2} \qquad (3)$$

$$\varepsilon'' = \frac{\lambda}{\varepsilon_o\omega} + \frac{\left(\varepsilon_s - \varepsilon_\infty\right)\omega\tau}{1 + \omega^2\tau^2} \qquad (4)$$

$\varepsilon''(\varepsilon')$ asılılığının qrafiki Koul-Koul diaqramını verir. Relaksasiya mexanizmlərinin sayı birdən çox olduqda Koul-Koul tənliyi (2) aşağıdakı kimi modifikasiya olunur:

$$\varepsilon = \varepsilon_\infty + \frac{\varepsilon_s - \varepsilon_\infty}{1 + (i\omega\tau)^{1-\alpha}} \qquad (5)$$

burada α - çox mexanizmli relaksasiya müddətlərinin paylanma əmsalı adlanır.

Bir relaksasiyalı halda (3) və (4) tənliklərindən $\omega\tau$-nu aradan çıxartmaqla alınan $\varepsilon''(\varepsilon')$ asılılığının qrafiki mərkəzi ε' oxu üzərində olan $\frac{\varepsilon_s - \varepsilon_\infty}{2}$ radiuslu yarım-

çevrə olur. Çoxrelaksasiyalı halda isə yarımçevrənin mərkəzi ε' oxuna nəzərən sürüşür.

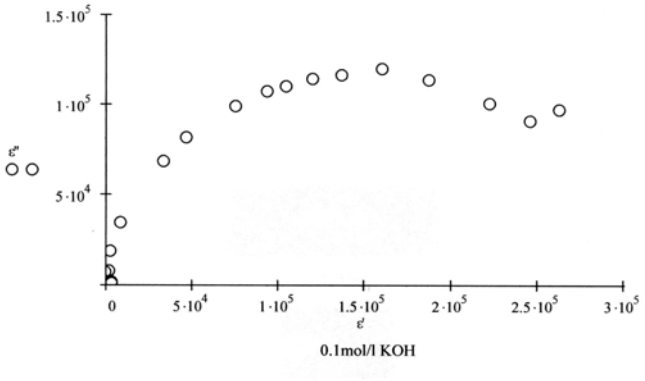

Şəkil 1a. 0.1 mol/l KOH –ın sulu məhlulu üçün Koul-Koul diaqramı.

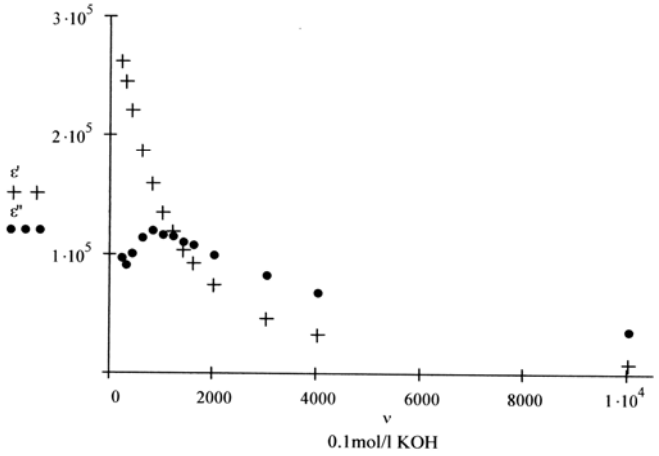

Şəkil 1b. 0.1 mol/l KOH –ın sulu məhlulunun dielektrik nüfuzluluğunun həqiqi və xəyali hissələrinin tezlik asılılığı

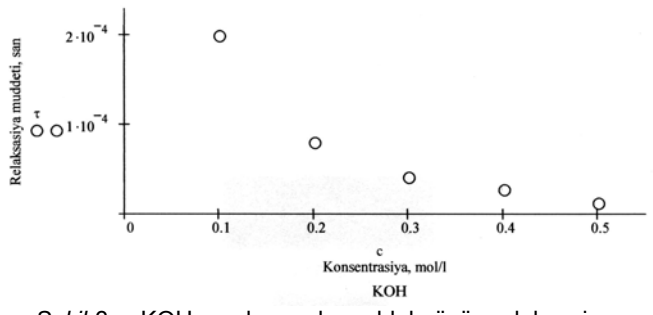

Şəkil 2a. KOH –ın duru sulu məhlulu üçün relaksasiya müddətinin KOH-ın konsentrasiyasından asılılığı.

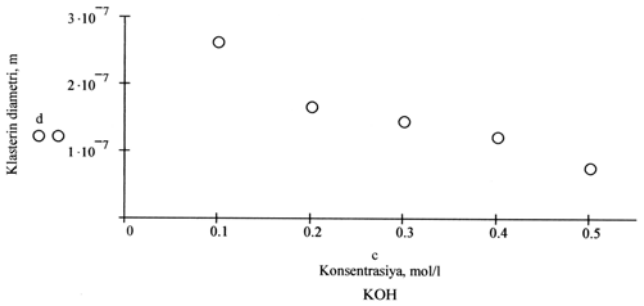

Şəkil 2b. KOH –ın duru sulu məhlulunda su klasterlərinin diametrinin KOH-ın konsentrasiyasından asılılığı.

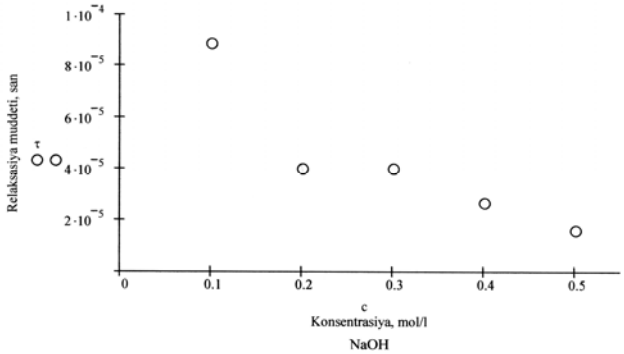

Şəkil 3a. NaOH –ın duru sulu məhlulu üçün relaksasiya müddətinin KOH-ın konsentrasiyasından asılılığı

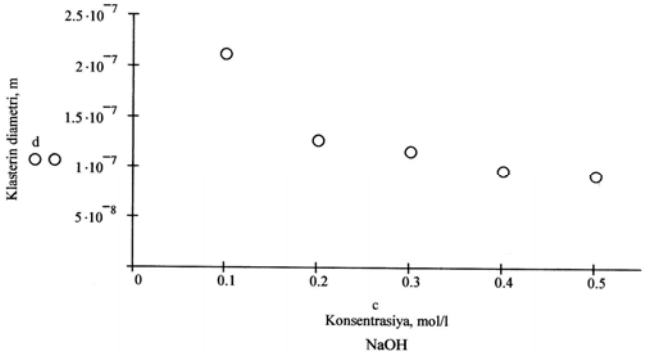

Şəkil 3b. NaOH –ın duru sulu məhlulunda su klasterlərinin diametrinin KOH-ın konsentrasiyasından asılılığı

K^+ və Na^+ ionları ilə aparılan təcrübələr göstərir ki, Koul-Koul diaqramlarından müəyyən olunan relaksasiya müddətləri hər iki ion halında ionların konsentrasiyası artdıqca azalır (şəkil 2a,3a). Nümunə kimi şəkil 1-də 0.1mol/l KOH sulu məhlulu üçün Koul-Koul diaqramı (a) və $\varepsilon'(\nu)$, $\varepsilon''(\nu)$ asılılıqlarının qrafikləri (b) göstərilmişdir.

İonların diffuziyası ilə bağlı polyarizasiyanın Skanavi tərəfindən verilən modelindən istifadə etməklə, Koul-Koul diaqramından uyğun relaksatorun ölçülərini qiymətləndirmək olar [6]:

$$P = \varepsilon_o\left(\varepsilon_S - \varepsilon_\infty\right)E_o\left(1 - e^{-\frac{t}{\tau}}\right) = \frac{n_o q^2 d^2}{12\,kT}E\left(1 - e^{-\frac{t}{\tau}}\right) \qquad (7)$$

Burada ε_S- statik dielektrik nüfuzluğu, ε_∞ - optik dielektrik nüfuzluğu, ε_0 - elektrik sabiti, n_0- ionların konsentrasiyası, q- ionların yükü, d – potensial çəpərin eni, k- Bolsman sabiti, T - mütləq temperatur, E – elektrik sahəsinin intensivliyi, τ - relaksasiya müddətidir.

(7) düsturunda *d*-ni relaksatorun ölçüsü qəbul etsək alarıq:

$$d = \frac{2}{q}\sqrt{\frac{3kT\varepsilon_o\left(\varepsilon_s - \varepsilon_\infty\right)}{n_o}} = \frac{2}{q}\sqrt{\frac{6kT\,\varepsilon_o\varepsilon''_{\max}}{n_o}} \qquad (8)$$

$\varepsilon''_{\max} = \frac{\varepsilon_s - \varepsilon_\infty}{2}$ -yə bərabərdir.

(8) düsturunu KOH və NaOH-ın duru sulu məhluluna tətbiq etməklə uyğun Koul-Koul diaqramlarının köməyilə məhluldakı su klasterlərinin diametrləri qiymətləndirilmişdir. Su klasterlərinin diametrlinin məhluldakı ionların konsentrasiyasından asılılıq qrafikləri şəkil 2b və 3b-də göstərilmişdir. Göründüyü kimi K^+ və Na^+ ionlarının konsentrasiyası artdıqca su klasterləri kiçilir. Bu faktı K^+ və Na^+ ionlarının məhluldakı konsentrasiyası artdıqca yeni-yeni su molekullarının klasterlərdən qoparaq ionların hidratasiyasına cəlb olunması ilə izah etmək olar. Yaxşı məlumdur ki, bioloji membranın daxilində K^+ ionları (0.140mol/l), xaricində isə Na^+ ionları (0.142mol/l) üstünlük təşkil edir [5]. Şəkil 2b ilə 3b-nin müqayisəsi göstərir ki, göstərilən konsentrasiyalı məhlullarda su klasterlərinin ölçüləri NaOH məhlulunda KOH məhluluna nisbətən ~1.5 dəfə kiçikdir. Deməli, hüceyrənin daxilindəki su klasterlərinin ölçüləri xaricindəkindən böyükdür, yəni suyun termodinamik halı membranın daxilində və xaricində fərqlidir. Bu fərq hüceyrənin fəaliyyətinə ciddi təsir edir: göstərilən konsentrasiyada suyun hüceyrənin daxilinə keçməsi hüceyrədən xaricə çıxmasına nisbətən asandır. Deməli, suyun membrandan keçmə istiqaməti K^+ və Na^+ ionlarının balansı ilə müəyyən olunur. Onu da qeyd edək ki, bu balansdan, həm də membran potensialı ciddi şəkildə asılıdır. Digər maddələrin də suyun strukturuna ayrılıqda və birgə təsirini öyrənmək istiqamətində işlər davam etdirilir.

[1] *H.P. Schwan*. “Electrical Properties of Tissue and Cell Suspensions”. Advences in Biological and Medical Physics; *J.H. Lawrence, C.A.Tobias*, Acad Press: New York, 1957, vol.V, 147-209.

[2] *P.T. Oreşkin*. «Fizika poluprovodnikov i dielektrikov», 1977, Moskva «Vısşaya şkola». (Rusca).

[3] *G. Schwartr*. “A theory of the low frequency dispersion of colloid particles in electrolyte solution”, J.Phys. Chem., 1962,66, 2636-2642.

[4] *R.D. Stoy, K.R. Foster, H.P. Schwan*. Dielectric properties of mammalian tissues from 0,1 to 100 MHz ; a summay of resent data. “Phys Med.Biol.”, 1982, 27, 501-513.

[5] *G. Martinsen, S. Grimnes, H.P. Schwan*. “Interface phenomena and dielejtrij properties of biological tissue”, Encyclopedia of Surface and Colloid Science; 2002, by Marcel Dekker.

[6] Q.İ. Skanavi. Fizika dielektrikov. I çast, 1949, qos. izd. tex. teor. lit. Moskva-Leninqrad.(Rusca).

Э.А. Масимов, Г.Ш. Гасанов, Х.Ф. Аббасов, Б.Г. Пашаев

ДИЭЛЕКТРИЧЕСКИЕ СВОЙСТВА РАЗБАВЛЕННОГО ВОДНОГО РАСТВОРА NaOH и KOH

Были исследованы диэлектрические свойства водного раствора NaOH и KOH при их низких концентрациях. Полученные результаты показывают, что NaOH и KOH при рассмотренных интервалах температур и концентраций разрушают структуру воды. Из диаграмм Коул-Коуля были определены времена релаксации и были оценены размеры водных кластеров на основе модели Сканави.

E.A. Masimov, H.Sh. Hasanov, H.F. Abbasov, B.G. Pashayev

DIELECTRIC PROPERTIES OF WATER SOLUTION OF NaOH and KOH

The dielectric properties of water solution of NaOH and KOH were investigated at lower concentration. The obtained results show that NaOH and KOH destroy the water structure in the considered temperature and concentrations. The relaxation times were found by Cole-Cole diagrams and the dimensions of the water clasters were estimated on the base of Skanavi model.

Received: 08.07.06

+

++

+

$MnGa_2S_4$ MONOKRİSTALININ ELEKTRİK XASSƏLƏRİ

N.N. NİFTİYEV
Azərbaycan Dövlət Pedoqoji Universiteti, Az. 1000, Bakı, Ü. Hacıbəyov, 34.
O.B. TAĞIYEV
AMEA Fizika İnstitutu, Az. 1143, Bakı, H. Cavid, 33.
M.B. MURADOV
Bakı Dövlət Universitet, Az. 1145, Z. Xəlilov, 23.
F.M. MƏMMƏDOV
AMEA kimya problemləri institutu, Az. 1143, H. Cavid,33

$MnGa_2S_4$ monokristalında müxtəlif temperaturlarda VAX, $\sigma(T)$ və TDC tədqiq edilmişdir. Tələlərin xarakteri müəyyən edilmiş, onların yerləşmə dərinliyi və konsetrasiyası hesablanmışdır.

Maqnit və yarımkeçirici xassələrini özündə cəmləşdirən və maqnit yarımkeçiriciləri adlanan AB_2X_4(A-Mn, Fe, Co, Ni; B-Ga, İn; X-S, Se, Te) tipli birləşmələr qeyri-adi xüsusiyyətləri sayəsində geniş tədqiqatların obyektinə çevrilmişdir. [1-6]. Bu birləşmələr onları əsasında lazerlər, işıq modulyatorları, fotodetektorlar və maqnit sahəsində idarə oluna bilən digər funksional qurğuların yaradılmasında perspektivlidir. $MnGa_2S_4$ birləşməsinin müxtəlif modifikasiyaları mövcuddur: aşağı temperaturlu α-$MnGa_2S_4$ fazası kristal qəfəs parametrləri *a=12,746, b=22,609, c=6,394Å* və fəza qrupu C_2^6c, *z=12* olan monoklin qəfəsə kristallaşır, yuxarı temperaturlu β-$MnGa_2S_4$ fazası kristal qəfəs parametrləri *a=12,90, b=745, c=6,13Å* və fəza qrupu *PnaZ,* olan rombik qrupa kristallaşır [1-2; 7-8]. Hər iki fazanın monokristalı kimyəvi köçürmə metodu ilə alınmışdır. Bundan başqa $MnGa_2S_4$ birləşməsinin $MnGa_2Se_4$ quruluşuna analoji olaraq qəfəs parametrləri *a=5,46, c=10,50Å, c/a=1,92* olan I4 fəza qrupuna kristallaşan yeni fazası alınmış və onun elektrik və optik xassələri tətqiq edilmişdir [9-10].

Bu işdə Bricmen metodu ilə alınmış β-$MnGa_2S_4$ monokristalının Volt amper xarakteristikası (VAX), elektrik keçiriciliyinin temperatur asılılığı $(\sigma(T))$ və termostimullaşmış depolyarizasiya cərəyanları (TDC) tədqiq edilmişdir. Ölçmələri aparmaq üçün kontakt kimi nümunənin səthinə çəkilmiş indium- qalium ərintisindən istifadə edilmişdir.

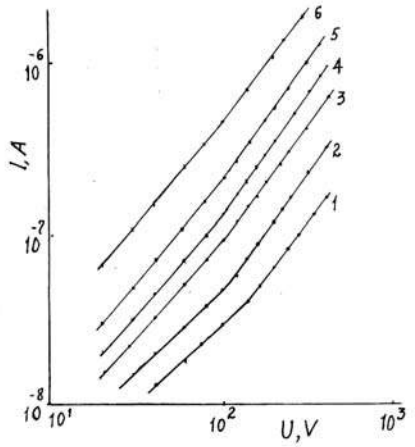

Şəkil 1. $MnGa_2S_4$ monokristalında qaranlıqda müxtəlif temperaturlarda VAX:-T.: 1-293; 2-308; 3-323; 4-338; 5-353; 6-373.

Şəkil 1-də $MnGa_2S_4$ monokristalının müxtəlif temperaturlarda VAX- i verilmişdir. Buradan iki oblast aşkara çıxarılmışdır: 1) Om qanununa tabe olan oblast ($İ$-U) və 2) $İ$-$U^{3/2}$ oblastı. Aşağı gərginliklərdə VAX-ın xətti oblastında cərəyanın gərginlikdən asılılığı

$$I=\frac{e\mu n_0 US}{L} \qquad (1)$$

kimi olur [11]. Burada U- nümunəyə tətbiq olunan gərginlik, n_0- tarazlıqda olan yükdaşıyıcıların konsentrasiyası, μ- yüdaşıyıcıların yürüklüyü, e- yükdaşıyıcıların yükü, L-kontaktlar arasında məsafə, S-kontaktların sahəsidir. Yükdaşıyıcıların konsentrasiyası üçün $\sim 10^{10} sm^{-3}$ qiyməti tapılmışdır. Temperatur yüksəldikcə qeyri- xətti oblasta keçid gərginliyi azalır. Bu onu göstərir ki, $MnGa_2S_4$ monokristalı qüvvətli kompensasiya olunmuş yarımkeçiricidir. $İ \sim U^{3/2}$ oblastında isə cərəyanın keçmə mexanizminin injeksiya ilə əlaqədar olması fərz olunar [11].

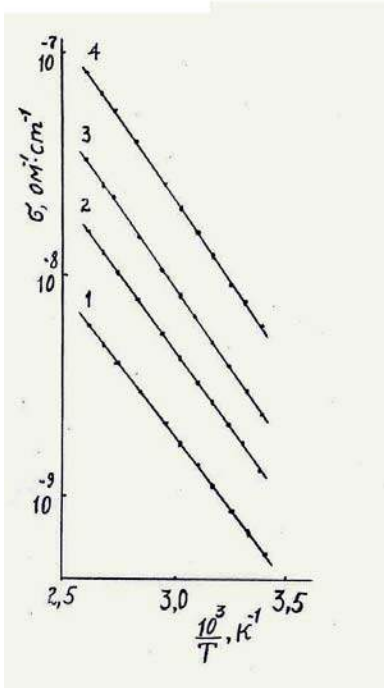

Şəkil 2. $MnGa_2S_4$ monokristalı üçün müxtəlif sabit gərginliklərdə elektrik keçiriciliyinin temperatur asılılığı: (U-V): 1-40; 2-100; 3-180; 4-300.

Şəkil 2- də müxtəlif sabit gərginliklərdə elektrik keçiriciliyinin temperaturdan asılılıq qrafiki verilmişdir. Düz xətlərin meylləri demək olar ki, bir-birindən o qədər də fərqlənmir. $lg\sigma \sim 10^3/T$ asılılıq əyrisindən yükdaşıyıcıların aktivasiya enerjisi hesablanmışdır və $E=0,28\pm0,2$ *eV*-a bərabərdir.

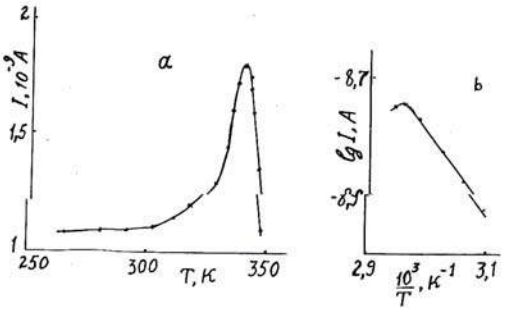

Şəkil 3. a) 300V polyarizasiya gərginliyində TDC əyrisi.
b) 300V polyarizasiya gərginliyində TDC cərəyan pikinin başlanğıc hissəsinin temperaturdan asılılığı.

Şəkil 3a- da $MnGa_2S_4$ monokristalı üçün *300V* polyarizasiya gərginliyində TDC əyrisi verilmişdir. TDC spektrində temperatur maksimumu *338K* olan pik müşahidə edilmişdir. TDC əyrisinin təhlili üçün yapışma səviyyələrinin tipini bilmək lazımdır. Bunun üçün «δ» kəmiyyətindən istifadə olunur və «δ» aşağıdakı ifadədən tapılır:

$$\delta = \frac{T_2 - T_M}{T_2 - T_1} \qquad (2)$$

Burada T_M- TDC- nin maksimumuna uyğun temperaturdur, T_1 və T_2- TDC- nin maksimum intensivliyinin yarısına uyğun aşağı və yuxarı temperaturlardır. TDC maksimumunun formasının təhlili göstərir ki, $MnGa_2S_4$ monokristalı üçün müşahdə edilən maksimumda

$$\delta \geq e^{-1}\left(1 + \frac{2KT_M}{E_t}\right) \qquad (3)$$

şərti ödənilir [12]. Bu şərtin ödənilməsi sürətli yanışma səviyyələrinin mövcudluğunu göstərir.

Şəkil 3b- də $MnGa_2S_4$ monokristalı üçün TDC cərəyan pikinin başlanğıc hissəsinin temperaturdan asılılıq əyrisi $I \sim 10^3/T$ miqyasında göstərilmişdir. Bu əyridən tələlərin aktivləşmə enerjisi hesablanmışdır və $E=0,28$ *eV* [13].

Göründüyü kimi bu enerji səviyyəsi $\sigma(T)$-dən də tapılmışdır. Bu onu göstərir ki, elektrik keçiriciliyi və termostimullaşmış depolyarizasiya cərəyanları eyni səviyyə ilə bağlıdır.

Beləliklə, $MnGa_2S_4$ monokristalında müxtəlif temperaturlarda VAX, $\sigma(T)$ və TDC tədqiq edilmişdir. Tələlərn xarakteri müəyyən edilmiş, onların yerləşmə dərinliyi və konsentrasiyası hesablanmışdır.

[1] *T. Kanomata, H.İdo, T. Kaneko.* J.Phys. Japan,1973, M.34, №2, p.554.

[2] *B.K. Babayeva*. V sb. Troynıye poluprovodniki i ix primeneie. Kişinev. Ştntsa. 1976.s.96. (Rus dilində)

[3] *G.A. Medvedkin. Yu.V. Rud M.V. Tairov*. Phys.Status solidi (a) 1989,V.3, p.289

[4] *Q.K. Averkieva, R.N. Bekimbetov, N.N. Konstantinova i dr*. Neorqaniçeskie materialı, 1988, t.24, №4, s.591-594. (Rus dilində)

[5] *N.N. Niftiyev, O.B. Taqiyev*. İnorqanik materials, 2003,V.39, №6 p.576-578.

[6] *N.N. Niftiyev, M.A. Alidjanov, O.B. Taqiyev, F.M. Mamedov*. FTP, 2004, t.38. №. 5, s.550-552. (Rus dilində).

[7] *R. Rimet, R. Buder, C. Sehlenker, B. Roques, T. Zanchetta*. Sol. St. Commun., 1981,v.37,P.693-697.

[8] *M.P. Pardo, M. Julien-Pourol.* C.r.Acad.sci, 1973, №20, p.1021-1023.

[9] *N.N. Niftiyev*. İntermetallics, 2003, №11, p. 975-977.

[10] *N.N. Niftiyev, O.B. Taqiev*. FTP, 2004, t.38, v.2, c.166-167. (Rus dilində).

[11] *M. Lampert, P. Mark*. İnjekulonnıye toni v tverdıx telax, M.Mir., 1973, 473s.

[12] *P.Q. Litevçenko, V.İ. Ustinev*. Aktualnıe voprosı fiziki poluprovodnikovıx priborov, Vilnyus, Mokslas, 1960, 153s.

[13] *Yu.A. Qoroxovatskiy*. Osnovi termodepolyarizatsion-noqo analiza, Nauka, 1981, 176s.

Н.Н. Нифтиев, О.Б. Тагиев, М.Б. Мурадов, Ф.М. Мамедов

ЭЛЕКТРИЧЕСКИЕ СВОЙСТВА МОНОКРИСТАЛЛОВ $MnGa_2S_4$

Исследованы вольтамперные характеристики ВАХ, электропроводность $\sigma(T)$ и токи термостимулированной деполяризации (ТСД) для кристаллов $MnGa_2S_4$ при различных температурах. Найден характер ловушек, определена их глубина залегания и концентрация.

N.N. Niftiyev, O.B. Tagiyev, M.B. Muradov, F.M. Mamedov

ELECTRICAL PROPERTIES Of $MnGa_2S_4$ SINGLE CRYSTALS

Volt-ampere characteristics VAC, electric conduction $\sigma(T)$ and thermostimulated depolarization (TSD) currents for $MnGa_2S_4$ crystals at different temperatures are investigated. Trap character is found and its occurrence depths and concentration are obtained.

Received: 08.07.06

REAL QAZLARIN DROSSELLƏNMƏSİNƏ DAİR

C.Y. NAZİYEV
Azərbaycan Dövlət Neft Akademiyası
370012, Bakı, Azadlıq pr., 20

Klauzius hal tənliyinə tabe olan real qazın axması zamanı adiabatik drosselənməyə baxılıb. Qazın kritik parametrləri, inversiya temperaturu və inversiya əyrisinin maksimal parametrləri təyin edilib.

Qazların və mayelərin drosselənməsi (əzilməsi) məsələsi termodinamikada xüsusi əhəmiyyət kəsb edir. Texnikanın bir çox sahələrində drosselənmədən geniş istifadə edilir: soyuducu maşınlarda, kriogen qurğularında, daxili yanma mühərriklərində, buxar və qaz turbinlərində, reaktiv mühərriklərdə, raket texnikasında, qaz borularında və i.a.

Bu, baxımdan hər bir real qazın drosselləndikdə özünü necə aparmasını həm nəzəri, həm də praktiki cəhətdən öyrənmək vacibdir.

Drosselənmə adiabatik və dönməyən prosesdir [1-3]. Ümumiyyətlə, o zərərli hadisədir. Çünki axma zamanı qaz mexaniki müqavimətdən keçir. Lakin texnikada ondan səmərəli istifadə edirlər.

Drosselənmə zamanı ideal qazın temperaturu dəyişmir. Amma real qaz drosselləndikdə o qıza da bilər, soyuya da bilər və onun temperaturu sabit da qala bilər. Bu qazın təbiətindən və onun başlanğıc parametrlərindən asılıdır.

Ədəbiyyatdan məlumdur ki, Klauzius hal tənliyi belədir [4]

$$\left[p-\frac{a}{T(\upsilon+c)^2}\right](\upsilon-b)=RT\,, \qquad (1)$$

burada p – qazın təzyiqi; T – temperaturu; υ - xüsusi həcmi; a,b,c – tənliyin sabitləridir.

Tənlikdən istifadə etmək üçün onu aşağıdakı şəkildə yazmaq əlverişlidir

$$p=\frac{RT}{\upsilon-b}-\frac{a}{T(\upsilon+c)^2}\,. \qquad (2)$$

Maddənin kritik (böhran) halının şərtlərindən istifadə edərək Klauzius qazının kritik parametrlərini (p_k, υ_k, T_k) təyin edək.

Kritik şərtə görə

$$\left(\frac{\partial p}{\partial \upsilon}\right)_T=0;\quad \left(\frac{\partial^2 p}{\partial \upsilon^2}\right)_T=0\,. \qquad (3)$$

(2) tənliyindən T=*const* halında birinci və ikinci törəmələri alaq

$$\left(\frac{\partial p}{\partial \upsilon}\right)_T=-\frac{RT}{(\upsilon-b)^2}+\frac{2a}{T(\upsilon+c)^3}=0 \qquad (4)$$

$$\left(\frac{\partial^2 p}{\partial \upsilon^2}\right)_T=\frac{2RT}{(\upsilon-b)^3}-\frac{6a}{T(\upsilon+c)^4}=0 \qquad (5)$$

(4) asılılığını (5)-ə bölsək alarıq ki,

$$\frac{\upsilon-b}{2}=\frac{\upsilon+c}{3} \qquad (6)$$

buradan

$$\upsilon_k=3b+2c. \qquad (7)$$

İndi (4) bərabərliyindən T_k-i tapaq

$$T_k^2=\frac{2a(\upsilon_k-b)^2}{R(\upsilon_k+c)^3}=\frac{8a}{27R(b+c)}\,.$$

Onda

$$T_k=\sqrt{\frac{8a}{27R(b+c)}}=\frac{2}{3}\sqrt{\frac{2a}{3R(b+c)}}\,. \qquad (8)$$

(2) tənliyindən p_k-ı tapmaq olar

$$p_k=\frac{RT_k}{\upsilon_k-b}-\frac{a}{T_k(\upsilon_k+c)^2}\,. \qquad (9)$$

Məlum T_k və υ_k-in qiymətlərini (7) və (8) ifadələrindən (9) tənliyinə qoysaq alarıq

$$p_k=\frac{a}{18(b+c)^2\sqrt{\frac{2a}{3R(b+c)}}}\,. \qquad (10)$$

İndi, əksinə, a, b və c sabitlərini kritik parametrlərlə ifadə edək.

Köməkçi düsturlardan istifadə edək. Təyin edə bilərik ki,

$$T_k p_k=\frac{a}{27(b+c)^2}, \qquad \square \qquad (11)$$

$$\frac{T_k}{p_k}=\frac{8(b+c)}{R}\,. \qquad (12)$$

(7), (11) və (12) asılılıqlarından təyin etmək olar

$$c=\frac{3RT_k}{8p_k}-\upsilon_k\,, \qquad (13)$$

$$b=\upsilon_k-\frac{RT_k}{4p_k}\,, \qquad (14)$$

$$a=\frac{27R^2T_k^3}{64p_k}\,. \qquad (15)$$

Universal tənlik üçün çox vacib olan kritik sıxılma əmsalını tapaq

$$z_k = \frac{p_k \upsilon_k}{RT_k} = \frac{3b+2c}{8(b+c)} = \frac{3}{8} - \frac{c}{8(b+c)}. \qquad (15,a)$$

İndi də Klauzius qazının drosselləmməsinə baxaq. Axının termodinamikasından məlumdur ki, qaz drosselləndikdə onun temperaturu aşağıdakı qanunla dəyişir

$$dT = \frac{T\left(\frac{\partial \upsilon}{\partial T}\right)_p - \upsilon}{c_p} dp, \qquad (16)$$

burada c_p – qazın izobar istilik tutumudur, $c_p>0$.

(16) tənliyini təhlil edək. Drosselləmədə həmişə təzyiq düşür, $dp<0$ olur. Deməli, temperaturun keyfiyyətcə dəyişməsi $[T(\partial\upsilon/\partial T)_p-\upsilon]$ kəmiyyətinin işarəsindən asılı olacaq, çünki $c_p>0$. Kəsrin surəti mənfi olsa $dT>0$, deməli drosselləndikdə qaz qızacaq; müsbət olsa $dT<0$, yəni qaz soyuyacaq; əgər surət sıfra bərabər olsa $dT=0$, deməli drosselləmədən sonra qazın temperaturu dəyişməz. Üçüncü halı texnikada bilmək çox vacibdir. Bu hala qazın inversiyası deyilir, temperatur isə inversiya temperaturu adlanır. Diaqramlarda inversiya əyrisi temperaturun dəyişməsinin sərhəd əyrisi olur.

İnversiya əyrisinin tənliyi (16) tənliyindən alınır.

$$T\left(\frac{\partial \upsilon}{\partial T}\right)_p - \upsilon = 0. \qquad (17)$$

Bəzən inversiya əyrisinin tənliyi kimi identik tənlik götürülür

$$T\left(\frac{\partial p}{\partial T}\right)_\upsilon + \upsilon\left(\frac{\partial p}{\partial \upsilon}\right)_T = 0. \qquad (18)$$

Alçaq təzyiqlər üçün (atmosfer təzyiqi ətrafında) inversiya temperaturunu tapaq.

(2) tənliyinə belə forma verək

$$p\upsilon = pb + RT - \frac{a(\upsilon-b)}{T(\upsilon+c)^2}. \qquad (19)$$

$p=const$ şəklində bu tənliyi differensiallayaq və (17) ifadəsində nəzərə alaraq

$$T\left(\frac{\partial \upsilon}{\partial T}\right)_p - \upsilon = \frac{RT^2(\upsilon+c)^3 + a(\upsilon-b)(\upsilon+c) - p\upsilon T(\upsilon+c)^3 + a\upsilon(\upsilon-2b-c)}{pT(\upsilon+c)^3 - a(\upsilon-2b-c)} = 0.$$

(19) tənliyindən $p\upsilon$-nin qiymətyini burada yerinə yazaq

$$T\left(\frac{\partial \upsilon}{\partial T}\right)_p - \upsilon = \frac{-pbT(\upsilon+c)^3 + 3a\upsilon^2 - 4a\upsilon b + a\upsilon c - 2abc}{pT(\upsilon+c)^3 - a(\upsilon-2b-c)} = 0. \qquad (20)$$

Alçaq təzyiqlər üçün $p=RT/\upsilon$ yazaq

$$\begin{aligned} T\left(\frac{\partial \upsilon}{\partial T}\right)_p - \upsilon &= \frac{-RT^2 b(\upsilon+c)^3/\upsilon + 3a\upsilon^2 - 4a\upsilon b + a\upsilon c - 2abc}{RT^2(\upsilon+c)^3/\upsilon - a(\upsilon-2b-c)} = \\ &= \frac{-RT^2 b + 3a\upsilon^3/(\upsilon+c)^3 - (4a\upsilon b - a\upsilon c + 2abc)\upsilon/(\upsilon+c)^3}{RT^2 - a(\upsilon-2b-c)\upsilon/(\upsilon+c)^3} = 0. \end{aligned} \qquad (21)$$

Kiçik təzyiqlərdə qəbul edək ki, $p\to 0$, $1/\upsilon\to 0$, onda (21) ifadəsi sadələşər; eyni zamanda $\upsilon^3/(\upsilon+c)^3\approx 1$ olduğundan

$$T\left(\frac{\partial \upsilon}{\partial T}\right)_p - \upsilon = \frac{-RT^2 b + 3a\dfrac{\upsilon^3}{(\upsilon+c)^3}}{RT^2} = 0,$$

$$-b \approx \frac{3a}{RT^2}, \qquad T_{inv}^2 \approx \frac{3a}{Rb}, \qquad (22)$$

$$T_{inv} \approx \sqrt{\frac{3a}{Rb}} \approx 3{,}21 T_k.$$

İnversiya tənliyinə (17) görə pT diaqramında inversiya əyrisi temperatur azaldıqca əvvəl yuxarı qalxır, sonra maksimum nöqtəni M keçərək azalmağa başlayır (şəkil 1).

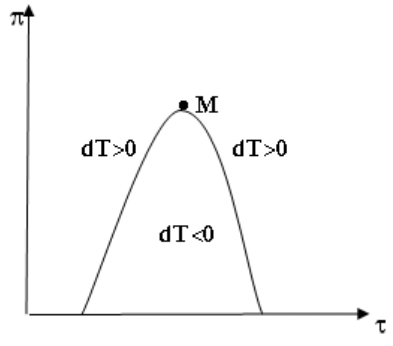

Şəkil π-τ koordinatlarında göstərilib, haradakı π və τ uyğun olaraq gətirilmiş təzyiq və temperaturdur.

Əgər qazın halı əyri içərisindəki sahəyə düşərsə o dros-

selləndikdə soyuyar, əyridən xaricdəki sahəyə düşərsə o qızar, əyri üzərinə düşərsə qazın temperaturu dəyişməz. Beləliklə, əyrinin təyini xüsusi əhəmiyyət kəsb edir.

(19) tənliyindən birinci törəməni alsaq (p=const)

$$\left[p-\frac{a\upsilon}{T(\upsilon+c)^3}+\frac{a(2b+c)}{T(\upsilon+c)^3}\right]\left(\frac{\partial\upsilon}{\partial T}\right)_p=R+\frac{a\upsilon}{T^3(\upsilon+c)^2}-\frac{ab}{T^2(\upsilon+c)^2}. \quad (23)$$

İkinci törəməni alaq ($p=const$)

$$\left[p-\frac{a(\upsilon-2b-c)}{T(\upsilon+c)^3}\right]\cdot\left(\frac{\partial^2\upsilon}{\partial T^2}\right)_p+\left[\frac{2a(\upsilon-3b-2c)}{T(\upsilon+c)^4}\right]\cdot\left(\frac{\partial\upsilon}{\partial T}\right)_p^2+\left[\frac{2a(\upsilon-2b-c)}{T^2(\upsilon+c)^3}\right]\cdot\left(\frac{\partial\upsilon}{\partial T}\right)_p+\frac{2a(\upsilon-b)}{T^3(\upsilon+c)^2}=0. \quad (24)$$

(23) bərabərliyini sadələşdirək. Qəbul edək ki, $p(\partial\upsilon/\partial T)_p=R$. Onda (23)-dən alarıq

$$\frac{2a(\upsilon-2b-c)}{T^2(\upsilon+c)^3}\cdot\left(\frac{\partial\upsilon}{\partial T}\right)_p=\frac{-2a(\upsilon-b)}{T^3(\upsilon+c)^2} \quad (25)$$

Bu qiyməti (24) tənliyində nəzərə alaq

$$\left[p-\frac{a(\upsilon-2b-c)}{T(\upsilon+c)^3}\right]\cdot\left(\frac{\partial^2\upsilon}{\partial T^2}\right)_p+\left[\frac{2a(\upsilon-3b-2c)}{T(\upsilon+c)^4}\right]\cdot\left(\frac{\partial\upsilon}{\partial T}\right)_p^2=0 \quad (26)$$

(26) ifadəsindən istifadə etmək üçün inversiyanın tənliyindən əlavə şərti alaq. (17) tənliyindən T və p-yə görə törəmə alaq.

$$T\left(\frac{\partial^2\upsilon}{\partial T^2}\right)+\left[T\left(\frac{\partial^2\upsilon}{\partial T\partial p}\right)-2\left(\frac{\partial\upsilon}{\partial p}\right)_T\right]\left(\frac{\partial p}{\partial T}\right)_{inv}=0 \quad (27)$$

İnversiya əyrisinin maksimum şərtinə görə $\left(\frac{\partial p}{\partial T}\right)_{inv}=0$; deməli $\left(\frac{\partial^2\upsilon}{\partial T^2}\right)$ da sıfır olacaq. Bunu (26) ifadəsində nəzərə alsaq ikinci həddi də sıfır olacaq.

(17) tənliyindən inversiya şərtinə görə $\left(\frac{\partial\upsilon}{\partial T}\right)_p=\frac{\upsilon}{T}$; $\left(\frac{\partial\upsilon}{\partial T}\right)^2=\frac{\upsilon^2}{T^2}$, deməli

$$\frac{2a(\upsilon-3b-2c)}{T(\upsilon+c)^4}=0$$

olar.

Buradan

$$\upsilon_{max}=3b+2c=\upsilon_k. \quad (28)$$

T_{max} temperaturunu tapmaq üçün (18) tənliyindən istifadə edək. Tənliyin ikinci həddini (4) tənliyindən alaq

$$\upsilon\left(\frac{\partial p}{\partial\upsilon}\right)_T=-\frac{RT\upsilon}{(\upsilon-b)^2}+\frac{2a\upsilon}{T(\upsilon+c)^3}. \quad (29)$$

(18) tənliyinin birinci həddini (2) tənliyini $\upsilon=const$ şərtində differensialladıqda almaq olar

$$T\left(\frac{\partial p}{\partial T}\right)_\upsilon=\frac{RT}{\upsilon-b}+\frac{a}{T(\upsilon+c)^2}. \quad (30)$$

Onda

$$T\left(\frac{\partial p}{\partial T}\right)_\upsilon+\upsilon\left(\frac{\partial p}{\partial\upsilon}\right)_T=\frac{-RTb}{(\upsilon-b)^2}+\frac{a(3\upsilon+c)}{T(\upsilon+c)^3}=0.$$

Buradan

$$T_{\max}^2=\frac{4a(9b+7c)}{27Rb(b+c)}=T_k^2\,\frac{9b+7c}{2b}.$$

Belləiklə,

$$T_{\max}=\sqrt{\frac{9b+7c}{2b}}\cdot T_k \quad (31)$$

Maksimal təzyiqi (20) tənliyindən almaq olar

$$-pbT(\upsilon+c)^3+a(3\upsilon^2-4\upsilon b+\upsilon c-2bc)=0,$$

$$p_{\max}=\frac{a\left(3\upsilon_{\max}^2-4\upsilon_{\max}b+\upsilon_{\max}c-2bc\right)}{bT_{\max}(\upsilon_{\max}+c)^3}.$$

T_{max} və υ_{max}-un qiymətlərini yerinə yazsaq alarıq

$$p_{\max}=\frac{2p_k}{3b}(15b+14c)\sqrt{\frac{9b}{2(9b+7c)}}\approx 7{,}1p_k\left(1+\frac{c}{b}\right)\sqrt{\frac{9b}{9b+7c}}. \quad (32)$$

υ_{max}, T_{max} və p_{max}-u bilərək z_{max}-u təyin etmək olar

$$z_{\max} = \frac{p_{\max} \cdot \upsilon_{\max}}{RT_{\max}} = \frac{(15b + 14c)(3b + 2c)}{4(b + c)(9b + 7c)} . \qquad (33)$$

[1] V.A. Kirillin, V.V. Sıçev, A.E. Şeyndlin. Texniçeskaya termodinamika. M.: Enerqiya. 1968. 472 s. (Rusca).
[2] E.E. Şpilrayn, P.M. Kesselman. Osnovı teorii teplofiziçeskix svoystv veşşestv. M.: Enerqiya. 1977. 248 s. (Rusca).
[3] S.O. Hüseynov, Y.M.Naziyev. Termodinamika (axının termodinamikası). Bakı. AzPİ. 1981. 53 s.
[4] Obzorı po teplofiziçeskim svoystvam veşşestv. M.: İVTAN. 1986. №1, 57, 127 s. (Rusca).

Дж.Я. Назиев

О ДРОССЕЛИРОВАНИИ РЕАЛЬНЫХ ГАЗОВ

В статье рассмотрено дросселирование реальных газов, подчиняющихся уравнению Клаузиуса. Определены критические параметры газа и максимальные параметры кривой инверсии.

J.Y. Naziyev

ON THROTTLİNG OF REAL GASES

The throttling of real gases, submitted to Klauzius equation is considered in the given paper. The critical gas parameters and maximal parameters of inversion curve are defined.

Received: 16.09.06

CRITERION OF THE CONTROL OF EXPERIMENTAL DATA

E.M. FARHADZADEH, A.Z. MURADALIYEV, Y.Z. FARZALIYEV
Azerbaijan Scientific-Research and Design-Prospecting Institute of Energetic
Zardabi ave., 94

The cases are frequent, when at check of the assumption about expediency of classification of the experimental data to the given attribute it appears, that the results application of the appropriate criteria are opposite. The method of an estimation of a mistake the second sort for the data on duration of condition power block electrical station and method of comparison of a number of criteria is resulted.

There is enough often results of passive or active experiment appear connected with a number of attributes which versions can be submitted by a discrete number of values. Display of these versions casually also does not depend on the experimenter. The importance of attributes and their versions at the best is clear at an intuitive level. Classification of the data on the set versions of attributes results in sharp decrease in number of the data of experiment and is connected to an opportunity of fallacies and wrong decisions. The method below is resulted, allowing to avoid the specified mistakes. We shall enter some concepts. We shall present the data of experiment as some set of results of measurement of concrete parameter (P) and we shall designate it through $\{P\}_M$, where M - number of experiments. But the data with preset values of versions of attributes we shall present as sample and we shall designate through $\{P\}_m$, where m - number of the data of sample

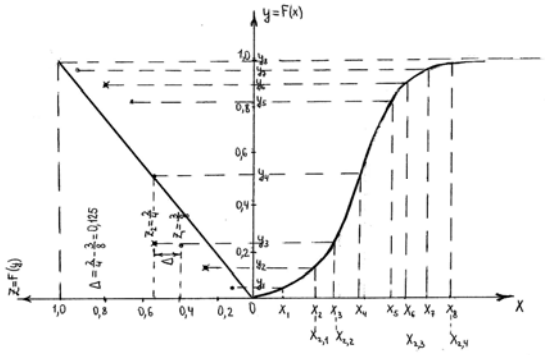

Fig. 1. A graphic illustration of consecutive calculation of statistics Δ_m for hypothesis H_1.

In [1] the new criterion of the control of imposing appearance of sample (if sample is representative an attribute of classification of the data insignificant) Δ_m, describing the maximal value of a divergence of sample and a data set and its updating - factor of imposing appearance of sample K_{II}, describing average quadratic value of a divergence of distributions and Δ_{cp}, describing average value of divergences has been offered. Being analogues of Smirnov's nonparametric criterion $D_{m.n}$ [2], they had and the certain advantages among discrete values of sizes of divergences that reduced an interval between probabilities of adjacent values of the possible divergences, an including significance value α.

Application of one of the criteria marked above demands development of methodology of their automated comparison, including development of methodology of an estimation of distributions of the criteria Δ_m, K_{II}, Δ_{cp} and $D_{m.n}$ provided that sample is not present. To distinguish distributions at hypotheses H_0 and H_1 we shall agree to represent them as $F^*(\Delta_m/H_0)$, $F^*(K_{II}/H_0)$, $F^*(\Delta_{cp}/H_0)$ and $F^*(\Delta_{mn}/H_0)$, $F^*(K_{II}/H_1)$, $F^*(\Delta_{cp}/H_1)$, $F^*(\Delta_{mn}/H_1)$.

The graphic illustration of consecutive calculation of statistics Δ_m for hypothesis H_1 is resulted on fig. 1. for m=4 and M=10

It is accepted, that sample is $\{X_{2,i}\}_m$, the random variables supplementing sample up to set is $\{X_{1,i}\}_n$, and set of random variables are $\{X_i\}_M$.

From fig. 1 it is evidently visible, that at calculation Δ_m for hypothesis H_1 biunique conformity between members of variations lines of random variables of set $\{X_i\}_M$ and members of variations lines $Y_j=F(X_i)_M$ is broken. For example, to the fifth member of lines $\{X_i\}_M$ there corresponds the seventh member of lines $\{Y_j\}_M$. Hence, *property of nonparametric (independence of criteria Δ_m , K_{II} , Δ_{cp} and $D_{m,n}$ from type of distributions $F_m(X)$ and $F_n(X)$) at check of hypothesis H_1 considered criteria lose).* Change of the law of distribution $F_m(x)$ and $F_n(x)$ is reflected in absolute size of each criterion. However, at any distributions $F_m(x)$ and $Fn(x)$ parity of each of N realizations of statistic Δ_m, K_{II} and Δ_{cp} and $D_{m.n}$ remains constant, namely $D_{m,n}>\Delta_m >K_{II}>\Delta_{cp}$ Therefore change $F_m(x)$ and $F_n(x)$ will not influence result of comparison of these criteria.

On fig. 2 experimental dependences of distributions of the statistics Δ_m are resulted, allow us estimate character of change of distributions $F(\Delta_m)=\beta(\Delta_m)$ depending on change m and n. As follows from fig. 2 with increase in number of random variables of sample (m) average value Δ_m and an average quadratic deviation $\sigma(\Delta_m)$ will decrease (we compare distributions 1 and 3 fig. 2).

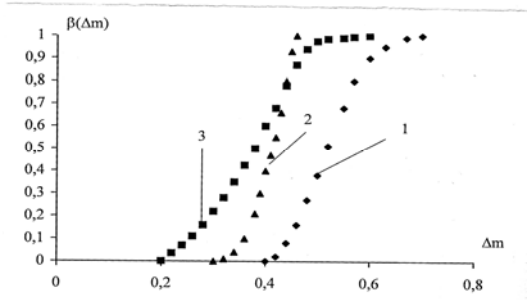

Fig. 2. Distribution of the greatest disorder of distributions $F_m(x)$ and $F_M(x)$ at hypothesis $H_1(\delta$=0,5) 1 - m =10; n =200; 2 - m =10; n =20; 3 - m=50; n=200

Distributions of random variables samples with identical m, taken of sets with differing number of random variables (for example $M_1>>M_2$), will have various $(\Delta_m)_{cp}$ and $\sigma(\Delta_m)$. Than M is more, the $(\Delta_m)_{cp}$ more and $\sigma(\Delta_m)$ less. The increase $\sigma(\Delta_m)$ at reduction of M is caused by growing influence of casual character of distribution $F_M(\tau)$.

Method of comparison of the criteria. As it has been marked above, the preference is given to theories of check of statistical hypotheses to criterion for which at the fixed mistake of the first sort, the mistake of the second sort is

minimal. Hence, to compare criteria it is necessary to compare dependencies $\beta(S) = f[\alpha(S)]$, where S - one of considered (Δ_m, $K_П$, Δ_{cp} and $D_{m,n}$) statistic.

Thus it is necessary to take into account:

1. Discrete character of sizes of the greatest deviation S. Addition α and β also is allowable only on condition α and β that are determined for same value S with i=1, r_Σ where r_Σ - number of identical digitizations of distributions $F^*(S/H_0)$ and $F^*(S/H_1)$.

The size r_Σ is defined:

- number distributions $F^*(S/H_0)$ and $F^*(S/H_1)$ (accordingly r_1 and r_2);

- a parity of boundary values of a confidential interval of average values of statistics S. The overlapping of these intervals is more, the more and r_Σ ;

The certain difficulties at construction $\beta(S) = f[\alpha(S)]$ arise both at small, and at great values m and M. At small values m and M, sizes r_1 and r_2 also are small, $r_\Sigma << r_i$ and $r_\Sigma << r_2$. At great value m and M, despite of essential increase r_1 and r_2, the size r_Σ remains enough small though distinction between separate realizations S does not exceed 1%. The increase r_Σ without decrease in accuracy can be achieved by a method of a rounding off of values of realizations S up to the second significant figure.

2. Features of statistical modeling. One of the basic difficulties at modeling estimations of optimum values of criterion checking to representativenesses of the sample) CRS $\Delta^*_{m,onm}$ is decrease in influence of casual character modeled samples on result of calculation. Fluctuations of numerical values $\Delta^*_{m,onm}$ cause the certain probability of the erroneous decision which, in particular, is more, than it is less number of realizations of sample and depends on number of iterations a little. Overcoming of this difficulty has been achieved as application of some known methods, as a method of the general random numbers together with a method of supplementing random variables [3], and new approaches, in particular:

- applications of criterion of Kolmogorov for the control of conformity programmed random numbers modeled sample to the uniform law "Sorting" samples at a significance value (0,3-0,4) not only reduces a mistake of the second sort, but also carries out protective functions from imperfection of program realizations samples and failures of the COMPUTER.

It is necessary to note, that the further increase in a significance value (more 0,3÷0,4) conducts to essential reduction of number of discrete values Δ_m and absence of identical values Δ_m for distributions [$1-F^*(\Delta_m/H_0)$] and $F^*(\Delta_m/H_1)$.

- elimination of influence of the random variables supplementing sample up to a data set;

- alignment of number of discrete values of distributions $[1 - F^*(\Delta_m / H_o)]$ and $F^*(\Delta_m / H_1)$ by assignment by absent discrete value zero frequency. Application of these methods has allowed to provide high stability of the decision. The control of objectivity of recommended methods was provided with application of a method of the decision of a «return problem».

On fig. 3. experimental dependencies $\beta(S) = f[\alpha(S)]$, for the values marked above m, M and δ for criteria Δ_m, $K_П$, Δ_{cp} and $D_{m,n}$. Similar dependencies are received and for lines of other values m_1, M and δ. The analysis of these data has allowed concluding:

- the least value β at $0<\alpha<1$ takes place for criterion Δ_m;

- values β at $0<\alpha<1$ for criteria $K_П$ and Δ_{cp} also are practically equal and is essentially higher, than at criterion Δ_m. In other words, distinction of distributions $F_m(P)$ and $F_m(P)$ also is defined not so much by average or average quadratic value of deviations, how many the greatest divergence.

- the indirect method of an estimation of representativenesses of sample (Smirnov's criterion) concedes to a direct method recommended authors, i.s. $\beta(D_m)>\beta(\Delta_m)$ at $0<\alpha<1$.

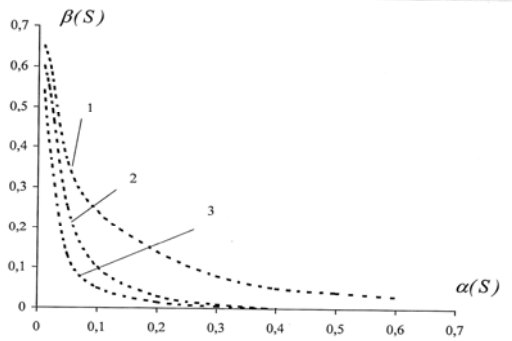

Fig. 3. Curve changes of dependence $\beta(S)=f[\alpha(S)]$ at m =10; M=30 and δ=0,5 for criteria (S): 1- $K_П$ и Δ_{cp}; 2 – $D_{m,n}$; 3 - Δ_m

[1] *B.V. Gnedenko, J.K. Beljaev, A.D. Solovyov*. Mathematician's methods in the theory of reliability. M; "Science", 1965, with 524.

[2] *E.M. Farhadzadeh, A.Z. Muradaliyev, J.Z. Farzaliyev*. Estimation of accuracy of parameters of individual reliability of power units. Ekoenerji №2, 2006.

[3] *I.A. Ryabinin*. Bases of the theory and calculation of reliability of ship power systems. L., "Shipbuilding", 1971.

[4] *J. Kleynen*. Statistical methods in imitating modeling. M.: "Statistics", 1978, 224 with.

Э.М. Фархадзаде, А.З. Мурадалиев, Ю.З. Фарзалиев

КРИТЕРИЙ КОНТРОЛЯ ЭКСПЕРИМЕНТАЛЬНЫХ ДАННЫХ

При проверке предположения о целесообразности классификации экспериментальных данных по заданному признаку результаты применения соответствующих критериев часто оказываются противоположными. Приводится метод оценки ошибки второго рода и метод сопоставления критериев.

E.M. Fərhadzadə, A.Z. Muradəliyev, Y.Z. Fərzəliyev

TƏCRÜBİ VERİLƏNLƏRİN YOXLANMASI KRİTERİYALARI

Verilən əlamətlərə görə təcrübi verilənlərin təsnifatlarının məqsədəuyğunluğu haqqında olan gümanın yoxlanması zamanı uyğun kriteriyaların tətbiqi nəticələrə çox zaman əks olur. Bunun üçün aşağıda ikinci növ səhvlərin qiymətləndirilməsi və kriteriyalarının müqayisəsi üsulları göstərilir.

Received: 08.07.06

ON ONE GENERALIZATION OF BOUGER – BEER LAW ON THE BASIS OF NEW INVARIANT PARAMETER OF SOLAR SPECTRAL IRRADIATION. APPLICATION FOR CALIBRATION OF GROUND SOLAR PHOTOMETERS

H.H. ASADOV, M.M. ALIYEV, E.S. ABBASZADEH
Azerbaijan National Aerospace Agency,
Azadlig ave., AZ-1033, Baku, Azerbaijan

In the given paper the possibility of introduction of invariant indexes of sun spectral radiation, obtained in the result of the summarizing of Bouger-Beer law for the case of three-wave atmosphere measurements has been considered. It is shown, that calibration of three-wave photometer on proposed invariant allows us to eliminate the influence of atmosphere parameter changeability on wave length.

The solar energy is the main source of energy for biosphere of the Earth. It directly controls the atmospheric and oceanic circulations and climate. The proper understanding of this energy is essential for true assessment of processes taken place in the system Earth – atmosphere. Historically, prior the satellite measurements the total solar energy calculated for average value of distance between the Sun and the Earth was considered as "Solar Constant". The systematic ground measurements of variations of solar constant are carried out during more than one hundred years, on Program of Solar Constant of Smithsonian Astrophysical Observatory [1]. At the basis of multi-number experimental researches, including satellite measurements of "Solar Constant", at present time existing prevailing scientific opinion states that only satellite measurements are really capable to detect the variations of solar constant, linked with magnetic activity of the Sun, for example, 11 years, 27 days and other cycles of variation [2].

At the same time methods and equipment for ground atmospheric measurements suffered great changes and modifications. The world-wide network AERONET was specially organized to carry out dynamic components of atmosphere [3]. The possibility of obtaining components extra-atmospheric data from satellites and synchronous data from ground networks allows us to carry out direct comparison of them to determine adequacy of ground measurements of solar constant. Results of one of such researches are described in [2] where comparison of synchronous measurements is carried out. These data were obtained from the instrument SOLSTICE installed in satellite UARS and AERONET network photometers beginning from January 1, 1998 till October 28, 1999.

As a result of held research it was revealed, that measured by instrument SOLSTICE the variation of solar-spectral radiation, determined as standard deviation divided to average value was equal to 0.12 % and 0.14 % in wavelength 340 nm and 380 nm.

But variations of ground measurements in aforementioned wavelengths were equal to 2,0 % and 1,8 %. These values of variation are more than one order in comparison with values of variation of solar irradiation measured by help of satellite instruments SOLSTICE. On the basis of aforesaid data it was concluded, that ground measurements cannot be used for research of variability of solar constant. Such a dubious conclusion is dangerous, because it rejects any possibility of calibration of ground photometer using solar irradiation. This conclusion is justified by such a wrong suggestion, that variability of atmosphere cannot be removed from results of ground measurements. The purpose of this article is demonstration of fallibility of such opinions on an example of recently proposed three-wave lengths technology of atmospheric measurements [4, 5].

As it was noted earlier, the accuracy of ground methods of determination of the solar constant is mainly depends on variability of atmosphere.

Further in this article we shall speak about UV band and mentioning the variability of atmosphere or optical depth of atmosphere we shall consider not temporal changes, but changes on wavelength of measurements. It is well-known, that one of major parameters of variability of random processes is autocorrelation function. For example, the changeability of function $\tau_A = f(\lambda, t)$, where τ_A - optical depth of atmosphere; λ - wavelength; t - time parameter of current measurements, can be characterized by following two – measured autocorrelation function:

$$R_\tau(\Delta\lambda, \Delta t) = \frac{1}{B(\tau)} \int_0^{\Delta\lambda_{max}} \int_0^{\Delta t_{max}} \tau(\lambda + \Delta\lambda; t + \Delta t) \cdot \tau(\lambda; t) d(\Delta\lambda) d(\Delta t). \quad (1)$$

At present, there are many sources, where the data on correlation dependence of optical depth of atmosphere separately on time and wavelength of measurements are given. For example, the results of atmospheric variability research in UV band are given [6]. These results are obtained on the basis of 19,568 measurements of direct solar irradiation carried out in Riverside site and similar series of measurements, by number of 21,972 measurements carried out in Mt. Wilson site.

The computed valued of correlation indices for all pairs of wavelength are shown in Table 1[6]. It is shown, that Riverside site is characterized with strong correlation between results of measurements in all wavelengths. For the Mt. Wilson site, the correlation indices are slightly weak.

Table 1

Riverside	306 nm	312 nm	318 nm	326 nm	333 nm	368 nm
300 nm	0,99	0,97	0,93	0,94	0,92	0,92
306 nm		0,99	0,95	0,97	0,95	0,95
312 nm			0,97	0,99	0,97	0,97
318 nm				0,99	1,00	0,99
326 nm					1,00	0,99
333 nm						1,00
Mt. Wilson	306 nm	312 nm	318 nm	326 nm	333 nm	368 nm
300 nm	0,94	0,85	0,76	0,69	0,62	0,59
306 nm		0,92	0,85	0,82	0,77	0,74
312 nm			0,98	0,96	0,93	0,91
318 nm				0,98	0,96	0,95
326 nm					0,99	0,98
333 nm						1,00

Thus, the results of research described in [6] have shown, that autocorrelation function (1) of optical depth of atmosphere, calculated on wavelength,

$$R_{\tau}(\Delta\lambda)=\frac{1}{B(\tau)}\int_{0}^{\Delta\lambda_{max}}\tau(\lambda+\Delta\lambda;t)\cdot\tau(\lambda,t)d(\Delta\lambda) \quad (2)$$

has a positive and higher values. Physically, it may be explained by such a fact, that the optical depth of atmosphere in UV band is mainly formed with aerosol and ozone, the quantitative and qualitative parameters of which are not changing during the short period of measurements.

It should be noted, that this phenomenon is rightful also for atmospheric measurements on horizontal route. For example as it is shown in [7], the higher correlation values exist for results of measurements of optical depth of aerosol in UV and visible bands carried out in on-earth layer of atmosphere.

According to the method of Langly plots, each deviation of measured value of solar constant is directly determined with deviation of optical depth of atmosphere, if optical mass is constant. From well-known formula of Bouger-Beer one can obtain following equation, which is basis of Langly plot method:

$$ln\,I_0 = m\,\tau_{\Sigma} + ln\,I\,, \quad (3)$$

where I_0 - «Solar constant»; m - optical mass; τ_{Σ} - total optical depth of atmosphere; I - the measured value of solar spectral irradiation.

It is obvious, that upon condition of stability of solar constant, $m=const$, and stability of parameters of ground photometer, each differed from zero measured value of $\frac{d\,ln\,I_0}{d\,\lambda}$ is caused by differed from zero value $\frac{d\,\tau_{\Sigma}}{d\,\lambda}$.

The presence of strong correlation in values of τ_{Σ} on λ leads to strong correlation of $ln\,I_0$ on λ, i.e. there is the error of measurement of I_0, depending from λ, which is caused by variation of τ_{Σ}. Therefore, the error of ground measurements of I_0 in comparison with the satellite measurements has a systematic feature and depends on λ.

But if we by modification of method of ground measurements, can succeed to generalize the relevant form of equation of Bouger-Beer, writing it in following form

$$P(I)=P(I_0)\cdot e^{-mP(\tau_{\Sigma})}, \quad (4)$$

where $P(I)$ - generalized parameter of solar-spectral irradiation, measured at the level of the Earth; $P(I_0)$ - the generalized parameter of solar-spectral irradiation at the external border of atmosphere; $P(\tau_{\Sigma})$ - the generalized parameter of optical depth of atmosphere, meeting the following conditions

$$\frac{dP(\tau_{\Sigma})}{d\,\lambda}=0 \quad (5a)$$

$$P(\tau_{\Sigma})=0\,, \quad (5b)$$

and consequently, following conditions

$$\frac{dP(I)}{d\,\lambda}=0 \quad (6a)$$

$$\frac{dP(I_0)}{d\,\lambda}=0\,, \quad (6b)$$

while any variation of I_0 due to variation of magnetic activity of the Sun is lacking, we could, in principle, succeed to carry out ground measurements of parameter of solar-spectral radiation, where the obtained result would not depend on variation of λ.

It can be shown, that as a result of application of recently proposed 3 wavelength technology of atmospheric measurements, we can formulate the generalized parameters $P(\tau_{\Sigma}); P(I)$ and $P(I)$, and in this case, the equation of Bouger-Beer may be generalized in the form of (4).

By the aim to form the generalized parameter of optical depth of atmosphere and generalized parameter of solar constant, we describe in brief the main provisions of method of three-wave lengths measurements. Let us assume, that there are wavelengths λ_1, λ_2 and λ_3, where $\lambda_1 < \lambda_2 < \lambda_3$ and we carry out following measurements

$$\left.\begin{aligned} I(\lambda_1) &= I_0(\lambda_1)\cdot e^{-m_1\tau(\lambda_1)} \\ I(\lambda_2) &= I_0(\lambda_2)\cdot e^{-m_1\tau(\lambda_2)} \\ I(\lambda_3) &= I_0(\lambda_3)\cdot e^{-m_1\tau(\lambda_3)} \end{aligned}\right\}. \qquad (7)$$

Now we should calculate generalized parameter $P(I)$ as follows:

$$P(I) = \frac{\sqrt[\chi]{I(\lambda_1)\cdot I(\lambda_3)}}{I(\lambda_2)}. \qquad (8)$$

Taking into account (7) and (8) we have following generalized form of writing of Bouger-Beer law

$$P(I) = \frac{\sqrt[\chi]{I(\lambda_1)\cdot I(\lambda_3)}}{I(\lambda_2)}\cdot e^{-m\left[\frac{\tau(\lambda_1)+\tau(\lambda_3)}{\chi}-\tau(\lambda_2)\right]}. \qquad (9)$$

Therefore, the generalized parameter of solar constant in (9) may be written as

$$P(I_0) = \frac{\sqrt[\chi]{I_0(\lambda_1)\cdot I_0(\lambda_3)}}{I_0(\lambda_2)}. \qquad (10)$$

The generalized parameter of optical depth of atmosphere may be written as

$$P(\tau) = \frac{\tau(\lambda_1)+\tau(\lambda_3)}{\chi} - \tau(\lambda_2). \qquad (11)$$

From the equation (11) it is obvious, that if by proper selection of $\lambda_1, \lambda_2, \lambda_3$ and χ we could ensure following conditions

$$P(\tau) = 0 \qquad (12a)$$

and

$$\frac{dP(\tau)}{d\lambda} = 0 \qquad (12b)$$

then the measured value of *Z* will be equal to generalized solar constant's parameter $\frac{\sqrt[\chi]{I_0(\lambda_1)\cdot I_0(\lambda_3)}}{I_0(\lambda_2)}$, which will not depend on wavelength.

Therefore, equations (12a) and (12b) are conditions for ensuring of accurate ground measurements of value of generalized solar constant (10).

From conditions (12a) and (12b) we have

$$\chi = \frac{\tau(\lambda_1)+\tau(\lambda_3)}{\tau(\lambda_2)}. \qquad (13)$$

As it is shown in [5] 2 variants of realization of equation (13) are possible.

1) We should select $\chi = 2$; Wavelengths λ_1 and λ_3 are fixed; and wavelength λ_2 should be chosen using following formula

$$\tau(\lambda_2) = \frac{\tau(\lambda_1)+\tau(\lambda_3)}{2}. \qquad (14)$$

2) The wavelengths $\lambda_1, \lambda_2, \lambda_3$ are fixed. The index χ should be chosen using equation (13).

In line with (12b) following condition should be met (if $\chi = 2$)

$$dP(\tau) = 0$$

or

$$\Delta P(\tau) = 0$$

or

$$\frac{\Delta\tau(\lambda_1)+\Delta\tau(\lambda_3)}{2} = \Delta\tau(\lambda_2). \qquad (15)$$

For example, it easily can be shown that in small interval $\Delta\lambda = \lambda_1 \div \lambda_3$, upon linear approximation of dependence $\tau = \tau(\lambda) = k\lambda$, the conditions (14) and (15) easily may be met.

Therefore, we may conclude that the invariant of spectral solar radiation (10) exists and this invariant not depends on wavelength.

Wavelengths $\lambda_1, \lambda_2, \lambda_3$ may be chosen using conditions (12a) and (12b).

The practical value of the proposed invariant is linked with necessity initial calibration of ground measurement systems on extra-atmospheric sources.

As it is noted in [6], the satellite means of measurements are calibrated using stable UV irradiation of blue stellar. Calibration of ground meters on Sun irradiation using previous methods turned out impossible due to influence of variability of atmosphere. In this situation the suggested three-wavelengths invariant should be applied.

The single instrument to be chosen in this case should be the previously suggested [4, 5] three-wavelengths meters, the application of which will open the era in the theory and practice of ground atmospheric measurements.

[1] *D.V. Hoyt* The Smithonian astrophysical observatory solar constant program, Rev. Geophys. Space Phys., 17, 427-458, 1979.

[2] *G. Wen, R.F. Cahalan, B.N. Holben*. Limitations of ground based solar irradiance estimates due to atmospheric variations. Journal of Geophysical Research, v. 108, No. D14, 4400.

[3] *B.N. Holben et. al.* AERONET: A federated instrument network and data archive for aerosol characterization. Remote Sensing Environment, 66, 1-16, 1998.
[4] *H.H. Asadov, A.A. Isayev.* Proc. XX Quadrennial ozone symp. – Kos (Greece), 2004, v. 1, p. 477.
[5] *H.H. Asadov, A.A. Isayev.* Common theory of three-wavelengths ozonometric measurements. Izmeritelnaya tekhnika, 2005, No. 8, p. 66-68.
[6] *L. Vuillenmier, R.A. Harley, N.J. Brown, J.R. Slusser, D. Kolinski, D.S. Bigelow.* Variability in ultraviolet total optical depth during the Southern California Ozone Study. Atmospheric Environment 35 (2001), 1111 – 1122.
[7] Optical properties of coastial atmospheric have. Edited: *G.K. Grekov*. Novosibirsk. 1988.

H.H. Əsədov, M.M. Əliyev, E.S. Abbaszadə

GÜNƏŞİN SPEKTRAL ŞÜALANMASININ YENİ İNVARİANT PARAMETRİ ƏSASINDA BUGER-BER QANUNUNUN BİR ÜMUMİLƏŞDİRİLMƏSİ BARƏDƏ. YERÜSTÜ GÜNƏŞ FOTOMETRLƏRİNİN KALİBRASİYASINDA TƏTBİQİ

Məqalədə göstərilmişdir ki, atmosfer dəyişiklikləri ilə əlaqədar olaraq yerüstü ölçmə vasitələri ilə Günəş şüalanmasında olan dəyişikliklərin müşahidə edilə bilməsinin qeyri-mümkünlüyü barədə qərarlaşmış elmi rəyə baxmayaraq, əvvəllər təklif edilmiş üç dalğa uzunluqlu ölçmə metodu və müvafiq qurğunun kalibrasiyası üçün Buger-Beer qanununun təklif edilmiş ümumiləş-dirilməsindən alınan Günəş spektral şüalanmasının yeni invariantı tətbiq edildiyi halda bu cür müşahidələr mümkündür.

Г.Г. Асадов, М.М. Алиев, Е.С. Аббасзаде

О ВОЗМОЖНОСТИ КАЛИБРОВКИ НАЗЕМНЫХ СОЛНЕЧНЫХ ФОТОМЕТРОВ С ПОМОЩЬЮ ИНВАРИАНТНОГО ПОКАЗАТЕЛЯ СОЛНЕЧНОЙ СПЕКТРАЛЬНОЙ РАДИАЦИИ

В данной статье рассмотрена возможность введения инвариантного показателя солнечной спектральной радиации, полученной в результате обобщения закона Бугера-Бера для случая трехволновых атмосферных измерений. Показано, что калибровка трех-волновых фотометров по предложенному инварианту позволяет устранить влияние изменчивости параметров атмосферы по длине волны.

Received: 02.06.06

THE TRANSMISSION OF LIGHT THROUGH A LOW-ABSORBING THIN COATING

R.A. KARAMALIYEV
Baku State University, AZ1148, Baku, Azerbaijan, Z. Khalilov str., 23

R.M. KASIMOV
Institute of Chemical problems of National Academy of Sciences, AZ1143, Baku, Azerbaijan, H.Javid av., 29

The transmission of light waves through a low- absorbing dielectric thin coating on semi-infinite dielectric substrate is considered. It is shown that in this system under certain conditions may be realized the effect of antireflection of light. Expressions for selective thin film thickness and wavelengths in which occur non-reflective absorption and transmission of light have been obtained.

The theory of optical design of multilayers is quite complex and tedious, and has been presented for some simple cases [1-3]. For microwave region of spectrum the effect of reflectionless absorption in layered medium both theoretically and experimentally was investigated in [4, 5]. This method of investigation was extended to include optical wavelengths in [6].

In this paper, we have presented the approximative method for calculating transmittance, reflectance and absorptance of optical waves by low – absorbing dielectric coating. We start by considering the reflection and transmission of light in an absorbing dielectric film on semi-infinite non-absorbing dielectric substrate. Incident light is considered normally and plane polarized. In order to find expressions for the reflectance and transmittance of a dielectric film illuminated by a parallel beam of light at wavelength λ, we must consider the multiple reflections of light at each surface of the film and perform a multiple beam summation. Thus, reflected and transmitted complex amplitudes are given by [2]

$$\tilde{R} = \frac{\tilde{r}_1 + \tilde{r}_2 e^{-2ikl}}{1 + \tilde{r}_1\tilde{r}_2 e^{-2ikl}} \quad , \qquad \tilde{T} = \frac{\tilde{t}_1\tilde{t}_2 e^{-ikl}}{1 + \tilde{r}_1\tilde{r}_2 e^{-2ikl}} , \tag{1}$$

where $\tilde{r}_1 = r_1 e^{i\varphi_1}$; $\tilde{r}_2 = r_2 e^{i\varphi_2}$; $r_1, r_2, \varphi_1, \varphi_2$ are complex amplitudes, modules and phases of reflection coefficients, respectively, κ is complex wave number. In these equations the subscripts 1and 2 refer to the first and second surface of the layer. The layer is assumed to be plane and parallel sided of thickness *l* and complex refractive index $\tilde{n}$ and is bounded by semi-infinite layers of indices 1 and n_1.

The Fresnel coefficients of reflection and transmission are

$$\tilde{r}_1 = \frac{1-\tilde{n}}{1+\tilde{n}}, \quad \tilde{r}_2 = \frac{\tilde{n}-n_1}{\tilde{n}+n_1}, \quad \tilde{t}_1 = \frac{2}{1+\tilde{n}}, \quad \tilde{t}_2 = \frac{2\tilde{n}}{n_1+\tilde{n}} \tag{2}$$

In formula (1), propagation constant k of the wave traveling in the covering material is

$$\kappa = \frac{2\pi}{\lambda}\left(n - i\chi\right) = \frac{2\pi}{\lambda_d}(1 - iy) \tag{3}$$

where $\lambda_d = \lambda/n$, $y = \chi/n$, n is the refractive index of the layer material, χ is the extinction coefficient of the material.

For the considered layered structures modules and phases of reflection coefficients are given by the well-known relations

$$r_1 = \sqrt{\frac{(1-n)^2 + \chi^2}{(1+n)^2 + \chi^2}} \quad , \qquad \varphi_1 = arctg\frac{2\chi}{1-n^2-\chi^2}$$
$$r_2 = \sqrt{\frac{(n-n_1)^2 + \chi^2}{(n+n_1)^2 + \chi^2}} \quad , \qquad \varphi_2 = arctg\frac{2n_1\chi}{n_1^2-n^2-\chi^2} \tag{4}$$

Let introduce $x = l/\lambda_d$ .The expressions for energy reflectance and transmittance may be obtained from equation (1)

$$R^2 = \frac{\left(r_1 - r_2 e^{-4\pi xy}\right)^2 + 4r_1 r_2 e^{-4\pi xy}\cos^2\left(2\pi x + \frac{\varphi_1 - \varphi_2}{2}\right)}{\left(1 - r_1 r_2 e^{-4\pi xy}\right)^2 + 4r_1 r_2 e^{-4\pi xy}\cos^2\left(2\pi x - \frac{\varphi_1 + \varphi_2}{2}\right)} \tag{5}$$

$$T^2 = \frac{(1-r_1)(1-r_2)e^{-4\pi xy}}{\left(1-r_1 r_2 e^{-4\pi xy}\right)^2 + 4r_1 r_2 e^{-4\pi xy}\cos^2\left(2\pi x - \frac{\varphi_1+\varphi_2}{2}\right)} \qquad (6)$$

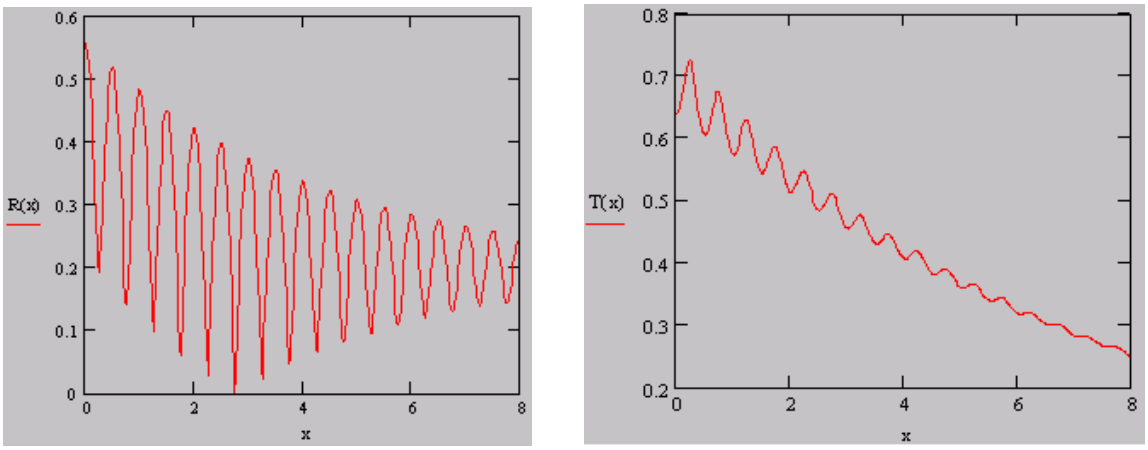

Fig.1. Absolute values of reflection *R(x)* and transmission *T(x)* coefficients .vs. thickness of the covering material in the two-layer dielectric-dielectric structure: r_1=0.2; r_2=0.4; n=1.5; y=0.02.

Fig.1 represents dependence of reflection coefficient amplitude R and transmission coefficient amplitude *T* on absorbing layer thickness when the coating is low-absorbing. One can see that these coefficients have damping oscillations. Thus, a standing of extremes of curves $R(l)$ are realized at thickness of an absorbing layer of distinct from quantities of multiple $\lambda_d/4$.There are two regions in the $R(l)$ dependence which differ by character of changing of extrema in increasing of thickness of the layer. The lower absorption coefficient is the higher the number of minimum which takes place without reflection.

It is well – known that in its simplest form (when $\chi = 0$) anti- reflecting coating is homogeneous, its thickness is a quarter wavelength and its refractive index equals the geometric mean of the indices of the two adjoining media:

$$n = \sqrt{n_1} \qquad (7)$$

In this connection we shall introduce the suggestion that the specified zero minimum of function $R(l)$ is realized at thickness of a layer of the substance a little differing from quantities of multiple $\lambda_d/4$

$$x = \frac{2N-1}{4} + \Delta \qquad (8)$$

where N is ordinal number of the zeroth minimum of function $R(l)$; Δ is the quantity to be determined by optical parameters of coating material.

Substituting equations (3) and (8) into equation (1), we find

$$\ln\frac{r_2}{r_1} = y\left[\pi(2N-1) + \varphi_2 - \varphi_1\right] \qquad (9)$$

$$\frac{l}{\lambda} = \frac{1}{n}\left(\frac{2N-1}{4} + \frac{\varphi_2-\varphi_1}{4\pi}\right) \qquad (10)$$

$$\Delta = \frac{\varphi_2-\varphi_1}{4\pi} \qquad (11)$$

Equations (8)- (11) allow functional relation between incident light wavelength λ, layer thicknees l and its optical parameters n and χ, for to arise reflectionlees absorption in the coating.

According to dispersion theory of light the real and imaginary parts of dielectric constant may be expressed as [2]

$$n^2 - \chi^2 = n_\infty^2 + \frac{4\pi N_0 q^2}{m}\frac{\omega_1^2-\omega^2}{\left(\omega_1^2-\omega^2\right)^2+\gamma^2\omega^2}\ ;\quad 2n\chi = \frac{4\pi N_0 q^2}{m}\frac{\gamma\omega}{\left(\omega_1^2-\omega^2\right)^2+\gamma^2\omega^2} \qquad (12)$$

where n_∞ is refractive index far from the resonance; q, m are charge and mass of electron, N_0 is concentration, γ is damping coefficient, ω is frequency. Resonance frequency ω_1 according to Lorentzs field in condensed matter may be expressed by frequency ω_0 and concentration

$$\omega_1^2 = \omega_0^2 - \frac{4\pi N_0 q^2}{m} \qquad (13)$$

It is easy in the first approximation from (12) to have the relation between n and χ

$$\left(n - n_\infty\right)^2 + \left(\chi - d\right)^2 = d^2 \qquad (14)$$

where

$$d = \frac{\pi N_0 q^2}{m\gamma\omega_1 n_\infty} \qquad (15)$$

Solution of equations (9) and (14) allows us to find optical parameters of absorbing dielectric layer.

To determine the frequency which the effect of reflectionless absorption takes place may be used next equation

$$\frac{\chi}{n - n_\infty} = \frac{\gamma}{2(\omega_1 - \omega)} \qquad (16)$$

We have been presented basic expressions to solve the problem of reflection and transmission in absorbing coating. But in learn this problem by practice often we deal with low – absorbing layers $\left(\chi << n\right)$ when $\chi << n$ from equations (4) may be obtained

$$r_1 = \frac{n-1}{n+1}, r_2 = \frac{n_1 - n}{n_1 + n}; \varphi_2 - \varphi_1 = \frac{2n_1\chi}{n_1^2 - n^2 - \chi^2} - \frac{2\chi}{1 - n^2 - \chi^2} \qquad (17)$$

From equations (9) and (17) in the first approximation one can obtain the next relation

$$\chi = \frac{1}{\pi\left(2N-1\right)} \frac{2n\left(n_1 - n^2\right)}{\left(n-1\right)\left(n+n_1\right)} \qquad (18)$$

Combined solution of equations (4) and (18) allows us to determine selective quantities of n and χ for low – absorbing dielectric layer.

In Fig.2 the dependence of selective values of χ on n calculated from equation (18) for low-absorbing dielectric thin film applied on dielectric substrate is presented. There also is given the dependence between χ and n for rhodamine layer with concentration of dye molecules $N_0 = 6.10^{21} cm^{-3}$. The crossing points of straight lines and circle allow to find selective values of n and χ. Then using equations (16) and (8) we have calculated selective wavelength λ_0 and thickness of coating l_0, respectively. The results of these calculations are given in Table. One can see from Table the values of n and χ of coating for given N and appropriate values of λ_0 and l_0 for to realise the effect of antireflection of light.

The energy absorbed in low – absorbing layer in the reflectionless absorption may be expressed by

$$W = 1 - n_1 \left|\tilde{T}\right|^2 = n_1 \sqrt{\frac{(1-n^2)^2 + 2\chi^2(1+n^2)}{(n_1^2 - n^2)^2 + 2\chi^2(n_1^2 + n^2)}} \qquad (19)$$

Optical parameters n_1, n and χ in (19) are quantities which satisfied condition of reflectionless absorption and related in equation (9).

The reflection and transmission of light by absorbing two-layer dielectric- dielectric structure is theoretically considered. Expressions for selective layer thickness and frequencies in which occur reflectionless absorption of light in this system have been obtained. The conditions for to realize anti-reflecting coatings in optical medium with resonance type dispersion have been found.

Propagation of light in low-absorbing layered system has been analyzed. The energy transmitted from low-absorbing layer when reflectionless absorption takes place was calculated.

Table.

Selective values of incident radiation wavelength λ_0, refraction index n, extinction coefficient χ, rhodamine layer thickness l_0 applied on dielectric substrate. N is number of the minimum of curve R; W is absorbed energy in the rhodamine layer. Refraction index of the dielectric substrate $n_1 = 4$.

N	Low-frequency branch					High-frequency branch				
	N	χ	$\lambda_0 \cdot 10^{-5} cm$	$l_0 \cdot 10^{-5} cm$	W	n	χ	$\lambda_0 \cdot 10^{-5} cm$	$l_0 \cdot 10^{-5} cm$	W
1	-	-	-	-	-	-	-	-	-	-
2	1,84	0,05	5,96	2,54	0,24	1,67	0,11	5,35	2,28	0,46
3	1,83	0,03	6,10	4,34	0,26	1,67	0,07	5,19	3,68	0,46
4	1,82	0,02	6,20	6,16	0,27	1,68	0,05	5,17	5,15	0,45
5	1,81	0,02	6,51	8,32	0,28	1,69	0,04	5,09	6,51	0,43

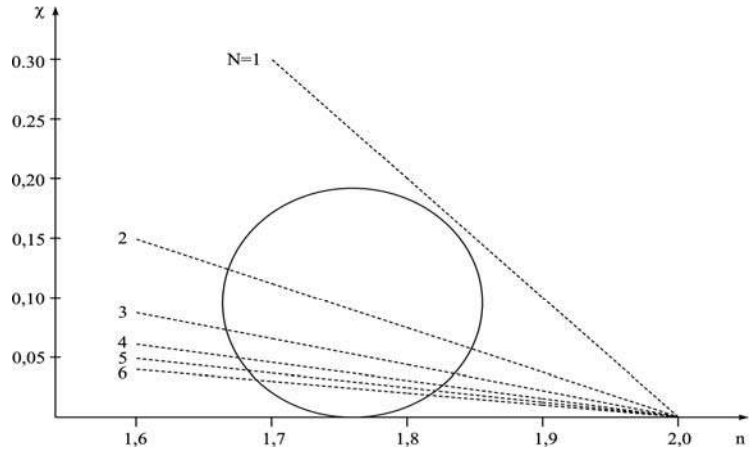

Fig.2. Dependences of extinction coefficient χ on refraction index n of the dielectric thin film:
a) applied on dielectric substrate (-------);
b) according to its resonance type dispersion in the range of optical wavelengths for rhodamine layer with concentration of dye molecules $N_0 = 6.10^{21} cm^{-3}$ (circle).

[1] *L.M. Brehovskih*. Waves in layered media, M., 1957 (Russian).
[2] *M. Born., E. Volf.* Principles of optics, M., 1970.
[3] *A. Yariv., P.Yeh.* Optical waves in crystals, M. 1987.
[4] *R.M.Kasimov, M.A.Kalafi, Ch.O. Kajar, E.R. Kasimov.* J. Engineering - physics, v. 71, 2, 1998, pp. 282 - 285 (Russian).
[5] *R.M. Kasimov, M.A. Kalafi, E.R. Kasimov, etc.* J. Technical physics. v.66, №5, 1996, pp. 167-171 (Russian).
[6] *R.M. Kasimov., R.A. Karamaliyev., V.M. Salmanov* (to be published).
[7] *Juan I . Larruquert*. J. Opt. Soc. Am. A 18, 2001, pp. 2617 – 2627

R.Ə. Kərəməliyev. R.M. Qasımov

İŞIĞIN ZƏİF UDAN NAZİK ÖRTÜKDƏN KEÇMƏSİ

Yarımsonsuz dielektrik səthinə çəkilmiş zəif udan nazik dielektrik örtükdən işıq dalğalarının keçməsinə baxılmışdır. Göstərilmişdir ki, bu sistemdə müəyyən şərtlər ödənildikdə işığın əks olunmadan udulması hadisəsi mümkündür. İşığın əks olunmadan udulması və keçməsinin baş verməsinə uyğun selektiv örtük qalınlıqları və dalğa uzunluqları üçün ifadələr alınmışdır.

Р.А. Карамалиев, Р.М. Касимов

ПРОХОЖДЕНИЕ СВЕТА ЧЕРЕЗ СЛАБОПОГЛОЩАЮЩЕЕ ТОНКОЕ ПОКРЫТИЕ

Рассматривается прохождение световых волн через слабопоглощающее тонкое диэлектрическое покрытие на полубесконечной диэлектрической подложке. Показано, что в этой системе при определенных условиях возможен эффект безотражательного поглощения света. Получены выражения для селективных значений толщины тонкой пленки и длин волн, при которых происходит безотражательное поглощение и прохождение света.

Received: 11.07.06

THE NUCLEUS EXCITATION BY ELECTRON INELASTIC SCATTERING

M.M. MIRABUTALIBOV
Azerbaijan State Oil Academy, AZ-1010, Baku, Azadlig av., 20

It is supposed to describe the dipole resonance with the help of the shell model, and the quadrupole resonance – with the help of the dynamic collective theory with the aim of the explanation of the simultaneous appearance of the giant dipole and quadrupole resonance in nuclei at the inelastic electron scattering in experiment. Moreover, Tassi model is used for the oscillation of the surface of nucleus shell. The matrix element of transition of excited nucleus is calculated in distorted-wave approximation. The form-factors of dipole and quadrupole excitations had been calculated for ^{60}Ni nucleus. The GDR and GQR energies and also deformation parameters at the proton and neutron transition in nucleus are defined.

The inelastic electron scattering on the nuclei at the different energies allows us to study comprehensively angular, energetic, mass and other distribution of particles-products, energy of final nucleus and canals of its decay. The carried out analysis of these large body of data allows to achieve the real information about nucleus construction.

In experimental works on the inelastic electron scattering on the nuclei it is established, that the prominently expressed maximums, which are called as giant dipole, quadrupole and monopole resonances are observed in energetic and angular dependencies of the cross-section of this process. Also resonances of more high multipolarities are observed in some nuclei [1].

The explanations of experiment data on the excitation mainly of giant resonances were carried out in frameworks of half-classis hydrodynamic and shell nuclear models. The join development of both approaches allows us to describe not only formation processes of giant multipole resonances at inelastic electron scattering on nuclei, but the canals of the decay of giant resonances in reactions with the emanation of different particles.

After the appearance of giant resonances, the nucleus is in the strongly excitated state, i.e. the nucleus heats. At the taking away of the introduced excitation in evaporation form, the nucleus emanates the separate nucleons and their combinations. The nucleus with most probability emanates the one nucleon, the nucleus with low probability emanates two and more number nucleons and moreover, the process of nucleus cooling is carried out.

The cross-sections of giant dipole and quadrupole resonances for light and average nuclei are achieved by the sum of emanated neutrons and protons.

The ratio of cross-sections of reactions with nucleon emanations depends on structure of giant dipole resonance (GDR) and giant quadrupole resonance (GQR), i.e. on width, energetic state and resonance amplitude.

Thus, we can conclude, that detail definition of main parameters of GDR and GQR (state, value and form) for different nuclei allows us to do the right choice about decay production of final nucleus.

That's why we use the theory of distorted-wave high-energetic approximation (DHEA), developed in [2] for the inelastic electron scattering on nuclei with the aim of the exact calculation of amplitude of process of inelastic electron scattering on nuclei. The workings out this theory for real type of charge densities show, that this theory works to a high accuracy [3].

For the study of giant resonances the transition matrix element is written in following form [2]:

$$T_{if} = -4\pi e^2 < f\left|\sum_{\alpha=1}^{A}\frac{1-\tau_z}{2}D(\mathbf{x}_\alpha)\rho(\mathbf{x}_\alpha)\ell^{i\mathbf{q}\mathbf{x}_\alpha}d\mathbf{x}_\alpha\right|i> \qquad (1)$$

Here

$$D(\mathbf{x}_\alpha)=\frac{R(\mathbf{x}_\alpha)}{q_{eff}^2(\mathbf{x}_\alpha)}. \qquad (2)$$

For the calculation of (1) the nucleus will be considered as the system, consisting on the nucleon and core. Moreover, nucleon transition on the one from high-excitated states will reveal the effective electric charge, taking under the consideration the relative movement of nucleon with mass m_N, charge $(1-\tau_z)/2$ and radius-vector $\mathbf{x}_1$ and the core with mass $m_N(A-1)$, charge $Z-(1-\tau_z)/2$ and radius-vector $\mathbf{x}_{ост}$, where radius is vector of the inertion center of nucleus is expressed as $\boldsymbol{R}_0=\{\mathbf{x}_1+\mathbf{x}_{0cm}(A-1)\}/A$.

Further, expressed in (1) the coordinates of particles through relative coordinate of particle-shell, we have the possibility to write the transition matrix element in the form of sum of matrix element of single-particle transition

$$T_{if}^{час} = -4\pi e^2 < f\left|\int D(\mathbf{x}')\rho_{час}(\mathbf{x}')\ell^{i\mathbf{q}\mathbf{x}'}d\mathbf{x}'\right|i.> \qquad (3)$$

and transition matrix element of nucleus core -

$$T_{if}^{ocm} = -4\pi e^2 < f\left|\int D(\mathbf{x}'')\rho_{ocm}(\mathbf{x}'')\ell^{i\mathbf{q}\mathbf{x}''}d\mathbf{x}''\right|i> \qquad (4)$$

Where $\mathbf{x}'=\varepsilon_h\mathbf{x}$, $\mathbf{x}''=\varepsilon_{sh}\mathbf{x}$, here $\mathbf{x}=\mathbf{x}_1-\mathbf{x}_{sh}$ defines the relative state of nucleon and core

$$\varepsilon_{час}=\frac{1-\tau_z}{2}\frac{A-1}{A} \qquad (5)$$

-effective charge of nucleon,

$$\varepsilon_{ocm} = (Z - \frac{1-\tau_z}{2})(-\frac{1}{A}) \quad (6)$$

- effective electric charge of nucleus core.
- At the calculation of (3) the wave functions of beginning and final states of nucleons are expressed in the form

$$\frac{1}{2}u_{nlj}(x')\sum_{\mathbf{m}_l m_s} < lm_l \frac{1}{2} m_s \Big| jm > i^l \mathrm{Y}_l(\theta.\varphi)\chi_{1/2}(m_s), \quad (7)$$

which are solutions of Schrödinger equation with oscillated potential.

The Danos and Grainer dynamic collective theory (DCT), joined with Tassi model [2], in which it is supposed, that spherical core surface in excitated state deforms vacillating with the aim of study of giant multipole resonances in excited nucleus core. The elementary excitations, appearing at the movement of protons relatively neutrons, are carried out with the oscillation frequency of surface of nucleus core.

In this theory the total proton (neutron) density are present in the form of sum of equilibrium density and fluctuation density, responsible for transitional part of density, which has the form

$$\rho^{tr}(\mathbf{x}'',t) = \sum_{\lambda\mu} \alpha_{\lambda\mu}(t)\rho_{\lambda\mu}(x'')\mathrm{Y}^*_{\lambda\mu}(\hat{x}''). \quad (8)$$

Here $\alpha_{\lambda\mu}$ is parameter, defining the form of distribution of nucleon density on the surface of nucleus core.

The radial multipole transitional density $\rho_{\lambda\mu}(x'')(\mu = 0)$ has the form [2].

$$\rho_\lambda(x'') = \frac{\nabla_x x''^{\lambda+k_\lambda}}{(\lambda+k_\lambda)c^{\lambda+k_\lambda-2}}\nabla_x^{(\lambda)}\rho_p(x''), \quad (9)$$

where $k_\lambda = 2\delta_{\lambda 0}$

$$\nabla_x^{(\lambda)}\rho_p(x'') = x''^{-3}\nabla_{x''}[x''^3\rho_N(x'')] \quad \lambda = 0$$

$$= \nabla_{x''}\rho_N(x'') \quad \lambda \geq 1. \quad (10)$$

The distribution of nucleon density in nucleus in equilibrium state is chosen in Fermi function form:

$$\rho_N(x'') = \rho^{(0)}\frac{sh\,c/d}{ch\,c/d + ch\,x''/d} \quad (11)$$

where $c = 1.05A^{1/3}(Fm)$.

The final expression for the cross-section of inelastic electron scattering is expressed through the given transition probabilities

$$\sigma_{i\to f} = (2e^2 k\cos\theta/2)^2 \frac{2j_f+1}{2j_i+1}\{B(j_i \to j_f) + \sum_\lambda \frac{B(E\lambda)}{2\lambda+1}\} \quad (12)$$

Where

$$B(j_i \to j_f) = \left|\int D(\mathbf{x}')\ell^{i\mathbf{q}\mathbf{x}'}u_f(\mathbf{x}')u_i(\mathbf{x}')d\mathbf{x}'\right|^2 \quad (13)$$

-is given single-particle transition probability, and

$$B(E\lambda) = \left|\alpha_\lambda \int D(\mathbf{x}'')\rho_\lambda(\mathbf{x}'')\ell^{\mathbf{i}\mathbf{q}\mathbf{x}''}\mathrm{Y}_{\lambda 0}d\mathbf{x}''\right|^2 \quad (14)$$

-is given transition probability of nucleus core.

Here

$$\alpha_\lambda = \sqrt{\frac{\hbar\omega_\lambda}{2C_\lambda}} \quad (15)$$

$$\hbar\varpi_\lambda = \hbar\sqrt{\frac{C_\lambda}{B_\lambda}}. \quad (16)$$

We obtain the following expressions for so-called hardness parameter C_λ and mass parameter B_λ with the help of DCT.

$$C_\lambda = 8K\int \frac{\left|\rho_\lambda(x'')\mathrm{Y}^*_{\lambda 0}\right|^2}{\rho_N(x'')}d\mathbf{x}'' \quad (17)$$

Here K is constant in mass Bete-Weizzekera formula.

$$B_\lambda = \frac{m_N ZN}{\lambda c^{\lambda-2}A^2}\rho^{(0)}\int\left|\nabla\rho_\lambda(x'')\mathrm{Y}^*_{\lambda 0}\right|^2 d\mathbf{x}''. \quad (18)$$

The mechanisms of appearance of giant dipole and quadrupole excitations are considered in ^{60}Ni nucleus.

The subshells of different parity are in complex nuclei inside the external shell, that's why the transitions can be between subshells inside the one shell and between subshells of neighbour shells, i.e. the change of parity is need at the single-particle dipole transition. That's why in ^{60}Ni nuclei, if the final proton participates in single-particle transition, so $1f_{7/2} \to 1g_{9/2}$ takes place, if final neutron participates, so $3P_{3/2} \to 2d_{5/2}$ takes place.

The energy of single-particle level of harmonic oscillator with spin-orbital interaction is defined with the help of following known expression.

$$E_{nlj} = \frac{\hbar^2}{ma^2}(2n+l+3/2) - 20\mathbf{ls}A^{-2/3}. \quad (19)$$

The oscillator parameter *a* is free at the calculation of cross-section process.

The form-factors of dipole and quadrupole resonances in ^{60}Ni nucleus have been calculated for the electron scattering with incident energy 200 MeV. Moreover, the nucleus characteristics parameters at proton and neutron nucleus transitions are defined correspondingly.

p-transition: $\hbar\omega_1$=16.2 MeV, $\hbar\omega_2$=14.1 MeV, deformation parameters α_2 = 0.19.

n-transition: $\hbar\omega_1$ = 20.1 MeV, $\hbar\omega_2$ = 10.3, α_2 = 0.16.

As it is seen, the values of energy of quadrupole resonances, appearing in excited core, are less, than values of energies of dipole resonances, obtained as in proton transition, so in neutron one.

[1] *V.V. Varlamov, B.S.Ishkhanov.* EChAY 35,858 (2004).
[2] *M.M. Mirabutalibov.* Vesti BGU ser. fiz-mat. nauk. 3,25 (2005).
[3] *M.M. Mirabutalibov*. Yadernaya fizika, 67,2171 (2004).

М.М. Мирабуталыбов

ВОЗБУЖДЕНИЕ ЯДЕР НЕУПРУГИМ РАССЕЯНИЕМ ЭЛЕКТРОНОВ

С целью объяснения одновременного появления в эксперименте гигантских дипольных и квадрупольных резонансов в ядрах, при неупругом рассеянии электронов, предлагается дипольный резонанс описывать с помощью оболочечной модели, а квадрупольный – динамической коллективной теорией. При этом для колебания поверхности остова ядра применяется модель Тасси. Матричный элемент перехода возбужденного ядра вычислен в искаженно волновом приближении. Форм-факторы гигантского дипольного и квадрупольного возбуждений были рассчитаны для ядра ^{60}Ni. Определены энергии ГДР и ГКР, а также параметры деформации при протонном и нейтронном переходах в ядре.

M.M. Mirabutalıbov

ELEKTRONLARIN QEYRİ -ELASTİKİ SƏPİLMƏSİLƏ NÜVƏLƏRİN HƏYƏCANLAŞMASI

Təcrübədə elektronların nüvədən qeyri-elastiki səpilməsi zamanı onlarda dipol və kvadrupol nəhəng rezonanslarının yaranmasının nəzəri izahı təbəqəli nüvə modeli və dinamik kollektiv nəzəriyyə əsasında verilmişdir. Nüvə özəyinin səthinin rəqsinin izahı üçün Tassi modelindən istifadə olunmuşdur. ^{60}Ni nüvəsində yaranmış NDR və NKR – ın enerjisi, həmçinin həyəcanlaşma zamanı proton və neytron keçidlərində deformasiya parametrləri təyin edilmişdir.

Received: 18.09.06

THE HOPPING OF INTERCALATED Ag RELAXORS $TlInS_2$<Ge>

R.M. SARDARLY, O.A. SAMEDOV, I.Sh. SADIKHOV, G.R. SAFAROVA, E.A. ZEYNALOVA
The Institute of Radiation Problems of NAS of Azerbaijan
AZ 1143, Baku, H.Javid av., 31a

The conductivity of intercalated layered relaxors-ferroelectrics $TlInS_2$<Ge> has been investigated. The presence of hopping has been established and parameters, characterizing the given mechanism have been defined.

There are many works in the literature, dedicated to the study of intercalation influence on electric, photo-electric and optical properties of layered crystals by A^3B^3 and $A^3B^3C^6_2$ types [1-4]. Summing the different aspects of intercalation influence on these properties we can conclude, that the common trait of this influence is the possibility of managing of parameters of these materials, in particular, electric and ferroelectric properties, by the means of introduction of foreign atoms in Van-der-Waals connections.

The $TlInS_2$ compound is the crystal, in which the temperature instabilities of crystal lattice are observed, leading to the ferroelectric order. Nowadays, it is clearly established, that these compounds of stochiometric composition are improper ferroelectrics with disproportionate phase.

Our previous investigations showed, that Ge doping of $TlInS_2$ crystals leads to the appearance of the stable relaxing state [5]. The intercalation of ferroelectric crystals independently leads to the strong relaxation of dielectric receptivity [6], which as in the first case coincides with temperature region of existing of disproportionate phase. Thus, the charge disorder inside the layer is the reason of dielectric relaxation in the first case, and the charge disorder between the layers in the second case. Both these factors influence on ferroelectric order, leading to the fact, that the state of ferroelectric glass precedes the order phase.

In the given paper the results of the investigation of electroconductivity of non-intercalated and intercalated relaxing ferroelectrics $TlInS_2$<Ge> are presented.

The measurements of electroconductivity were carried out at the constant current in two directions: parallel ($\sigma_{\|}$) and perpendicular ($\sigma_{\perp}$) obliquely to c axes, as for the intercalated, so for the non-intercalated compositions $TlInS_2$<Ge> in temperature interval 90÷300K.

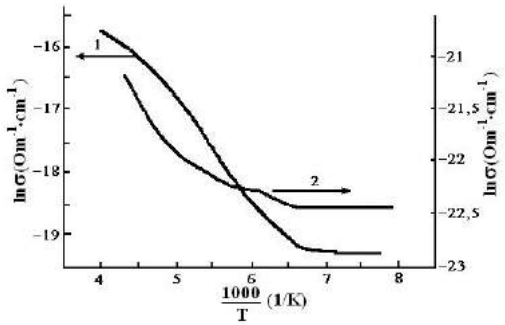

Fig.1. The temperature dependence of conductivity `$\sigma(T)$ along (1) and perpendicular (2) to layers for non-intercalated relaxor ferroelectrics $TlInS_2$<Ge>.

The changes of temperature dependence of electroconductivity $\sigma(T)$ in Arrenius coordinates for the non-intercalated crystals $TlInS_2$<Ge> (curve 1 is perpendicular to *c* axes, curve 2 is parallel to *c* axes) are given on the fig.1. As it is seen from the fig.1 (curve 1), the dependence $\sigma_{\|}(10^3/T)$ in temperature region 210-150K in direction (100) has the long exponential region. Further temperature decrease till 150K leads to the $\sigma_{\|}$ decrease, and $\sigma_{\|}$ doesn't depend on temperature below 150K. The activation energy $E_a \approx 0.08$ eV was defined from curve inclination.

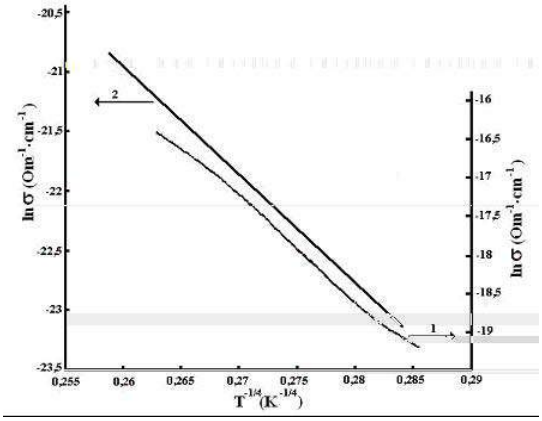

Fig.2. The conductivity of $TlInS_2$<Ge> crystals in Mott's coordinates, along (1) and perpendicular to (2) layers.

The dependence $ln\sigma_{\|}$ on $T^{-1/4}$ is shown on the fig.2 (curve 1). As it is seen from the figure, the rectification of all experimental points takes place on the given dependence, that allows us to say about the fact, that the charge transfer along the layers takes place in given temperature region in non-intercalated crystal $TlInS_2$<Ge> by the means of the hopping. This transfer is carried out on the states, which lie in narrow energy band near Fermi level [7], $ln\sigma \sim T^{-1/4}$. The curve inclination $ln\sigma_{\|}$ on $T^{-1/4}$ was $T_0 \approx 1{,}6\ 10^6$ K.

The density of localized states near Fermi level can be obtained from the formula:

$$N_F = \frac{16}{T_0 \cdot K \cdot a^3},$$

Where *K* is Bolzman constant, *a* is localization radius. The of state density value (nano-blast-furnace state) of crystal is $TlInS_2$<Ge> $N_F \sim 4.3 \cdot 10^{17}$ $eV^{-1} \cdot cm^{-3}$.

The length of *R* jumps of charge carriers at the different temperatures was defined from the formula:

$$R(T) = \frac{3}{8} a \cdot T_o^{1/4} T^{-1/4} = 191 \mathring{A},$$

and for the studied temperature interval average jump length was 191Å.

The given value in 6,3 times exceeds the average distance between localization centers of charge carriers (a=30Å). As it was already mentioned, the conductivity of non-intercalated monocrystals $TlInS_2$<Ge> doesn't depend on temperature region 150-170K. This means, that non-activated hopping takes place along the crystal layers.

The big value N_F, obtained for the non-intercalated crystals $TlInS_2$<Ge>, shows on their similarity with strongly disorder semiconductors. The existence of the defects caused by the introduction of Ge impurity influences on the increase of the degree of disorder, that explains the existence of the high density of the states near Fermi level. By other words, $TlInS_2$<Ge> samples, treated by doping by Ge, present themselves the disorder joint of the regions of short range ordering. The high conductivity on the localized states in the forbidden band caused by the existence of defect centers of high concentrations N_t=3,44·10^{16}cm^{-3}.

The temperature dependence of the conductivity $TlInS_2$<Ge> along c axis of relaxor had other character. The high-temperature branch of $\sigma_\perp$ dependence had exponential character. The inclination of this dependence in temperature interval 210÷300K was E_a=0,41eV. The activation energy of conductivity constantly decreases and at T<145K $\sigma_\perp$ almost didn't depend on temperature below 210K.

The droningly decreasing $TlInS_2$<Ge> conductivity with temperature decrease connects with jumps of charge carriers on the localized states near Fermi level. The $\sigma_\perp T^{1/4}$ dependence of conductivity, reconstructed in coordinates, is presented on the fig.2. (curve 2). The inclination of this dependence was T_0=4,4·10^7K. The N_t=1,6·10^{17}eV^{-1}cm^{-3} has been obtained for the density of localized states near Fermi level, the jump distances of charge carriers have been defined as 95,25Å (table 1).

Thus, above temperature 210K the crystal conductivity is band one. The phonons are absorbed in the temperature region 150÷300K at jumps of charge carriers from one localized center on the other one. Finally, the moment comes, when the conductivity stops to depend on temperature. In this case jumps of charge carriers take place with of phonon ejection. The non-activated hopping takes place below temperature T<150K.

The temperature dependence of the conductivity on the c axis $\sigma_\parallel$ (curve 1) and perpendicular the layers $\sigma_\perp$ (curve 2) for the intercalated compositions $TlInS_2$<Ge> (a=30Å) is given on the fig.3. From the figure it is seen, that the conductivity of intercalated crystal $TlInS_2$<Ge> is significantly higher, than the initial $TlInS_2$<Ge> in the direction of natural axis c and perpendicular to it too. The increase of the electroconductivity in c direction at high intercalate concentrations connects with the introduction into semiconductor layer of $TlInS_2$ argentums. In this case the covering of wave functions of introduced atoms, accompanying with significant increase electroconductivity of intercalated crystal, which begins to introduce the significant contribution into crystal electroconductivity. The existence of the conducting Ge film between the $TlInS_2$ layers leads to the decrease of potential interlayer barrier, in the result of which the movement of the carriers in the direction of c axis of the crystal makes significantly easy. That's why the electroconductivity increases in c direction.

From the dependencies $\sigma(T)$ in Arrenius $\sigma(1/T)$ (fig.1, curves 1 and 2) and in Motts' coordinates $\sigma(1/T)^{1/4}$ (fig.2. curves 1 and 2) the density of localized states N_F; activation energy E_a; jump length R at different temperatures in direction of axis and perpendicular to it (table 1) are defined.

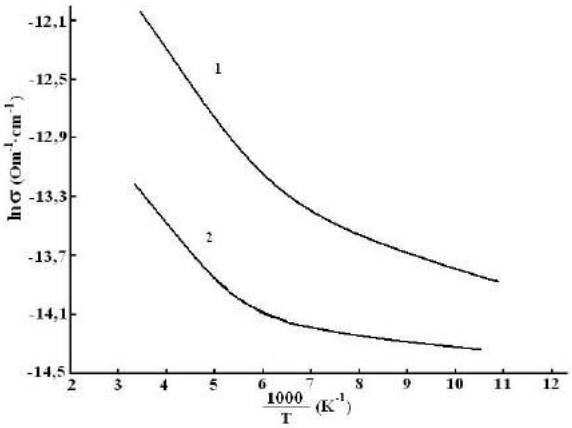

Fig.3. The temperature dependence of $\sigma(T)$ conductivity along (1) and perpendicular (2) layers for intercalated Ag relaxor ferroelectrics $TlInS_2$<Ge>.

The small mobility is the peculiarity of jump mechanism, as jumps of charge carriers are carried out on weak coverings of tail parts of wave functions of nearest acceptor levels. The speed devastation of charge carriers in the conduction band takes place with temperature decrease, and this leads to the fact, that the jumps of charge carriers on separate impurity states without activation in allowed band begin to play the biggest role.

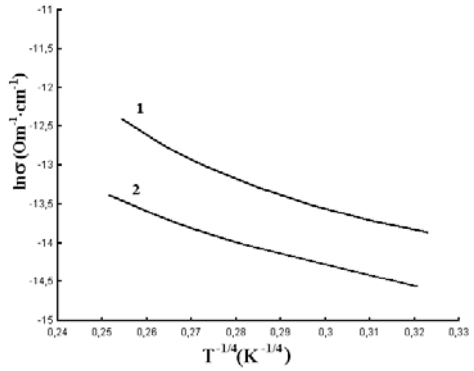

Fig.4. The conductivity of intercalated Ag crystals $TlInS_2$<Ge> in Mott's coordinates, along (1) and perpendicular (2) layers.

Thus, the experimental results on the study of processes of charge transfer in intercalated samples $TlInS_2$<Ge> as along, so perpendicular to c axis, allow to say that hopping with variable of jump length, which becomes non-activated one at further temperature decrease.

The investigation results of electrophysic parameters of non-intercalated and intercalated compounds $TlInS_2$<Ge> are given in table 1.

As it is known, the layered crystals are anisotropic ones. The anisotropy of electric properties of all layered compounds connects firstly with the fact, that electrons can freely move inside the layers, as covering between the layers of wave functions is small because of Van-der-Waals character of layer interaction. The layered compounds, in which anisotropy is extremely strong and leads to almost two-dimensional movement of electrons in crystal presented biggest interest.

Table 1.

Electrophysical parameters of non-intercalated and intercalated compounds $TlInS_2$<Ge> along the layers and perpendicular to them.

		E_a, eV	N_f, eV^{-1} cm^{-3}	R, Ω	N_t, cm^{-3}	ΔE, eV	T_0, K
Non-intercalated compound	Along the layers	0,31	$4,3 \cdot 10^{17}$	191	$3,44 \cdot 10^{16}$	0,08	$1,6 \cdot 10^{7}$
	Perpendicular to layers	0,41	$1,6 \cdot 10^{17}$	247,5	$1,44 \cdot 10^{16}$	0,09	$4,4 \cdot 10^{7}$
Intercalated compound	Along the layers	0,27	$4,7 \cdot 10^{18}$	95,25	$2,77 \cdot 10^{17}$	0,059	$4,9 \cdot 10^{6}$
	Perpendicular to layers	0,29	$3,6 \cdot 10^{18}$	102	$2,27 \cdot 10^{17}$	0,063	$6,4 \cdot 10^{6}$

Thus, at the intercalation $TlInS_2$<Ge> Ag atoms penetrate into interlayer space and create "metallic" layers. Accordingly, wave functions of introduced atoms also collid that is accompanied by significant increase of electroconductivity of intercalate layer, which begin to play the significant role in electroconductivity. As result, anisotropy of electroconductivity of $TlInS_2$<Ge> crystal decreases.

[1] *K.F.Tovstyuk*. Poluprovodnikovoye materialovedeniye. Kiyev, Naukova Dumka, 1984, 264 s. (in Russian).

[2] *Z.D.Kovalyuk, P.I.Savitskiy, K.D.Tovstyuk*. Neorqanicheskiye materiali. t.28, №2, 1982, s.209. (in Russian).

[3] *I.V.Mintyyanskiy, I.I.Grigorchak, Z.D.Kovalyuk, S.V.Gavrilyuk*. FTT. 1986, t.28, v.4, s.1263. (in Russian).

[4] *S.N.Mustafaeva, M.M.Asadov, V.A.Ramazanzade*. Neorqanicheskiye materialı, 1995, t.31, v.3, s.318. (in Russian).

[5] *R.M.Sardarly, O.A.Samedov, I.Sh.Sadigov* Inorganic Materials, 2005, v.40, n.10, p.1163.

[6] *R.M.Sardarlı, O.A.Samedov, İ.Ş.Sadıgov, G.A.Zeynalova, T.Yu.Sardarlı*. Proceedings International Conference "Fizika-2005", Baku, Elm, 2005.

[7] *N.F.Mott, G.A.Devis*. Elektronnıye processi v nekristallicheskix veshshestvax. Mir, M.: 1974, 472 s. (in Russian).

R.M. Sərdarlı, O.A. Səmədov, İ.Ş. Sadıxov, G.R. Səfərova, E.A. Zeynalova

Ag İLƏ İNTERKALYASİYA OLUNMUŞ $TlInS_2$<Ge> RELAKSORUNDA SIÇRAYIŞLI KEÇİRİCİLİK

İnterkalyasiya olunmuş laylı $TlInS_2$<Ge> relaksor-seqnetoelektrikinin keçiriciliyi tədqiq olunmuşdur. Sıçrayışlı keçiricilik müəyyən olunmuş və keçirici mexanizmini xarakterizə edən parametrlər təyin edilmişdir.

Р.М. Сардарлы, О.А. Самедов, И.Ш. Садыхов, Г.А. Сафарова, Э.А. Зейналова

ПРЫЖКОВАЯ ПРОВОДИМОСТЬ ИНТЕРКАЛИРОВАННЫХ Ag РЕЛАКСОРОВ $TlInS_2$<Ge>

Исследована проводимость интеркалированных слоистых релаксоров-сегнетоэлектриков $TlInS_2$<Ge>. Установлено наличие прыжковой проводимости и определены параметры, характеризующие данный механизм.

Received: 16.06.06

THE INFLUENCE OF THE HEATING OF THE CHARGE CARRIES ON PROPAGATION OF HIGH-FREQUENCY ELECTROMAGNETIC WAVES IN ELECTRON TYPE SEMICONDUCTORS

Kh.A. HASANOV, V.A. GUSEINOV
Department of General and Theoretical Physics, Nakhchivan State University, AZ 7000, Nakhchivan, Azerbaijan

The influence of the heating of the charge carries on propagation of electromagnetic waves of high frequency in non-degenerate electron type semiconductors is considered. It is considered the case when the long wave phonons form "the thermal reservoir" in the lattice. The case of normal skin effect is investigated. It is shown that the heating of the electrons leads to the considerable non-linear problem. The dependence of the penetration depth of the wave on the amplitude of the incident wave is obtained in the mechanisms of the scattering of the electrons both at the deformation potential and at the piezoelectric potential of the acoustical phonons.

Let us consider the propagation of high-frequency electromagnetic waves in degenerate semiconductors having one-type charge carriers (electrons) in the following model. Let us suppose that the electron-phonon system are heated by the field of the wave propagating in semiconductive crystal and the subsystem of long wave phonons forms "the thermal reservoir". In this case in the boundary of the crystal the energy got from the field are transferred to the medium at the expense of the electron- phonon scattering. Let us accept that the electron-electron scattering frequency is much less than the electron-phonon scattering frequency. In this case phonons are described by the Planck distribution of the temperature T_e and electrons are described by the Maxwell distribution of the same temperature.

Besides, we accept than the characteristic length of field change is much less than the linear size of the pattern in the direction of the propagation of the wave. It enables to consider the semiconductor in which the wave is propagated as a half endless one. To be satisfied the normal skin effect the characteristic length is to be much greater than the wave length in the medium and the characteristic length is to be much greater than the electron mean free path by transferring energy and momentum. Let us consider the case when the falling onto the semiconductor and propagating in it is circular polarized. This condition provides the time independence of the isotropic part of the distribution function for the electrons in the kinetic equation. Within all these conditions on the charge-drift velocity of the electrons found from the kinetic equation we obtain the following expression for the electric conductivity of high frequency:

$$\sigma = \frac{\Gamma\left(\frac{t+5}{2}\right)}{3\pi^{3/2}}\left(\frac{\omega_p}{\omega}\right)^2\left(\frac{T_e}{T_p}\right)^{t/2}\nu(T_p)\left(1+2\frac{\omega_H}{\omega}\right)+i\frac{1}{4\pi}\frac{\omega_p^2}{\omega}\left(1+\frac{\omega_H}{\omega}\right), \tag{1}$$

where ω is the frequency of the external electromagnetic field, $\nu(T_p)$ is the electron-phonon scattering frequency when the phonons are not heated and $\omega_H = eH/mc$ is the cyclotron frequency of the electrons, where c is the velocity of light in the vacuum, $\omega_p = (4\pi ne^2/m)^{1/2}$ is the plasma frequency of electrons, $\Gamma(z)$ is the Gamma-function,

$$T_e(E) = T_p\left(1+\frac{E^2}{E_1^2}\right) \tag{2}$$

is the electron temperature, T_p is the phonon temperature, $E_1 = \sqrt{3}s_0 m(\omega-\omega_H)/e$ is the strength of the characteristic field, t is the parameter characterizing the scattering mechanism. When we have dealings with the high-frequency waves $\omega_H/\omega << 1$ and the electromagnetic waves propagate in the direction of $k\|H\|Oz$, the Maxwell equation is given by

$$\frac{d^2E(z)}{dz^2}+\frac{\omega^2}{c^2}\left[\left(\varepsilon_0-\frac{\omega_p^2}{\omega^2}\right)+i\frac{4\Gamma\left(\frac{t+5}{2}\right)}{3\sqrt{\pi}}\frac{\omega_p^2}{\omega^2}\nu(T_p)\left(\frac{T_e}{T_p}\right)^{\frac{1}{2}}\right]E(z)=0, \tag{3}$$

where ε_0 is the relative permittivity of the crystalline lattice.

From the comparison of the expressions (1) and (2) it is visible that the electric conductivity depends on the strength of the electric field considerably. This dependence leads to the non-linearity.

Using [2], if we look for the solution of the equation (3) as

$$E(z) = U(z)\exp\left(i\frac{\omega}{c}\int_0^z n(z)dz\right), \tag{4}$$

we can obtain the equation

$$2n(z)\frac{dU(z)}{dz}+U(z)\frac{dn(z)}{dz}+\frac{4\Gamma\left(\frac{t+5}{2}\right)}{3\sqrt{\pi}}\left(\frac{T_e}{T_p}\right)^{\frac{1}{2}}\frac{\omega_p^2}{\omega^2}\frac{\nu(T_p)}{c}U(z)=0, \tag{5}$$

where $n(z)$ is refractive index of the medium. The condition $L_e >> \lambda$ refuses the transformation of the wave energy to the Joule heat by absorbing in the small thickness of the medium. Here λ is the wave length of the electromagnetic wave in the medium. It means that the electromagnetic waves penetrate till the definite depth. In that case the coordinate dependence of the refractive index of the medium can be neglected and the equation (5) can be easily integrated

$$U(z)=U_0\exp\left(-\frac{Z}{L_E}\right). \tag{6}$$

Here

$$L_E=\frac{3\sqrt{\pi}}{2\Gamma\left(\frac{5+t}{2}\right)}\frac{\omega^2 cn_0}{\omega_p^2\nu(T_p)}\left(\frac{1}{1+\frac{E^2}{E_1^2}}\right)^{\frac{t}{2}} \tag{7}$$

is the penetration depth of the electromagnetic wave. In a strong electric field $\left(\frac{E}{E_1}>>1\right)$, when the electrons scatter by the deformation potential of the acoustical oscillation of the lattice, i. e. when $t=+1$,

$$L_E=\frac{3\sqrt{\pi}}{4}\left(\frac{\omega}{\omega_p}\right)^2\frac{cn_0E_1}{\nu(T_p)}\frac{1}{E} \tag{8}$$

and in the case of scattering by the piezoelectric potential $t=-1$

$$L_E=\frac{3\sqrt{\pi}}{2}\left(\frac{\omega}{\omega_p}\right)^2\frac{cn_0}{\nu(T_p)E_1}E \tag{9}$$

And now let us perform the numerical estimation. For the strength $E=10E_1$ of the electric field, if we take into consideration the parameters $n_0=4$, $m=0.56m_e$, $n=2.5x10^{13}cm^{-3}$ of Ge and the field frequency $\omega\approx 3.2x10^{11}Hz$ in the formula (8), we obtain $L_E\approx 1.3x10^{-2}$ cm for the attenuation depth of the electromagnetic wave.

[1] *B.M. Askerov*. Electron transport phenomena in semiconductors, Singapore, World Scientific Publishing Company, 1994.

[2] *F.G. Bass, Y.G. Gurevich*. Goriachiie electroni i sil'nyie elektromagnitnyie volny v plazme polurovodnikov i gazovogo razriada (Hot electrons and strong electromagnetic waves in the plasma of the semiconductors and gas discharge), Moscow, Nauka, 1975.

X.A. Həsənov, V.A. Hüseynov

ELEKTRON TİPLİ YARIMKEÇİRİCİLƏRDƏ YÜKSƏK TEZLİKİLİ ELEKTROMAQNİT DALĞALARININ YAYILMASINA YÜKDAŞIYICILARIN QIZDIRILMASININ TƏSİRİ

İşdə elektron-fonon sisteminin qızmasının elektron-keçiricilikli cırlaşmamış yarımkeçiricilərdə yüksək tezlikli elektromaqnit dalğalarının yayılmasına təsirinə baxılmışdır. Bu zaman qəfəsdə uzundalğalı fononların "istilik rezervuarı" yaratdıqları nəzərə alınmışdır. Normal skin-effekt araşdırılmışdır. Göstərilmişdir ki, elektronların qızdırılması nəzərə çarpacaq qeyri-xəttilik yaradır. Elektronların həm akustik fononların deformasiya potensialından, həm də pyezoelektrik potensialdan səpilmə mexanizmlərində dalğanın nüfuzetmə dərinliyinin düşən dalğanın amplitudundan asılılıqları tapılmışdır.

Х.А. Гасанов, В.А. Гусейнов

ВЛИЯНИЕ НАГРЕВА НОСИТЕЛЕЙ ЗАРЯДА НА РАСПРОСТРАНЕНИЕ ВЫСОКОЧАСТОТНЫХ ЭЛЕКТРОМАГНИТНЫХ ВОЛН В ПОЛУПРОВОДНИКАХ ЭЛЕКТРОННОГО ТИПА

В работе рассмотрено влияние нагрева системы электрон-фонон на распространение высокочастотной электромагнитной волны в невырожденных электронных полупроводниках. При этом, рассмотрен случай, когда в решетке длинноволновые фононы образуют "тепловой резервуар". Исследуется случай нормального скин-эффекта. Показано, что разогрев электронов приводит к существенно нелинейной задаче.

Найдена зависимость глубины проникновения волны от амплитуды падающей волны в механизмах рассеяния электронов как на деформационном потенциале, так и на пьезоэлектрическом потенциале акустических фононов.

Received: 08.02.06

THE SUPRAMOLECULAR STRUCTURES ON THE BASE OF A^{IV} B^{VI} – Sb (NiSb) EUTECTIC SYSTEMS

K.Sh. KAGRAMANOV, S.Sh. KAGRAMANOV
Scientific-industrial community "Selen" of National Academy of Sciences of Azerbaijan Republic, Baku, Azerbaijan

E.D. MOROUDOR, M.G. PISHKIN
Stambul Technical University "Yildiz" , technical department, Stambul, Turkey

The processes of crystallization and morphology peculiarities of microstructure A^{IV} B^{VI} – Sb (NiSb) eutectic are evidence in favor of supramolecular conception with taking into account of substructure interactions.

The anomalous structures are revealed on the obtained direct-oriented (PbTe - Sb) and (PbS - Sb) eutectics, and the regular plane-fibrous structures are revealed on the (PbS - NiSb) and (PbTe - NiSb) eutectics.

The principle of the orientational and dimensional correspondence keeps in (PbS - NiSb) eutectic also as in the normal binary eutectic systems, the plane (111) PbS accretes with plane (0001) NiSb.

The morphology analysis of (PbS - NiSb) eutectic showed the presence of the different defects of types: plate shifting, surfaces of convergence, block (plate) inclinations and excess extra-plate. These defects are analogous to atom defects, obtaining in real one-phase crystals.

The investigations showed that eutectics can be considered as the supramolecular layered ensembles.

Introduction

The eutectic is the special melt (solution), the components of which restrictedly mix in solid and liquid (in some temperature interval) states and spontaneously form the thermodynamic equilibrium liophilic disperse system in this interval. The given disperse system is characterized by significant interphase interaction and salvation.

The main statements of eutectic theory have been analyzed in the ref [1] and the view of the more significant results, obtained at the investigation of eutectic melts of inorganic substances, is given. The evidences in the favor of supramolecular eutectic conception, taking into account the interaction ("non-autonomous phases") are presented. The many direct experimental provements of "interacting phases" conception exist.

The ability of the self-organizing supramolecular objects to the molecular recognition is their main property. The component recognition proposes the "complementarity", i.e., the compatibility of ensemble participants (substratum and receptor) – as geometrical one, so the level of the formation of intermolecular connections [2].

The theoretic analysis proves the possibility of suprastructure self-organizing from the structures, disproportionate in the one crystallographic direction. The consideration of eutectic compositions, in the limit case disproportionate on all three crystallographic directions, in terms of supramolecular chemistry allows us to obtain the answers on many questions and to escape the vaguenesses, mentioned at the discussion of existing eutectic conceptions [1]. The proposed supramolecular conception in eutectic theory [1] doesn't reject the classic conceptions. It duffers from them only by the fact, that abstract thermodynamic criterias, such as the surface energy or surface tension are changed by real parameters of interacting substructures: disproportion, hardness, interaction potential.

The given experimental data can be evidence in the proof of supramolecular eutectic conception. The statement about the fact, that interaction of these phases is need to consider in the eutectic melt, consisting the autonomous phases A and B is the base of this conception. The forming of the nonautonomous phases, similar to the supramolecular ensembles is the result of such interaction. The conditions of the formation of defect composite-nonautonomous phases with changed lattice parameters can be created in the dependence on the interaction potential,, disproportion of crystal lattice of suprastructures A and B, their harshness and extension, external mechanic influences. The special properties of eutectic melts, the dependence of their structures on the synthesis conditions (temperature, cooling velocity, mechanical interactions) are defined by the quantity of nonautonomous phase and the degree of it organization [1].

Many works are dedicated to the investigation of the morphology and crystallization peculiarities, physicochemical properties of eutectics [1,3-9]. They reveal the peculiarities in their microstructure. It was the base for the eutectic classification. The classification, on which all eutectics are divided on normal and anomalous ones, was separated.

Normal eutectics have mainly plate or fibrous (rod) microstructure. The definite crystallographic ratios, character for the given melt, should exist in normal eutectic between the phases. The anomalous eutectics form in only that case, when eutectic phases can't increase with the similar velocities.

Eutectic crystallization "is carried out by the way of the creation" and increase of colonies of two-phase formation, the each of them forms on the base of one center [10-11].

On authors' opinion the oriented crystallization, as in eutectic, so at the artificial crystallization of the one crystal on the substrate of another one, is possible only at the condition, that both materials already naturally have some geometric similar crystallographic atom complexes, well mating with each other [5-6]. Authors of the refs [5-6, 12-13], showing on the observance dimensional and oriented correspondence between the phases in eutectic, draw an analogy between atom interaction on the interphase boundary in eutectic melt and this interaction, which is realized at the artificial epitaxial growing of the one material on the substrate of the another one. However, the results of X-ray

and electron-microscopic investigations of eutectic set showed that such analogy can't be drawn. The electron-microscopic investigations of directed-oriented eutectics reveal the presence dislocation variance on the phase boundaries, decreasing the coherent deformations, caused by the convergence of phase lattices on the coupling boundary. As the investigations showed, the dislocation density of the variance on the interphase boundaries in eutectics is defined by the value of the convergence of lattice parameters of mating phases [3]. The dislocation forming in double-layer film structures, obtained by epitaxial growing, is caused not only by variance of crystal lattices, but mainly by interdiffusion [14].

The results of X-ray investigation of the thin structure of eutectic system Si - $ZrSi_2$ [14], obtained by the directed crystallization, showed that in eutectic the dislocation density of variance decreases exponentially into grain depth, and it is maximal on the interphase surface in the difference from the double-layer film structures, in which the dislocation density, caused by interdiffusion, is maximal in the grain center and decreases to the boundary side. As it was established in this paper, the lattice of Si matrix is pressed, and lattice of $ZrSi_2$ fibres is extended in the result of the variance of crystal lattices in the direction, which is parallel to the increase axis of Si - $ZrSi_2$ eutectic system. The given deformations are elastic as shows the selective etching. The lattice inclinations in the transverse direction are absent, that is the interest fact. The above mentioned fact is the important step in the statement of the fact that eutectic structures radically differ from the structures of another crystals.

It can be supposed, that eutectic is the system, which is characterized by the unite energy electron spectrum. The results of the refs [13-15] are the some statements of this supposition. So the authors of the ref [15], studying the possible interphase interaction in SnTe - NiSb by the method of nucleus-gamma resonance, have revealed, that Lorenz curve of tin atoms in this eutectic is asymmetric in comparison of one in SnTe, that is revealed in line broadening to the side of the low velocities. This asymmetry was explained by the authors [15] by the fact, that eutectic spectrum presented itself the superposition of two spectrums of different intensity. The spectrum of bigger intensity corresponds to the tin atoms in SnTe, and the spectrum of low intensity corresponds to tin atoms, situated on the boundaries with NiSb phase.

The analysis of literature data allows us to make the conclusion, that the some chemical interaction takes place in eutectics on the interphase boundaries. However, the electron structure of eutectics and reasons of its creation haven't clarified yet.

The given paper is dedicated to the study of the peculiarities of morphology microstructure, physicochemical properties of eutectic melts A^{IV} B^{VI} – Sb (NiSb) with the aim of the revealing of interphase interaction nature, proving in the proof of the supramolecular conception.

Investigation technique

The eutectic melts of the following systems: PbS(PbTe)-Sb, PbS(PbTe)-NiSb have been grown by Bridgman method at the velocity v=3 mm/h and temperature gradient ΔT=100°C between the heaters. The purity of the initial materials: Sb, Pb, S, Te was not less, than 99,999%.

The part of the microstructures on MIM-7 microscope, on raster electron microscope (REM) JSM-50A with the prefix for the local X-ray analysis and on electron microscope JSM-2000 in the beams of the secondary electron mission and in the beams of the transmission electrons, X-ray images had been investigated in Te, S, Ni, Sb beams.

The diffractograms of PbS-NiSb eutectic are obtained on DRON-2 installation. The photos are obtained at the beam directions, parallel to the direction of the axes of crystal growth and perpendicular to the surface plane of PbS and NiSb in eutectic. The diffractograms of eutectic powder PbS-NiSb were investigated for the comparison.

The lines of the characteristic X-ray radiation for the one beforehand chosen element (permission method 1000-2000 nm) are registered; white elements on the photos are more hard. For example, regions PbTe on NiSb phone are looked like white. The microstrictures of the anisotropic eutectic PbTe-NiSb, obtained on REM give the possibility to see the image of the investigated surface simultaneously as in electron, so in X-ray beams. The images in electron and X-ray beams are turned out interest not only by the fact, that they have best permission in principle, than the ones, obtained with the help of the metallographic microscope, but by only the fact, that they give the possibility to observe the boundary between the phases and to judge about the element distribution along sample surface.

The result discussion

The regular ordered microstructures are character to the eutectic melts (fig. 1-2). The high strength and superplasticity of the eutectics say about the special structure of interphase boundaries. All these peculiarities and many other properties differ eutectics from the homogeneous melts and from the mechanical ones and are evidence in the proof of the supramolecular eutectic conception.

The previous investigations showed that the structure in PbTe-NiSb systems is the one of the same type. Let's consider the crystallization in PbTe-NiSb and PbS-NiSb systems for the distinctness. The PbTe-NiSb eutectic (fig.1 (b)) has the fiber structure and PbS-NiSb has the plate structure (fig.2 (1-4)). The eutectics of (PbS-Sb) PbTe-Sb systems can be related to the anomalous, limited bar ones with the petalled structure of the rods and planes. The investigated eutectic PbS-NiSb (fig.2) can be related to the normal, i.e. to the "regular" ones on the form and phase distribution. Each substructure grows with the one strictly drawn crystallization front, clearly revealing the contact surface of subblocks. The defined crystallographic ratios, character for the given systems exist in the normal microstructures, investigated by us, between the phases which aren't observed in anomalous eutectics.

The element distribution in PbTe-NiSb eutectic, obtained by the local; X-ray analysis between two grains is given on the fig.3. As it is seen from the fig.3 the distribution of Pb, Te, Ni and Sb elements between the phases is clear; in the inclusion region the signal falling from Pb and Te and the increase of the signals from Ni and Sb take place. The insignificant distribution of Ni and Sb in NiSb region is paid attention. The results of the local X-ray analysis of the directed-oriented eutectic of PbTe-NiSb system are given here. According to them Ni and Sb, happen to the needles of the dispersed phase, coincide with minimal content of Pb and Te.

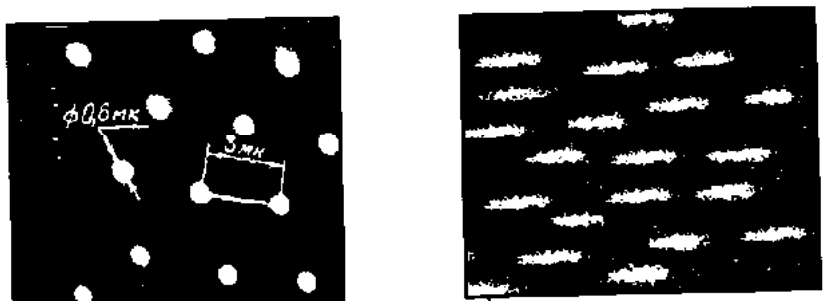

a) *b)*

Fig.1. Microstructure of transversal (a) and longitudinal (b) section of the directed-oriented PbTe-NiSb eutectic.

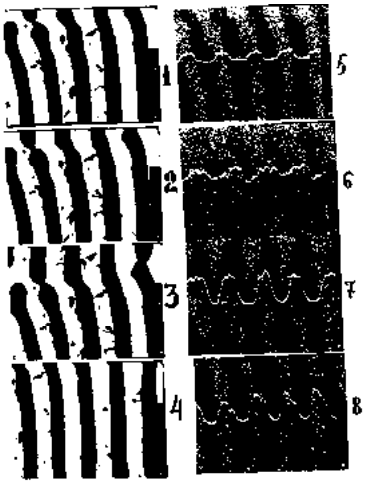

Fig.2. The photos of microstructure and local X-ray analysis of longitudinal section of the oriented eutectic PbS-NiSb (x300), obtained on JSM-50A: 1,2,3,4 – in Sotro mode; 5-8 are X-ray images in the characteristic beams (5 –Ni, 6-Pb, 7-Sb, 8-S) towards with linear distribution of Pb, S, Sb and Ni.

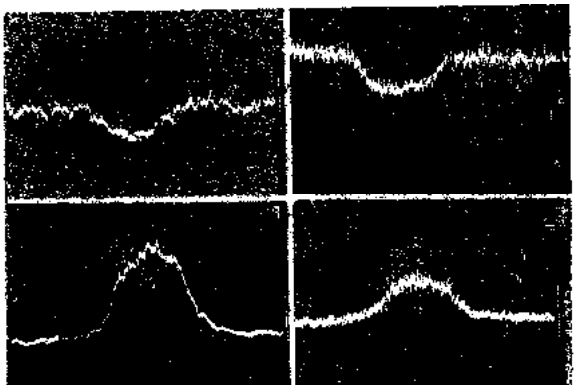

Fig.3. The figures of the local X-ray analysis of the transversal section of the oriented eutectic PbTe - NiSb: a) – X-ray images in characteristic Sb beams with linear distribution (x14000); b) - the same in Ni beams towards with Ni linear distribution (x14000); c) - the same in Pb beams (x15000); d) - the same in Te beams towards with Te linear distribution (x15000).

The images, obtained in characteristic beams of all four atoms, show that as the matrix, so the inclusions present themselves the suprastructures, consisting from the solid solutions. The data of local X-ray analysis is the total agreement with the state diagram of PbTe-NiSb system [16]. The same pictures of Pb, S, Ni, Sb element distribution in PbS-NiSb eutectic are presented on the fig.2, (5-8). The alternations of plates of the solid solutions on the base of the lead sulphide and planes of solid solutions on the base of nickel antimonide are clearly seen on the figure 2. Each phase in the system, being the independent subblock, belongs to the united eutectic supramolecular ensemble.

Let's consider the mechanism of the establishment of the oriented ratios in these systems (PbS-NiSb, PbTe-NiSb).

The length of the fibers in eutectic colony of PbTe-NiSb system varies in the interval from 200 nm till 7000 nm at the diameter 160-180 nm. The fibers have cigar-shaped form with the thickening on the one end and needle-shaped bevel on another one (fig. 1 (b)).

It can be said, that the obtaining of such eutectic supramolecular ensembles with regular structure (fig.1 and fig.2) is the enough complex technological task, which not always can be realized even on the one and the same composition on these or that reasons. Thus, the high concentration of convergence defects (mentioned by circle (A) fig.4) and terminations (mentioned by pointer (B), caused by the fact, that phase orientation in this case doesn't coincide with more profit one, is visually seen on transversal section of PbS-NiSb eutectic. The plates turn relatively each other round growth axis on small angles, mating moreover between each other by more successful form for the realization of minimum of interphase energy. The PbS and NiSb mate more successful in bend phase region; the plate shifting relatively each other increases as far as the region widening. The further widening in bend region leads to the plate break with the formation of convergence surfaces (fig.4). The convergence surfaces in energy meaning are comfortable places for termination creations. Though all details of creation and growth of plates of PbS and NiSb are hard to imagine, the profitable orientation relatively to neighbor plates, which endure the bend by the way of formation of subboundaries with off-orientation, causes to quick establishment of favorable crystallographic connections in eutectic.

The PbS-NiSb plates are continuous and parallel in the limits of small regions in eutectics. The excess plane of the one phase is present on the one of the sides. This extra-plate is analogous to atom extra-plane, connected with edge dislocation like the edge of atom half-plane forms the line

defect in space, which is called end substructure defect or termination [10].

Fig.4. The longitudinal section of PbS-NiSb eutectic.

The convergence surfaces are connected with terminations in plate eutectics. These convergence surfaces are situated perpendicular to the plates. Besides the regions with defects and the perfect regions, where the termination is absent, are present.

Thus, the defect density is defined not by crystallization conditions, but by crystallographic factor. The orientation, favorable for the growth of perfect phases, appears in creation process. The subblocks (PbS and NiSb plates) grow perpendicular to crystallization front in conditions of stationary growth, so that contact plane of plates necessarily has the growth direction. As PbS-NiSb has the plate structure, then the condition of regular accretion of phases is the more obvious, and between accreting planes of lead sulphide and nickel antimonide the orientation ratios should are exist. It is naturally, that the disparities of mating lattices on the period of crystal lattice and their mutual shifting appear at the mating of eutectic phases. The morphology analysis of subblocks of PbS-NiSb eutectic shows the presence of defect set of termination type, plate shifts, convergence surfaces and their contortions. The studied morphology and carried out analogies show that the big defect number of crystal structure can participate in the forming of interphase boundaries of suprastructure eutectic melts.

The order distribution of crystal directions in sample space is well demonstrated with diffractograms, given on the fig. 5 (a,b,c). The diffractograms are taken at the beam directions, parallel (a) to direction of crystal growth and perpendicular (b) to PbS and NiSb plates, and also in the case of use of eutectic powder PbS-NiSb (c). The obtained photos show on the fact, that the orientation ratio between blocks of eutectic melt, that can be caused by atom distribution along planes (0001) in NiSb and (111) in PbS is present.

It is obvious, that especially this correspondence between the structures of concerning verges is the reason of the creation of layered eutectic suprastructure.

The atom interaction of eutectic superstructures is direct physical reason, which causes the crystal accretions of these phases on the defined directions, more energetically profitable ones and supplies the high stability of interphase boundary.

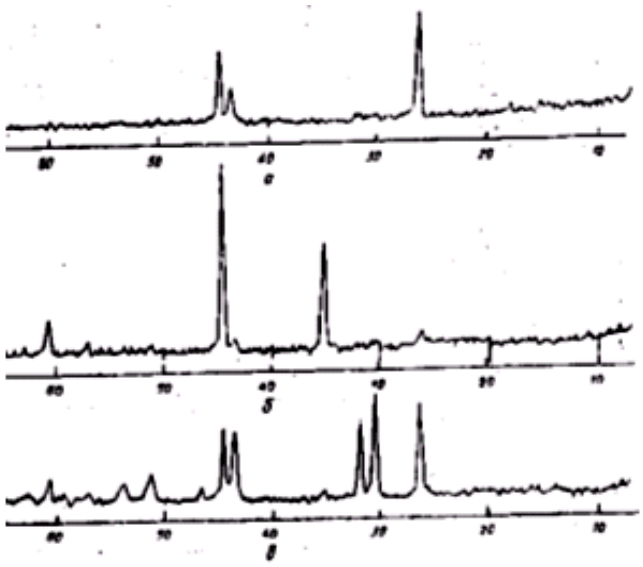

Fig.5. The diffractograms, taken on the beam directions, parallel (a) to direction of crystal growth and perpendicular (b) to plane of plate surfaces PbS and NiSb, and also diffractogram of eutectic powder (PbS-NiSb) – (c).

The investigations of possible orientation ratios in system eutectics by $A^{IV}B^{VI}$-NiSb type, carried out on the samples, directly grown eutectic of PbS-NiSb system showed, that plane (111) PbS accretes with plane (0001) NiSb in such way, that monatomic stibium layer is situated under the monatomic sulfur layer on the interphase boundary (fig.6). The lead chalcogenides and also SnTe have cubic lattices by NaCl type, differing from each other by the dimensions of elementary cell that is given in table. That's why the analogy to PbS-NiSb eutectic system it can be supposed, that such deorientation correspondence should take place between the phases in eutectics of PbSe(Te)-NiSb and SnTe-NiSb systems, i.e. the monatomic Sb layer should be situated under chalcogen monatomic layer in all eutectics of systems by $A^{IV}B^{VI}$-NiSb type.

The distances between the chalcogen atoms in direction (111) (a'), (table) had been calculated on the base of such supposition for semiconductor phases of all eutectics. The distance between Sb and NiSb atoms coincides with a parameter of elementary cell.

The circuit of interphase boundary of blocks eutectic of PbS-NiSb system in plane, perpendicular to plane of phase accreting, is given on the fig.6. The sulfur and stibium atoms are striving for the interaction and development in eutectic of high voltages. The crystal lattice of lead sulphide on boundary is situated under the influence of compression stress and crystal lattice of NiSb is situated under the influence of tensile one. The difference of parameters of phases of crystal lattices on coupling boundary (a' and a) at transfer from PbS to PbTe increases. As more this difference, the more voltage should develop on interphase boundary and the more influence should provide the creation of near boundary interaction on the connection weakening between atoms inside each eutectic phases. This supposition is well

evidenced by corresponding decrease of melting point of eutectics in the set of PbS(Se,Te) – NiSb system (table).

Table

The phase parameters, constituting the eutectics of systems by A^{IV} B^{VI} – NiSb type

The eutectic composition, mol %	T°K	α, Å	α', Å	$\Delta\alpha$, %
46 PbS	1420	5,93	4,19	6,35
54 NiSb		3,94	3,94	
68 PbSe	1170	6,147	4,44	12,7
32 NiSb		3,94	3,94	
92 PbTe	1143	6,45	4,49	13,9
8 NiSb		3,94	3,94	

Notion: $\Delta\alpha$ is difference between α' in lead chalcogenide and α in nickel antimonide.

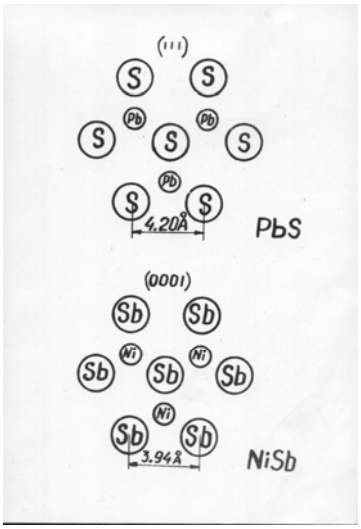

Fig.6. The circuit of atom situation on interphase boundary (111) of PbS and (0001) of NiSb planes.

The microstructure regularity should reflect on the course of periodic potential of all structure eutectic elements in total, in particular: periodic potential of one lattice should be changed by periodic potential of another lattice with some constant period for given eutectic and it is bigger than constant of lattice of each phase. The width of PbS plate is ~1800 nm, and NiSb is ~2500 nm have been considered on results of microstructure investigation, in the result of which the structure period of this eutectic is ~4300 nm (fig.1-4).

The supposition, that disparity compensation of elementary cell parameters on the boundary of phase couplings should be carried out not only by the way of the formation of dislocation grids on this boundary, but by some lattice stretching of one phase and pressing of another one, that is proved experimentally in the ref [14]. The elastic deformation of lattices is maximal one on the boundary and exponentially decreases in phase depth. Along with it, the connection weakening between atoms in near boundary region inside the phases should cause the decrease of order in the given region. That's why potential periodicity inside supramolecular formations in eutectic in the relation to that, which has the place in crystal of initial component, will significantly change.

According to above mentioned data, at eutectic crystallization of PbS-NiSb system, the (111) plane of one of its phase (97 mol.% PbS+3 mol.% NiSb) accretes with (001) of another phase (99 mol.% NiSb+1 mol.% PbS) in such way, that monatomic stibium layer is situated under monatomic sulfur layer (fig.6). In this connection the distance between Pb and S atoms is 4,2Å, between Sb atoms the distance is 3,94Å in direction, perpendicular to interphase boundary without taking consideration of elastic lattice deformation. These values of interatomic distances will be saved only in crystal center of each phase at taking under the consideration of the field of elastic deformation, about character of which has been mentioned above. The crystal lattice of solid solution on NiSb base will treat the tensile stress, and crystal lattice of solid solution on PbS base will treat compression stress (fig.7).

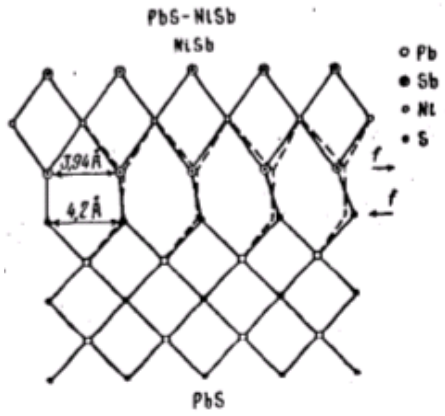

Fig.7. The circuit of possible strained PbS-NiSb eutectic in plane, perpendicular to plane of phase accretion.

The supposed change of periodic potential in eutectic of PbS-NiSb system in direction, perpendicular to plane of phase accretion, where the parameters of elementary cells of component phases with structure periods is shown on the fig.8.

The morphology analysis of plate eutectic of PbS-NiSb system allows to discuss the directed-oriented compositions as the especial class of crystal layered supramolecular systems.

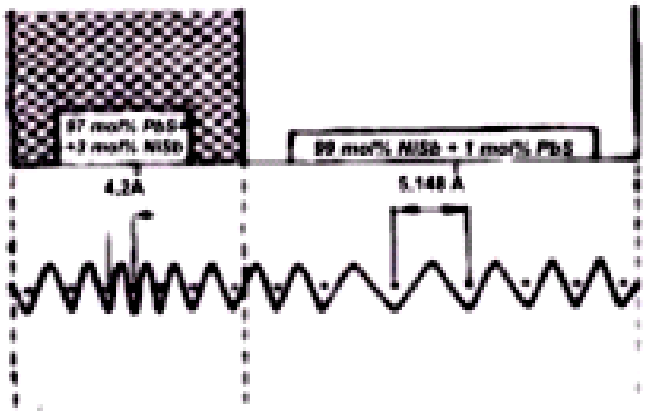

Fig.8. The schematic sketch of supposed change of periodic potential in oriented eutectic suprastructure (PbS-NiSb) in direction, perpendicular to accretion plane of suprastructures (phases).

The microstructure regularity, as we already described, should be reflected in the course of periodic potential of whole eutectic crystal in whole, and in particular: periodic potential of one lattice should be changed by periodic potential of another lattice with some period, constant for given eutectic and more bigger constant lattice of each phase.

The crystallization peculiarity and electron structure of eutectic causes the firm interphase connection, which reveal in such properties of eutectic melts as the high values of mechanical strength, plasticity, and also the microstructure stability to long heat influences.

Conclusion

The glassed eutectic is the supramolecular system, in which the redistribution of electron density, in the result of which the connection appears between the atoms of different blocks on the boundary, leading to the electron community, and connection becomes weak inside the each subblock in frontier region, takes place in the comparison with initial components.

The oriented crystal eutectic melts can be considered as solid suprastructures, in which the periodic potential of phase alternation is marked on periodic potentials of crystal lattices of each phase, that causes the unite energy structure for the electrons of whole crystal.

The totality of investigated of supramolecular eutectic compositions on A^{IV} B^{VI} base gives the possibility of their use as contact materials at the production of different sublayers for thermoelements in systems: A^{IV} B^{VI} eutectic-metal [17].

[1] *V.S. Pervov, I.D. Mikheykin, E.V. Makhonina, V.D. Butskiy*. J.Uspekhi khimii, 72(9), 2003, S.852-862.

[2] *J.M. Len.* Supramolekulyarnaya khimiya. Kontseptsii i perspektivi, Nauka, Novosibirsk. 1998.

[3] *R. Kraft.* Trans. Met., Soc. AIME, 1962, 224, n1., p.65-75.

[4] *R. Kraft.* Trans. Met., Soc, AIME, 1963, 227, n3, p.393-399.

[5] *V.M. Zalkin.* J. Fiz. khimii,1964, 38 vip.10, s.2524-2527.

[6] *V.M. Zalkin, R.E. Chigarkova, N.L. Smirnova*. Kristallografiya , 1974, 19, vip. 3, s.619-624.

[7] *R.H. Hopkins, R. Kossovsky*. Acta. Met. 1971, 19, N3, p.203-211.

[8] *I.S. Savchenko.* J. Neorgan. ximii. 1959, IV, vip. 2. s.417-423.

[9] *Ya.I. Dutchak, I.V. Kavich, I.I. Shevchuk, V.G. Siyushko*. Neorqan. materiali, 1976, 12, №4, s.589-591.

[10] *A.I. Somov, M.A. Tikhonovskiy*. Evtekticheskie kompozitsii . M.: Metallurgiya. 1975., 304 s.

[11] *Yu.N. Taran, V.I. Mazur*. Struktura evtekticheskikh splavov, M: Metallurgiya, 1978, 124 s.

[12] *K.Sh. Kakhramanov, R.M. Roshal, V.V. Didik*. Izv. AN SSSR. Neorgan. materiali, 1983. t.10, №19, s.1613.

[13] *K.Sh. Kakhramanov, R.M. Roshal, V.V. Didik*. Izv. AN SSSR. Neorgan. Materiali. 1983, t.19, №10, s.1613-1616.

[14] *L.K. Savitskaya, L.S. Derevyagina, L.M. Bitkevich, G.N. Safonova*. Izv. AN SSSR. Neorgan. Materiali. 1982, t.18. №7, s.1143.

[15] *K.Sh. Kakhramanov, G.D. Sultanov*. Izv. AN Az. SSR, Ser. Fiz-texn i mat. Nauk, 1980. №6. s.65-67.

[16] *M.I. Zargarova, K.Sh. Kakhramanov, R.M. Roshal*. Izv. AN Az. SSR. Ser. fiz. texn. i mat. Nauk, 1975. №4. s.107-109.

[17] *K.Sh. Kakhramanov, A.P. Alieva*. J. Tekhnika, Baku, AR, 2000, №4, s.82-85.

K.Ş. Qəhrəmanov, S.Ş. Qəhrəmanov, E.D. Moroydor, M.Q. Pişkin

$A^{IV}B^{VI}$-Sb (NiSb) EFTEKTİK SİSTEMLƏRDƏ SUPRAMOLEKULYAR ANSAMBLLAR

İşdə $A^{IV}B^{Vi}$-Sb (NiSb) eftektik nümunələrdə kristallizasiya proseslərini və mikrostrukturların morfoloji xüsusiyyətləri öyrənilib. Belə nəticəyə gəlmək olur ki, eftektikaların faza strukturu və onların fiziki əlaqələri molekulyar suprastruktur konsepsiyası ilə izah etmək olar.

(PbTe-Sb) və (PbS-Sb) eftektikalarda anomal, (PbS-NiSb) və (PbTe-NiSb) normal laylı suprastrukturlar almaq olur.

(PbS-NiSb) eftektik sistemində (111) PbS müstəvisi (0001) NiSb müstəvisinə paralel oriyentasiya və ölçü prinsiplərinə malik olurlar. Bu eftektikada yaranan atom defektləri real bircinsli kristallarda olan defektlərə bənzəyirlər.

К.Ш. Кахраманов, С.Ш. Кахраманов, Е.Д. Мойдор, М.Г. Пишкин

СУПРАМОЛЕКУЛЯРНЫЕ СТРУКТУРЫ НА ОСНОВЕ ЭВТЕКТИК СИСТЕМ $A^{IV}B^{VI}$ - Sb (Ni Sb)

Процессы кристаллизации и особенности морфологии микроструктуры эвтектик A^{IV} B^{VI} - S b (NiSb) свидетельствуют в пользу супрамолекулярной концепции с учетом взаимодействия субструктур.

На полученных направленно – ориентированных эвтектиках – (PbTe - Sb) и (PbS - Sb) выявлены аномальные структуры, а в эвтектиках (PbS - NiSb) и (PbTe - NiSb) - регулярные пластинчато-волокнистые.

В эвтектике (PbS - NiSb), также как и в нормальных бинарных эвтектических системах соблюдается принцип ориентационного и размерного соответствия: плоскость (111) PbS срастается с плоскостью (0001) NiSb;

Анализ морфологии эвтектики (PbS - NiSb) показал наличие различных дефектов типа сдвигов пластин, поверхностей несовпадения, искривлений блоков (пластин) и избыточной экстра - пластины. Эти дефекты аналогичны атомным дефектам, образующимся в реальных однофазных кристаллах.

Исследования показали, что эвтектики можно рассматривать как супрамолекулярные слоистые ансамбли.

Received: 20.06.06

THE INVESTIGATION OF THE ELECTRON STRUCTURE OF THE (010) GeSe SURFACE BY GREEN FUNCTION METHOD

Z.A. JAHANGIRLI

Azerbaijan Technic University,1024, Baku, H.Javid av., 25

The electron structure of (010) surface, limited by Ge atoms in the layered semiconductor GeSe has been considered on the base of Green function theory in the basis of Linear Combination of Atom Orbitals (LCAO). The electron states in the forbidden band, resonances and change of the density of energy states in crystal, connected with the defect have been discussed.

Introduction

The study of the electron structure of deep defect centers plays the important role in the understanding of electric and optic properties of semiconductors. It is shown, that the electron properties of semiconductor devices are especially sensitive to the character of the different defects and their concentration. Last years, Green function method is the one of the main methods of the defect studying with deep energy level, electron structures of the point defects and semiconductor surfaces.

The semiconductor compound GeSe is related to the layered semiconductors by A^4B^6 group [1-5]. The layered structure of the crystals, caused by anisotropy in chemical connections of atoms, from which the quazi-two-dimensional crystal lattice is built, is the main their peculiarity. The unit cell consists from the two layers, each layer includes two molecules, where the atoms of the neighbor layers are connected by weak Van-der-Waals forces between themselves and as the result, some physical properties of these crystals have two-dimensional character. In this work the electron structure of (010) surface, limited by Ge atoms of semiconductor compound GeSe is calculated by Green function method.

The crystal structure [4], electron structure and optical properties [6,7] of GeSe compound are well studied.

Green function method.

Green function method is well described in [8]. Here we give the main equations of this method. Let's H_0 is effective one-electron Hamiltonian of ideal crystal, U is defect potential, and $H=H_0+U$ is Hamiltonian of perturbed system. Then, the one-particle Green operator of ideal crystal

$$G^0(E) = \lim_{\varepsilon \to 0+} (E + i\varepsilon - H^0)^{-1}$$

And Green operator of perturbed system

$$G(E) = \lim_{\varepsilon \to 0+} (E + i\varepsilon - H)^{-1}$$

Are connected between each other by Dawson equation:

$$G = G^0 + G^0 U G$$

The formal solution of this equation for G is:

$$G = (1 - G^0 U)^{-1} G^0$$

The energy levels of perturbed system correspond to poles of G function. We obtain the following for the levels in the forbidden band:

$$[1 - G^0(E)\, U]\ \Psi = 0,$$

Ψ is wave function of perturbed system. The connected states correspond to determinant zero:

$$D(E) = Det\,||\, 1 - G^0 U\, ||\, = 0.$$

The change of the density of electron states is defined by the formula:

$$\Delta N(E) = \frac{1}{\pi} \frac{d\delta(E)}{dE},$$

Here,

$$\delta(E) = -\tan^{-1} [ImD(E)/ReD(E)]$$

Energy levels of connected states.

The LCAO, constructed from *s*- and *p*-orbitals was used for the definition of band structure of ideal crystal and then the same set was used for the calculation of localized states. The values of resonance integrals were taken from [9]. Further, these data became better by the way of the picking out of our results on the band structure with the previous calculations and with experiment data on photoemission [10].

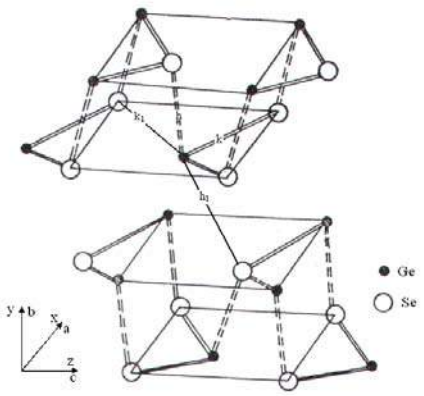

Fig. 1. Unit cell of GeSe-type compounds.

In calculations we took under consideration the contributions of only first four neighbors. The unit cell of the compounds by GeSe type is shown on the fig.1. *Y* axis is perpendicular to the crystal layers. The two-dimensional cell for (010) surface has one Ge atom and one Se atom in each layer. The

calculation results of projected band structure GeSe (PBS is E_{nk} projection of infinite crystal with $k=(q, k_{\perp})$ for each q in two-dimensional 3B) are shown on the fig.3. The projected valency band consists from three groups in the correspondence with photoemission spectrum [10]. The lowest group, situated in energy interval –14-15 eV, is far from others by wide energy gap and it comes from *s*-states (Se 4*s*). The next group in 6-8 eV interval comes from 4*s*-states of Ge and 4*p*-states of Se. The upper group of PBS mainly comes from *p*-states of Se and in lesser extent comes from *p*-states of Ge, at the same time the situation is vice versa for the six lowest conduction bands.

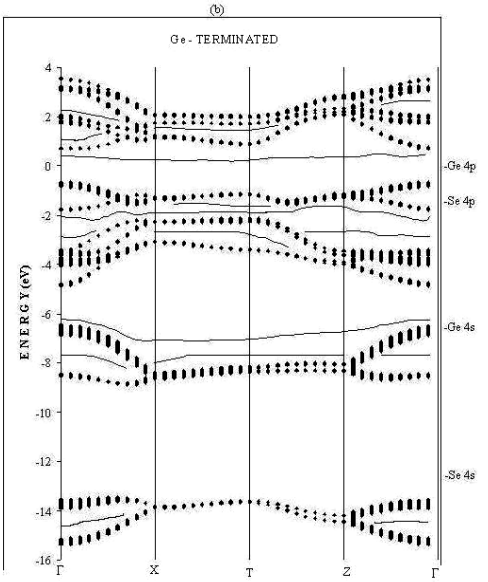

Fig.2. Projected bulk band structure and surface band structure for the Ge- terminated (010) surface of GeSe

In GeSe crystal the two nearest neighbors of cation (anion) situate on the one crimped plane, third nearest neighbor situates on the next crimped plane (010), that's why it is enough to delete plane having the cation (anion) with taking into consideration of interaction deposit of fourth nearest neighbor for the creation of the free surface. The one plane, having Se atoms, is deleted, the surface, limited by Ge atoms, is created. The chinks and "pockets", where it is need to calculate the localized states is well seen on the fig.2. The existence conditions of localized state ([8], (B1)]).

$$D(E) = Det|| G^{0}_{m,m`} || = 0 ,$$

Where indexes *m* and *m'* run on the *s*- and *p*-orbitals of the atom of deleted level. The surface band structure and localized states are shown on the fig.2. The amplitudes of wave functions, summed on *s*- and *p*-orbitals for the some surface levels for first ten layers with the help of formula ([8], (28)]) are shown on the fig.3.

$$f^{m}_{sq}(E_s) = \sum_{\alpha} || A^{m,\alpha}_{s,q}(E_s)|| .$$

The presence of the surface leads to the appearance of localized levels in forbidden band, and in permitted band the density of energy states changes. The local state density, the change of local state density, total change of state density on the first seven layers for the surfaces, limited by Ge atoms, are shown on the fig.4. It is seen from the figure, that in practices all surface states are strongly localized and in practices after third layer the local state density becomes an identical one with density of electron states of infinite crystal.

The common changes of local state density for each layer, where the resonances, anti-resonances and localization of wave function for each case are well seen, are shown on the fig.4. As it is seen from the fig.2 the surface states near –14,5 eV and –7,5 eV, which are localized in the limits of two layers and come from valency states, are present. Besides, two surface states near s-states of Ge near –7 eV are present. This shows that the character and energy situation of many surface states depend on atom nature on the first level.

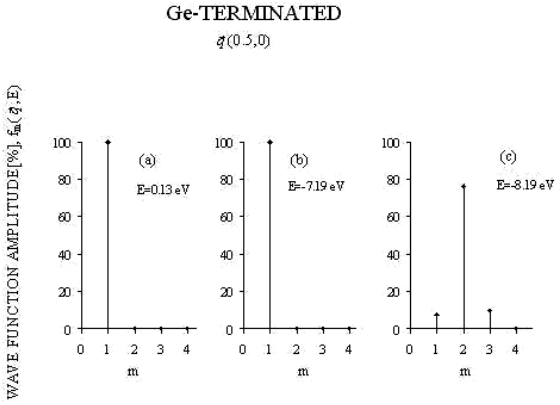

Fig.3. Wave-function amplitudes summed over the *s*- and *p*-orbitals as a function of the layer number for surface states for the Ge- terminated (010) surface of GeSe

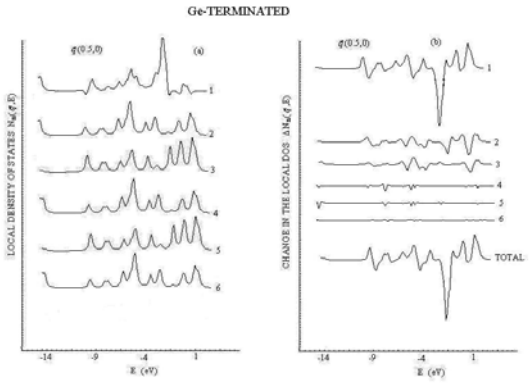

Fig. 4. (a)- Local densities of states at each of the first six layers for the Ge- terminated (010) surface of GeSe at the symmetry point *X* of the surface Brillouin zone
(b)- The changes in local density of states at each of the first six layers

The orbital situation of amplitudes of wave functions, the dependence of local densities of energy states on the level numbers show, that surface state near –7 eV is localized in the limits of three layers and is formed from s- and формула-orbitals. This well corresponds with the fact, that valency band near –7 eV mainly comes from cation states. As it is seen from the fig.2 in forbidden band the one almost dispersion-free localized state takes place. We have been integrated $\Delta N(E)$ in $q(0.5, 0.0)$ on projected valency band for the occurrence investigation,

$$\int_{E_{bot}}^{E_{top}} N(E)dE = \frac{2}{\pi}\left[\delta\left(E_{top}\right) - \delta\left(E_{bot}\right)\right],$$

Where E_{bot} and E_{top} are bottom and top of valency band. We have been revealed, that the one state in conduction band is chipped off in the forbidden band because of the presence of the surface. This shows, that local state in forbidden band comes from conduction band. The orbital situation of amplitudes of wave functions of this state shows, that this state mainly is p_z - typed one with small *s*-typed impurity and does as the connecting bridge between atoms of neighbor layers and totally is localized in surface plane.

Conclusion.

The electron structure of (010) surface, limited by Ge atoms in layered semiconductor GeSe has been considered on the base of Green function theory in basis of Linear Combination of Atom Orbitals. The calculation results show, that the presence of the surface leads to the appearance of one surface level in fundamental forbidden band. It is established, that this level is totally localized in surface plane, is p_z -typed level with small *s*-typed impurity and connects atoms of neighbor planes. Besides, the $\Delta N(E)$ -change of density of electron states, inducted by defect, and also the resonances and antiresonances, connected with surface presence, have been calculated.

[1] *N.Le. Nagard, C.Levy-Clement, A. Katty*. R.M.A. Lieth., Material Research Bulletin, 1990, v 25, Issue 4, p. 495.

[2] *P.K.Dwivedi, S.K. Tripathi, A. Pradhan, V.N. Kulkarni, S.C. Agarwal*. Journal of Non-Crystalline Solids, 2000, Volumes 266-269, Part 2, p. 924.

[3] *P.Petkov, S. Parvanov, C. Vodenicharov*. Materials Letters, 1999, v. 41, p. 27.

[4] *Okazaki*. J. Phys. Soc. Japan ,1958, v. 13 N 10, p. 1151.

[5] *T. Grandke and L. Ley*. Phys. Rev. B, 1977, v. 16 N 2 p. 832.

[6] *.G Valiukonis, F.M. Gashimzade, D.A. Guseinova, G. Krivaite, A.M. Kulibekov, G.S. Orudzhev and A. Sileika*. Phys. Status. Solidi b 117, 1983, p. 81.

[7] *.R Eymard, A. Otto*. Phys. Rev.B 16 ,1977, p. 1616.

[8] *J. Pollmann and T. Sokrates*. Pantelides, Phys. Rev. B 18 ,1978, p. 5524.

[9] *E. P.O'Reilly*. J. Phys. C: Solid State Phys., 1982, p. 151449.

[10] *P. Kemeny, J. Azoulay, M. Cardona et al.* Nuovo Cimento ,1977, v.39B, N2, p. 709

Z.A. Cahangirli

QRİN FUNKSİYASI METODU İLƏ GeSe YARIMKEÇİRİCİSİNİN SƏTH ELEKTRON STRUKTURUNUN HESABLANMASI

Qrin funksiyası nəzəriyyəsi vasitəsilə Atom Orbitallarının Xətti Kombinasiyası bazisində GeSe laylı kristalının Ge atomları ilə məhdudlaşan (010) səthinin elektron quruluşu təyin edilmişdir. Qadağan zolağında yerləşən enerji səviyyəsi, rezonanslar və defektin təsirilə enerji səviyyələri sıxlığının dəyişməsi müzakirə olunmuşdur.

З.А. Джахангирли

РАСЧЕТ ЭЛЕКТРОННОЙ СТРУКТУРЫ ПОВЕРХНОСТИ В GeSe МЕТОДОМ ФУНКЦИИ ГРИНА

На основе теории функции Грина в базисе линейной комбинации атомных орбиталей (ЛКАО) рассмотрена электронная структура поверхности (010), ограниченная атомами Ge в слоистом полупроводнике GeSe. Обсуждены электронные состояния в запрещенной зоне, резонансы и изменение плотности энергетических состояний в кристалле, связанные с дефектом.

Received: 28.06.06

EXACT SOLUTION OF WZNW MODEL

M.A. MUKHTAROV
Institute of Mathematics and Mechanics
370602, Baku, F.Agaev str. 9, Azerbaijan

One dimensional reduction of WZNW is integrated in the case of $A_1(SL(2,C)$ algebra.

1. The problem of constructing of the solutions of integrable models and its dimensional reductions, the one dimensional WZNW model in our case, in the explicit form remains important for the present time. The interest arises from the fact that almost all integrable models in one, two and (1+2)-dimensions are symmetry reductions of SDYM or they can be obtained from it by imposing the constraints on Yang-Mills potentials [1-13].

This work is a direct continuation of [14-16], where the exact solutions have been derived by discrete symmetry transformation method that allows generating new solutions from the old ones in much more easier way than applying methods from [11]. The Lax pair presentation of the model under consideration is the first step in this program [16] that we hope will give us a key to construct solutions for an arbitrary semisimple algebra.

2. The one dimensional reduction of self duality equations obtained in [11] is the equation for the element f, taking values in the semisimple algebra,

$$\frac{\partial^2 f}{\partial r^2}+\frac{\partial f}{\partial r}-[H,[H,f]]-2[X^-,[X^+,f]]-2[X^+,[X^-,f]]+ \\ +2[[\frac{\partial}{\partial r}-H,f],[X^+,f]]=0 \tag{1}$$

Here $H, X^{\pm}$ are generators of $A_1(SL(2,C)$ algebra

$$\left[X^+,X^-\right]=H,\left[H,X^{\pm}\right]=\pm 2X^{\pm} \tag{2}$$

embedded to gauge algebra in the half-integer way.

The equation (1) has been reduced [16] to the following form:

$$\frac{\partial}{\partial\tau}(\frac{\partial q}{\partial\tau}q^{-1})=[qF_0q^{-1},X^+] \tag{3}$$

Equation (2) is one-dimensional WZNW (Wess-Zumino-Novikov-Witten) equation [17-19].

We'll deal with the presentation of the equation under consideration in the form (1) and in the simplest case of f taking values in the algebra $A_1(SL(2,C)$:

$$f=xX^-+yH+zX^+, \tag{4}$$

where generators $H, X^{\pm}$ satisfy the same commutational relations (2).

Then the equation (1) can be rewritten for the components of (4) as the system of three nonlinear one dimensional second order equations, the general solution of which has to be dependent on six constants.

The system of equations has the form:

$$\begin{cases} x''+x'-2xx'-2x^2-2x=0 \\ y''+y'-2yx'-2yx-2y=0 \\ z''+z'+2z'x-2yz-2z+4yy'=0 \end{cases} \tag{5}$$

Consider the first equation of the system (5) representing it in a form:

$$(x'+2x+1)'-2x(x'+2x+1)=0 \quad \text{or} \quad \frac{\partial}{\partial\tau}\ln(x'+2x+1)=2x$$

Introducing new unknown function $u=\ln(x'+2x+1)$ we have:

$$u'=2x;\ u''+u'=2(x'+2x+1)-2=2e^u-2$$

Making again the change of variables: $u_1=u+2\tau$ we simplify last equation:

$$u_1''+u_1'=2e^{u_1-2\tau}$$

and after the substitution $t=e^{-\tau}$ we come to one-dimensional Liuville equation

$$\ddot{u}_1=2e^{u_1}$$

Multiplying both sides of the last equation by $\dot{u}_1$

$$\dot{u}_1\ddot{u}_1 = 2\dot{u}_1 e^{u_1}; \quad \frac{d}{dt}(\dot{u}_1)^2 = 4\frac{d}{dt}e^{u_1}$$

and integrating once, we have

$$\dot{u}_1 = 2\sqrt{e^{u_1} + k^2},$$

where k is a constant.

The second integration gives the following:

$$t - c = \int \frac{du_1}{2\sqrt{e^{u_1} + k^2}} = -\frac{1}{k}\int \frac{dw}{\sqrt{1+w^2}} = -\frac{1}{k}\left(w + \sqrt{1+w^2}\right),$$

where $w = ke^{-\frac{u_1}{2}}$.

Using all above introduced notation we have:

$$e^{u_1} = \frac{k^2}{sh^2(kt+c)}$$

and using the relations $t = e^{-\tau} = e^{-\ln R} = R^{-1}$ and $e^{u_1} = e^{u+2\tau} = R^2 e^u$, we eventually have the relation:

$$e^u = \frac{k^2}{R^2 sh^2\left(kR^{-1}+c\right)}$$

Taking into account the relation

$$x = \frac{1}{2}u' = \frac{1}{2}R\frac{du}{dR}$$

we derive the solution of the first equation of the system under consideration:

$$x = -1 + cth\left(kR^{-1}+c\right) \tag{6}$$

Let's rewrite the second equation of the system (5) in the form:

$$y'' + y' = 2(x' + 2x + 1) = 2ye^u$$

and introducing the same, as in first equation, variables (t, u_1), we have:

$$\ddot{y} = 2y\frac{k^2}{R^2 sh^2\left(kR^{-1}+c\right)} \text{ or}$$

$$\frac{d^2y}{dr^2} = 2y\frac{1}{sh^2 r}, \tag{7}$$

where $r = kR^{-1} + c$.

From the general theory of linear equations it follows that the Wronskian of two solutions of the equation (7) is a constant, that is if y_1 and y_2 are solutions of (7) then

$$W(y_1, y_2) = \det\begin{pmatrix} y_1 & y_2 \\ y_1' & y_2' \end{pmatrix} = c_1 \tag{8}$$

If one knows one partial solution of (7), saying y_1, then second solution can be obtained via the following relation:

$$y_2 = c_1 y_1 \int (y_1)^{-2} dr + c_2 y_1 \tag{9}$$

The equation (7) has the solution $y_1 = cthr$. Substituting it to (9) and making the corresponding integration, we come to the general solution of equation (7):

$$y_1 = c_1 cthr + c_2(rcthr - 1),$$

or in terms of original variables:

$$y_1 = c_1 cth\left(kR^{-1}+c\right) + c_2\left(kR^{-1}cth\left(kR^{-1}+c\right) - 1\right) \tag{10}$$

Consider the homogeneous part of the first equation of the system (5):

$$z'' + z' + 2z'x - 2yz - 2z = 0$$

Rewriting it in a form

$$(z' - z)' + 2(z' - z)(x+1) = 0$$

or

$$\frac{d}{dR}\left(R\frac{d}{dR}z - z\right) = -\frac{2}{R}(x+1) = -\frac{2k}{R^2}\,cth\left(kR^{-1}+c\right).$$

Here we used the expression for x from (6).

The first integration gives the equation:

$$R\frac{d}{dR}z - z = c_3 sh^2\left(kR^{-1}+c\right),$$

the second one gives the required solution:

$$z = \frac{c_3}{2k}\left(1 - \frac{R}{2}sh2\left(kR^{-1}+c\right)\right) + c_4 R$$

and the solution of the whole equation, whose inhomogeneous part is defined by the known solution y of the second equation of the system, is given by the following expression:

$$z = \frac{c_3}{2k}\left(1 - \frac{R}{2}sh2c\right) + c_4 R +$$

$$+ \frac{c_1^2}{2k} Rth\left(kR^{-1} + c\right) + 2c_1 c_2 th\left(kR^{-1} + c\right) + c_2^2 (kR^{-1} th\left(kR^{-1} + c\right) - 1)$$

As the solution of the system of three second order ordinary differential equations depends on six arbitrary constants, this solution is the general one.

Comparison of the solutions obtained with that ones obtained by means of Riemann-Hilbert problem is the subject of further publications.

[1] *R.S. Ward, Phil. Trans.* R. Soc. Lond.A315, 451 (1985); Lect. Notes Phys., 1987, 280, 106; Lond. Math. Soc. Lect. Notes Ser., 1990, 156, 246.

[2] *L.J. Mason and G.A. J.Sparling.* Phys. Lett., 1989, A137, 29; J. Geom. and Phys., 1992, 8, 243.

[3] *S. Chakravarty, M.J. Ablowitz and P.A. Clarkson.* Phys. Rev. Lett., 1990, 1085.

[4] *I. Bakas and D.A. Depireux.* Mod. Phys. Lett., 1991, A6, 399.

[5] *M.J. Ablowitz, S. Chakravarty and L.A. Takhtajan.* Comm. Math. Phys., 1993, 158, 1289.

[6] *T.A. Ivanova and A.D. Popov.* Phys. Lett., 1992, A170, 293.

[7] *L.J. Mason and N.M.J. Woodhouse.* Nonlinearity 1, 1988, 73; 1993, 6, 569.

[8] *M. Kovalyov, M. Legare and L. Gagnon.* J. Math. Phys., 1993, 34, 3425.

[9] *M. Legare and A.D. Popov.* Pis'ma Zh. Eksp. Teor. Fiz., 1994, 59, 845.

[10] *A.A. Belavin and V.E. Zakharov.* Phys. Lett., 1978, B73, 53.

[11] *A.N. Leznov and M.A. Mukhtarov.* J. Math. Phys., 1987, 28 (11), 2574; Prepr. IHEP, 1987, 87-90. Prepr. ICTP 163, Trieste, Italy, 1990; J. Sov. Lazer Research, 13 (4), 284, 1992.

[12] *A.N. Leznov.* IHEP preprint-92/87, 1990.

[13] *A.N. Leznov, M.A.Mukhtarov and W.J.Zakrzewski.* Tr. J. of Physics 1995, 19, 416.

[14] *M.A.Mukhtarov.* Fizika, 2002, v. 5, N 2, 38

[15] *M.A.Mukhtarov.* Fizika, 2002, v. 5, N 3, 3

[16] *M.A.Mukhtarov.* Fizika, 2005, v. 8, N 2, 40

[17] *V.G. Knizhnik and A.B. Zamolodchikov*, Nucl. Phys. B247 (1984) 83.

[18] *F. Bastianelli*, Nucl. Phys. B361 (1991) 555.

[19] *F. Bastianelli*, Nucl. Phys. B361 (1991) 555.

[20] *A.A. Tseytlin*, Nucl. Phys. B411 (1994) 509.

M.A. Muxtarov

WZNW MODELİNİN DƏQİQ HƏLLƏRİ

SL(2,C) cəbri halında WZNW modelinin birölçülü reduksiyası inteqrallanmışdır.

М.А. Мухтаров

ТОЧНЫЕ РЕШЕНИЯ МОДЕЛИ WZNW

Одномерная редукция модели WZNW проинтегрирована в случае алгебры SL(2,C)

Received: 18.09.06

ON STRUCTURE OF VALENCY BAND IN SEMICONDUCTOR MELTS $Bi_{1-x}Sb_x$

B.A. TAIROV, A.G. RAGIMOV, S.Z. DAMIROVA
Institute of Physics of Azerbaijan of National Academy of Azerbaijan
Az-1143 Baku, H.Javid av., 33

On the base of the investigations of all independent galvanomagnetic coefficients in semiconductor melts $Bi_{1-x}Sb_x$ at 77-300K, the kinetic parameters of all types of charge carriers have been defined.

It is established, that new hole ellipsoids in the comparison with hole and electron ones in basis plane are less elliptic, than in binary and bisector planes.

The galvanomagnetic effects are easily measured already at fields of order of oersted parts because of very high mobility of charge carriers in $Bi_{1-x}Sb_x$. That's why in refs [1, 2], dedicated to the investigations of electron properties of these materials, the galvanomagnetic phenomenon were used for the development of the presentations about the character of their energetic spectrum. In the result of set theoretic [3,4] and experiment [5,6,7,8] refs the main characters of reconstruction of band structure of energetic spectrum in $Bi_{1-x}Sb_x$ at x composition change in $x \leq 30$ at.% region had been revealed. In some region $Bi_{1-x}Sb_x$ composition has the semiconductor properties. This region at T=4,2K longs from $x \leq 0.06$ at.% till 0.25 at.%, and at T=77K $0.07 \leq x \leq 0.20$; this region disappears totally at $T>180$ with temperature growth.

The band structure changes with the composition change so strongly, that melts, the compositions of which differ on 1at.%, it is need to consider as significantly different materials with different parameters, peculiar to them, so as effective mass, relaxation time of impulse and energy, the distribution of charge carriers on energetic data.

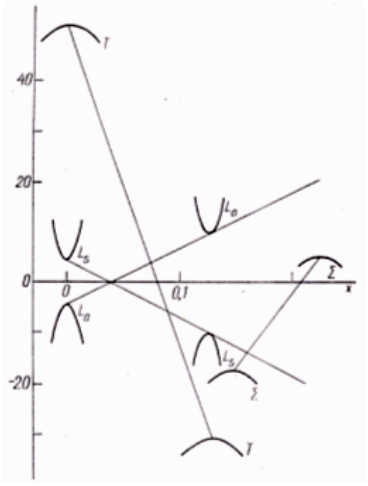

Fig.1. The scheme of reconstruction of energetic spectrum of bismuth-stibium melts at increase of stibium concentration.

From the reconstruction scheme of energetic spectrum of charge carriers of melt $Bi_{1-x}Sb_x$ on stibium [9] concentration of semiconductor melts of $0.15 \leq x \leq 0.22$ composition, presented on the fig.1., it is followed, that minimal energetic chink is defined by La and ∑ terms. However, La deposit of electrons in galvanomagnetic effects is so big in unalloyed melts, that it is difficult to study the structures of valency band. That's why, it is possible to obtain the information about structure of valency band of ∑ Brillouin, situating in formula, picking up the stibium content from the above mentioned interval and concentration of doped acceptor impurity of tin. The different parameters $Bi_{1-x}Sb_x$ were measured on the base of galvanomagnetic measurements at the temperature of liquid nitrogen [10, 11].

The new hole band, the extremum of which is in ∑ point, begins to play at further increase of stibium content.

Thus, in given ref the measurements of all independent galvanomagnetic coefficients at temperatures T=77-300K were carried out for the revealing of actuality of all these bands in transfers phenomenon and establishment of the form of isoenergetic surfaces in $Bi_{1-x}Sb_x$ melts with stibium content higher, than 15 at.%.

It is need to note, that above mentioned coefficients correspond to conditions of weak magnetic field. For the obtaining of such values the dependence of corresponding galvanomagnetic coefficient on the field is always taken. Moreover, the condition of weak magnetic field, i.e. the independence of coefficients R_{ikl} and $\rho_{ik,lm}$ on field, was checked. In many cases, however, the conditions of weak magnetic field are carried out at its tensity of order of one oersted and even, its parts because of very high values of mobility components and that's why it is need to take its value, obtained by extrapolation of the dependence to the zero field for the value of galvanomagnetic coefficient in weak field. The limit of weak magnetic field is different for different coefficients, and its change allows us to follow qualitatively for the change of energetic spectrum of charge carriers.

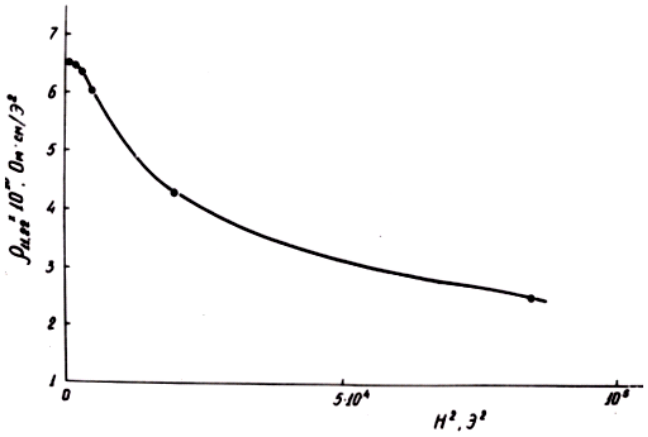

Fig.2. The dependence of magnetoresistance coefficient $\rho_{11,22}$ on H^2 for $Bi_{0,08}Sb_{0,20}$ melt at 77K.

The field dependences of coefficient of магнетосопротивление of $\rho_{11.22}$ on H^2 for $Bi_{0,08}Sb_{0,20}$ melt at 77K are shown on the fig.2.

The temperature dependencies of two components of specific resistance of $Bi_{1-x}Sb_x$ melts with different stibium content are shown on the figures 3 and 4.

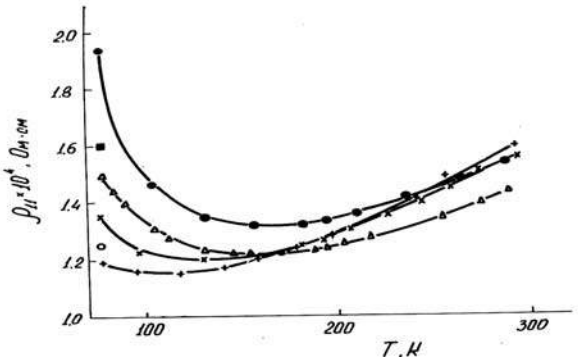

Fig.3. The temperature dependence of specific resistance ρ_{11}:Δ--$Bi_{0.92}Sb_{0..8}$
● $Bi_{0.84}Sb_{0.16}$ ⊕ $Bi_{0.82}Sb_{0.18}$
x -$Bi_{0.80}Sb_{0.20}$ ○ $Bi_{0.78}Sb_{0.22}$
\+ -$Bi_{0.75}Sb_{0.25}$.

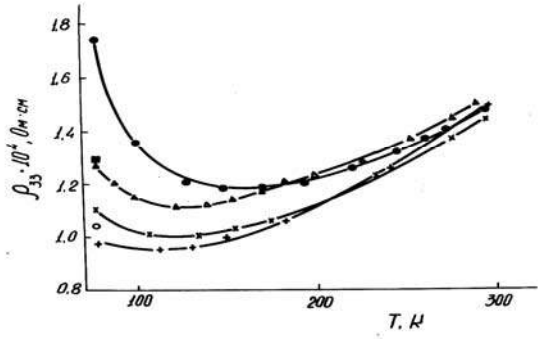

Fig.4. The temperature dependence of specific resistance . ρ_{33}: Δ--$Bi_{0.92}Sb_{0.08}$
● $Bi_{0.84}Sb_{0.16}$ $Bi_{0.82}Sb_{0.18}$
x -$Bi_{0.80}Sb_{0.20}$ ○ $Bi_{0.78}Sb_{0.22}$
\+ -$Bi_{0.75}Sb_{0.25}$

It is need to note, we can't judge about the value of width of forbidden band in $Bi_{1-x}Sb_x$ melts on the dependencies by type $ln\sigma \sim f(1/T)$, i.e. not only the width itself changes with temperature, but the participation in transfer of different actual extremums.

The temperature dependencies of components of Hall coefficient R_{231} and R_{123} for melts with 0,16%at are presented on the following figures 5 and 6.

As it is seen from the figures, both components of Hall coefficient for $Bi_{1-x}Sb_x$ melts of all investigated compositions significantly decrease with temperature. Such decrease evidences about concentration growth of current carriers. However, the conductivity of $Bi_{1-x}Sb_x$ melts in investigated temperature interval and changes of Hall coefficient can be connected with the change of ratio of mobility of electrons and holes. That's why the temperature change of components of Hall coefficients can't be quantitatively characterize the concentration change of charge carriers without calculations according to model of energetic spectrum. The carried out calculations will be in the next.

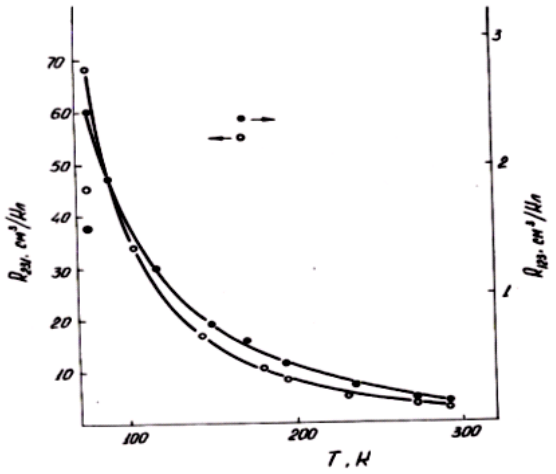

Fig.5. The temperature dependence of Hall R_{ijk} coefficients for $Bi_{0.84}Sb_{0.16}$ melt (separate points R_{ijk} at 77K for melt $Bi_{0.82}Sb_{0.18}$).

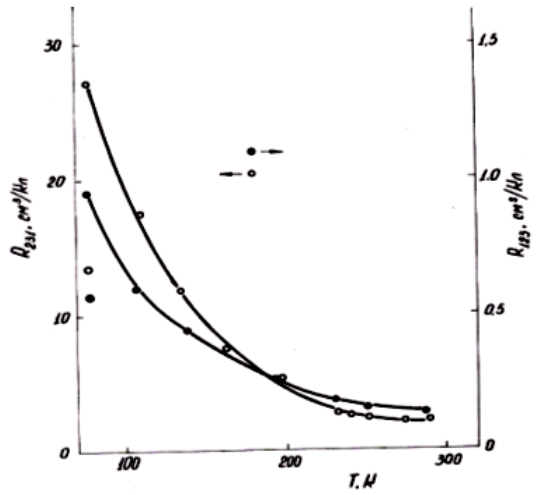

Fig.6. The temperature dependence of Hall R_{ijk} coefficients for $Bi_{0.80}Sb_{0.20}$ melt (separate points R_{ijk} at 77K for melt $Bi_{0.78}Sb_{0.22}$).

The temperature change of magnetoresistance $\rho_{11,22}$, $\rho_{11,33}$, $\rho_{11,11}$ and $\rho_{33,11}$ and $\rho_{33,33}$ for $Bi_{1-x}Sb_x$ melts with different stibium content are shown on the following figures 7,8,9.

The change character of all components of magnetoresistance with temperature stays constant.

It should be evidenced qualitatively about the saving of relations of mobility of electrons and holes. Indeed, the magnetoresistance is depended as on participation of different types of carriers in transfer phenomenon, so on ratios of components and their motilities in different crystallographic directions at participation of many-valley band structure. At the same time, if we propose, that ratios between components of mobility of separate groups of charge carriers don't change with temperature, the extremums of valency band and conduction band for transfer phenomena stay the same, and also the ratios of mobility of charge carriers don't change, so change dependencies with temperature of all components of magnetoresistance should be strongly similar.

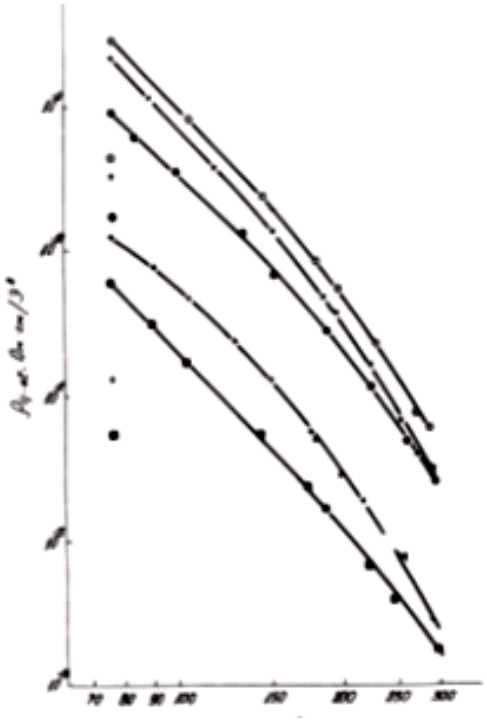

Fig.7. The temperature dependence of magnetoresistance coefficient $\rho_{ij,kl}$ of $Bi_{0.84}Sb_{0.16}$ melt (separate points $\rho_{ij,kl}$ at 77K for $Bi_{0.78}Sb_{0.22}$ melt) o- $\rho_{11.22}$, x -$\rho_{11.11}$, ●-$\rho_{33.11}$, + - $\rho_{11..33}$ ⊕ - $\rho_{33.33}$.

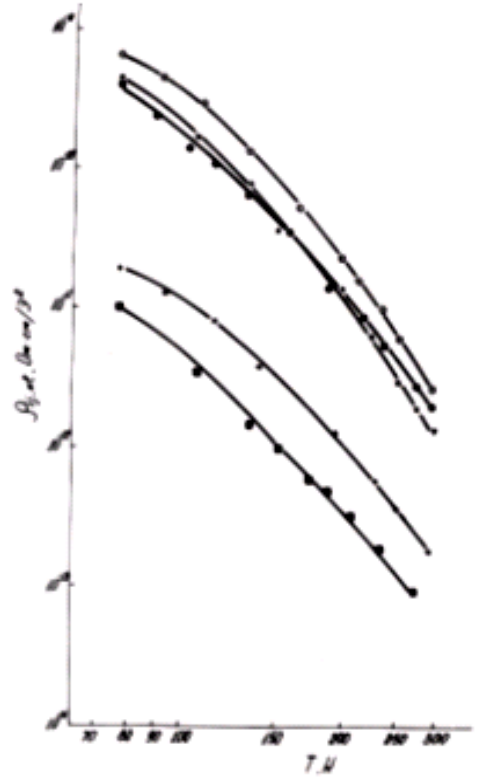

Fig.8. The temperature dependence of magnetoresistance coefficient $\rho_{ij,kl}$ of $Bi_{0.80}Sb_{0.20}$ melt, o - $\rho_{11.22}$, x -$\rho_{11.11}$, ●-$\rho_{33.11}$, +- $\rho_{11..33}$, ⊕ - $\rho_{33.33}$.

The components of Hall coefficients will be changed analogically to this. This gives the foundation on qualitative conclusion about weak change of all mentioned parameters in semiconductor melts $Bi_{1-x}Sb_x$ in interval 77-300K. The more detail data have been obtained on the base of quantitative calculations, which will be given further.

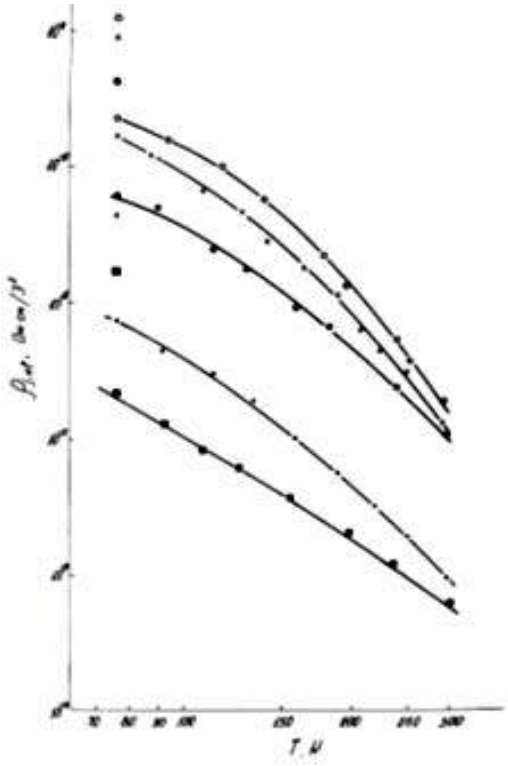

Fig.9. The temperature dependence of magnetoresistance coefficient $\rho_{ij,kl}$ of $Bi_{0.75}Sb_{0.25}$ melt (separate points $\rho_{ij,kl}$ at 77K for $Bi_{0.82}Sb_{0.18}$ melt) o- $\rho_{11.22}$, x -$\rho_{11.11}$, ●-$\rho_{33.11}$, + - $\rho_{11..33}$, ⊕ - $\rho_{33.33}$.

The ratios between components of tensors of galvanomagnetic coefficients of electron and hole mobilities, and also their concentrations, defined by model of energetic spectrum [12] were used for the quantitative interpretation of experimental results of galvanomagnetic properties $Bi_{1-x}Sb_x$ above mentioned. Such interpretation allows from the one side in the agreement of experimental and calculated values to judge about rightness of choice of energetic spectrum model and from another one to judge about change character of spectrum parameter, i.e. the component of tensor mobility is characterized by corresponding components of tensor effective mass with taking under consideration anisotropy of relaxation time or supposition of its anisotropy. From the above mentioned it is followed, that the model, presenting Fermi surface of electrons in three ellipsoids of common type, easily inclined relatively trigonal axis and transferring into each other at the turn on 120°C round this axis and situating in L in 3B point, was accepted by us for the interpretation of galvanomagnetic properties of $Bi_{1-x}Sb_x$ ($0.15 \le x \le 0.25$) melts. The Fermi surface of holes is presented by three or six ellipsoids of common type, inclined relatively trigonal axis and situated in ∑ and H 3B points.

Thus, for the actual phenomena of the phenomenon of transfer of carriers of all these bands and establishment of form of isoenergetic melt $Bi_{1-x}Sb_x$ (x=0,14-0,25)surface, measurements of all independent coefficients at temperatures T=77-300K were carried out.

The values of experimental and calculated values of galvanomagnetic coefficients for $Bi_{1-x}Sb_x$ melts with stibium content 0.16÷0.25 at.% at temperature 77K are given in table 1. As it is seen from the table, for all melt compositions the experimental and calculated values are in good state. The calculation was in such set of components of mobilites and concentrations, which supplied the best agreement of experimental and calculated values (table 2). As it is seen from the table 2 in the ration of hole components ∑ is equal to ν_2/ν_1=0,05, ν_3/ν_1=0,5 in all investigated melt compositions $Bi_{1-x}Sb_x$ (x=0.16, 0.25).

It is need to note, that analogical calculations were carried out in the refs [14,15].

In the ref [16] on the base of investigations of dispersion of electromagnetic magnetoplasma waves and galvanomagnetic effects it is established, that for L-electrons the ratios of mobility components is μ_2/μ_1=0,0001, μ_3/μ_1=0,7 and for L-holes one is ν_2/ν_1=0,009, ν_3/ν_1=0,7.

Table 1

The values of experimentally obtained and calculated galvanomagnetic coefficients in melts $Bi_{1-x}Sb_x$ at T=77K (ρ_{11}, ρ_{33} were measured with delicacy 3%, ρ_{123}, ρ_{231}-5%, $\rho_{11,22}$-10%, $\rho_{11,11}$ and $\rho_{33,11}$-15%, $\rho_{11,33}$ and $\rho_{33,33}$-20%; dimension is $\alpha_{ij.kl}$ –$\Omega^{-1}\cdot cm^{-1}$).

At,% Sb		σ_{11} 10^{-3}	σ_{33} 10^{-3}	σ_{231} 10^{-9}	σ_{123} 10^{-8}	
016	exp.	5,15	5,70	200	0,68	
	calc.	4,87	6,10	2,06	0,60	
018	exp.	6,25	7,80	2,20	0,58	
	calc.	6,03	7,70	2,26	0,59	
020	exp.	7,40	9,10	1,82	0,53	
	calc.	7,10	8,90	1,90	0,53	
022	exp.	7,94	9,60	1,28	0,34	
	calc.	7,53	9,38	1,38	0,31	
025	exp.	8,10	10,20	0,69	0,21	
	calc	7,27	9,10	0,86	0,19	
at,% Sb		$\sigma_{11,33}$ 10^{-12}	$\sigma_{33,11}$ 10^{-14}	$\sigma_{11,11}$ 10^{-14}	$\sigma_{11,22}$ 10^{-14}	$\sigma_{33,33}$ 10^{-12}
016	exp.	34,00	10,70	5,84	14,20	19,30
	calc.	39,00	14,30	5,10	15,6	20,00
018	exp.	17,50	10,30	3,55	11,1	10,50
	calc.	23,81	11,90	4,21	12,8	12,00
020	exp.	11,00	7,50	2,62	7,85	8,00
	calc.	23,17	7,20	2,60	7,85	7,00
022	exp.	8,60	2,90	1,74	4,30	5,72
	calc.	10,60	3,50	1,26	3,83	7,23
025	exp.	5,30	1,16	1,01	1,97	2,23
	calc	4,35	1,47	0,53	1,60	2,98

Table 2

The kinetic parameters of charge carriers for $Bi_{1-x}Sb_x$ melts at T=77K.

At.% Sb	016	018	020	022	025
φ_{oe}	5^0	$4^040'$	$4^010'$	$4^06'$	$4^06'$
φ_g	16^0	16^0	16^0	16^0	16^0
μ_1	9.00	7.15	5.20	3.44	2.32
(5)	(5)	(5)	(5)	(5)	
μ_2	8.10	6.43	6.48	3.09	2.09
(3)	(3)	(3)	(3)	(3)	
μ_3	6.30	5.00	3.64	2.41	1.62
(5)	(5)	(5)	(5)	(5)	
ν_1	3.00	1.80	1.3	9.10	5.80
(5)	(5)	(5)	(4)	(4)	
ν_2	1.50	0.9	0.65	4.55	2.90
(4)	(4)	(4)	(3)	(3)	
ν_3	1.50	0.9	0.65	4.55	2.90
(5)	(5)	(5)	(4)	(4)	
ν					
ν_2					
ν_3					
$N_э$	4,95	8,21	1,33	2,10	3,04
(16)	(16)	(17)	(17)	(17)	
N_g	4,95	8,21	1,33	2,10	3,04
(16)	(16)	(17)	(17)	(17)	

where N_e, N_g are concentrations of charge carriers measured in cm^{-3}.

μ_i and ν_i are tensor components of electron and hole mobilities correspondingly, measured in $cm^{-2}V^{-1}s^{-1}$.

We can make the following conclusions on obtained results:

1. The possibility of quantitative interpretation of galvanomagnetic effects in $Bi_{1-x}Sb_x$ ($0{,}16 \le x \le 0{,}25$) melts on base of model of Fermi electrons in the form of three ellipsoids of common type and holes, in form of three ellipsoids, situating in $\sum$ in 3B point is shown.

2. It is established, that new hole ellipsoids in the comparison with easy hole and electron ellipsoids are less elliptic ones in basis plane, than in binary and bisector planes.

[1] *H.J. Juretschke.* Acta Crystalloq., 1955, v.8, n.11, p. 716-722.

[2] *T. Okada.* J. Phys. Soc. Japan, 1957, v.12, n.12, p. 1327-1337.

[3] *S. Mase.* J. Phys. Soc. Japan, 1959, v. 14, n. 5, p. 584-589.

[4] *S. Golin.* Phys. Rev., 1968, v.166, n.3, p. 643-651.

[5] *L. Esaki*. J. Phys. Soc. Japan 21, 1968, suppl. 89.

[6] *N.B. Brandt, Kh. Dittmann, Ya.G. Ponomaryov*. FTT, 1971, t. 3, v.10, s. 2860-2872.

[7] *N.B. Brandt, Kh. Dittmann, Ya.G.Ponomaryov, S.M. Chudinov*. Pisma v JETF, 1970, n. 11, s. 250.

[8] *V.M. Grabov, G.A. Ivanov, V.L. Nalyotov, V.S. Ponaryadov, T.Ya. Yakovleva.* FTT, 1969, 11, s. 3653.

[9] *N.B. Brandt, B.A. Korchak, A.M. Chesnokov, S.M. Chudinov.* FTT, 1977, t. 19, v. 7, s. 2107-2116.

[10] *H. Goldsmid.* J. Phys. Stat. Sol. (a), 1970, 1, 7.

[11] *T. Yazaki, Y. Abe*. J Phys. Soc. Japan, 1968, v.24, n.2, p. 290-295.

[12] *A.Sh.Mekhtiev, B.A.Tairov, M.G. Shakhtakhtinskiy.* Metodologiya kineticheskikh parametrov v tverdikh telakh so slojnoy zonnoy strukturoy. «Məqalələr toplusu » Fizika 2005, iyun N 7-9, s.282-292.

[13] *R. Brazis, J.Pozela, B. Tairov and M. Shakhtakhtinskii.* Phys. Stat. Sol. (b), 1974, v.62, n.2, p. 697-708.

[14] *F.F. Aliev, S.A. Aliev.* FTP, 2002, t.36, vip.8, s.932-936.

[15] *F.F. Aliev.* FTP , 2003, t.37, N 9, c 1082-1085.

[16] *B.A. Tairov.* Dispersiya elektromagnitnikh maqnitoplazmennikh voln i galvanomagnitnie effekti v splavakh $Bi_{1-x}Sb_x$. Diss. na zvanie dok. fiz. - mat. nauk, Baku 1994, s. 259.

B.A. Tahirov, A.H. Rəhimov, S.Z. Dəmirova

YARIMKEÇİRİCİ $Bi_{1-x}Sb_x$ BƏRK MƏHLULARININ VALENT ZONASININ QURULUŞU HAQQINDA

Yarımkeçirici $Bi_{1-x}Sb_x$ məhlularının T=77-300K temperatur intervalında qeyri-asılı qalvanomaqnit əmsallarının tətqiqi əsasında bütün növ yükdaşıyıcıların kinetik parametrləri təyin edilmişdir.

Müəyyənləşdirilmişdir ki, yeni deşik ellipsoidləri yüngül deşik və elektron ellipsoidləri ilə müqayisədə bazis müstəvisində binar və bissektris müstəvilərinə nisbətən daha kiçik elliptikliyə malikdir.

Б.А.Таиров, А.Г.Рагимов, С.З. Дамирова

О СТРУКТУРЕ ВАЛЕНТНОЙ ЗОНЫ В ПОЛУПРОВОДНИКОВЫХ СПЛАВАХ $Bi_{1-x}Sb_x$

На основе исследований всех независимых гальваномагнитных коэффициентов в полупроводниковых сплавах $Bi_{1-x}Sb_x$ при 77-300К определены кинетические параметры всех сортов носителей заряда.

Установлено, что новые дырочные эллипсоиды по сравнению с легкими дырочными и электронными эллипсоидами в базисной плоскости менее эллиптичны, чем в бинарных и биссектрисных плоскостях.

Received: 22.05.06

RADIOGRAPHIC INVESTIGATIONS OF MELTS OF $TlInC_2^{VI} - InGaC_2^{VI}$ SYSTEMS

E.A. ALLAHYAROV
Azerbaijan Technical University, Baku
Baku, 1025, H. Javid av., 25

In the paper the parameters of elementary cells of melts of $TlInC_2^{VI} - InGaC_2^{VI}$ (C-Se, Te) systems are defined by the radiographic investigations.

The carrying out of the corresponding analysis it is need for the obtaining of the necessary information about nature of chemical connections between atoms as the elementary compounds, so the complex phases. In the connection with this fact, the crystal-structure investigations are the one of the important question of crystal chemistry. These investigations create the experimental base of crystal chemistry.

As it is known, the complex of physical properties of solid bodies is defined by chemical composition and spatial location its constituent atoms. The character of electron interaction between them though is defined by the position of constituent atoms; however, the clear conception is created in the limits of the one and the same concrete crystal structure. Thus, the solution of the one of concrete problems of physics and chemistry of semiconductors mainly is defined by the accurate definition of concrete bonds of physical peculiarities of semiconductors with chemical composition, crystal structure and bond nature. However, nowadays, the investigations of new complex semiconductors are carried out one-sidedly, often limited by the revealing and studying of their physical properties. The necessary attention doesn't pay to the study of the construction of crystal lattice structure. In spite of the fundamental meaning of crystal structure, it has been deciphered widely enough only for few complex semiconductors.

The state diagrams of $TlInC_2^{VI} - InGaC_2^{VI}$ systems have been constructed in [1,2] by the methods of differentially-thermal and microstructural analysis and it is revealed, that new compositions $TlIn_2GaC_2^{VI}$ are created in these systems and wide solubility regions on the base of initial compounds are observed. However, the roentgen-phase analysis of these melts wasn't carried out.

In this connection in present paper the melts of the $TlInC_2^{VI} - InGaC_2^{VI}$ systems are treated by roentgen-graphic investigations.

The powder had been prepared previously for the obtaining of roentgenograms of each $InTl_{1-x}Ga_xC_2$ composition. The notations of electronic reflections were carried out on CuK_α, ($\lambda_{Cu_\alpha} = 1{,}54178E$), DRON-2 difractometer of radiation with nickel filter at the similar modes. In the measurements of reflection angles the mistake didn't exceed the value $\theta = \pm 0{,}02°$.

The bar-diagram of the melts of $TlInSe_2$-$InGaSe_2$ system is given on the fig.1. As it is seen from the figure the some tendency to the increase of the intensity of corresponding reflexes is observed in the solubility regions at the partial replacement of thallium atoms by Ga atoms in $TlInSe_2$ lattice.

The increase of the intensity of the lines in the given system probably is connected with the fact, that Ga atoms have the big tendency to hybrid bond sp^3 creation in contrast to thallium atoms that is caused to the decrease of metallic part of chemical connection between the composing atoms. In this case the shifting of maximum of electron density to the skeletons of Se atoms at the partial replacement of thallium atoms by Ga atoms in $TlInSe_2$, i.e. the possibility of fitting out of external electron membrane of Se atoms till the stable configuration s^2p^6 increases. In this connection the bond ionicity of chemical bond between the atoms of given melts increases.

The roentgenograms of $InTl_{0,5}Ga_{0,5}Se_2$ composition and solid solutions on its base significantly differ from the roentgenograms of initial compositions of $TlInSe_2$, $InGaSe_2$ and solid solutions on their base that proves the creation of the new quadrantal phase $TlIn_2GaSe_4$ in $TlInSe_2$-$InGaSe_2$ system.

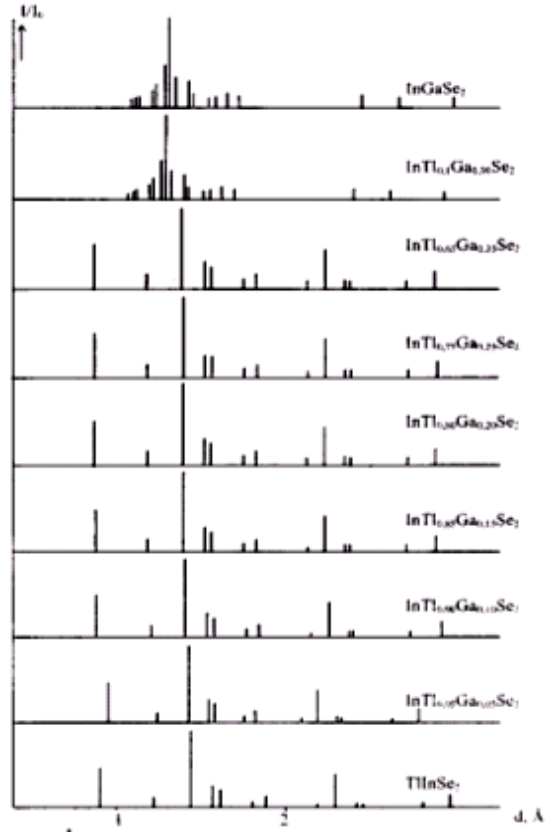

Fig.1. The bar-diagram of the melts of $TlInSe_2$-$InGaSe_2$ system.

The indicating results of obtained roentgenograms showed, that the investigated melts of $InTl_{1-x}Ga_xC_2$ systems are crystallized in tetragonal syngony.

Table 1.1

Interfacial distances (on Å), indexes on melt roentgen grams of $InTl_{1-x}Ga_xSe_2$ system

hkl	$TlInSe_2$			$InTl_{0,95}Ga_{0,05}Se_2$			$InTl_{0,9}Ga_{0,1}Se_2$			$InTl_{0,85}Ga_{0,15}Se_2$			$InTl_{0,3}Ga_{0,7}Se_2$			$InTl_{0,72}Ga_{0,28}Se_2$		
	$a=8.02$, $c=7.15$ Å			$a=8.00$, $c=7.13$ Å			$a=7,97$, $c=7.10$ Å			$a=7,94$, $c=7.07$ Å			$a=7,90$, $c=7.05$ Å			$a=7,88$, $c=7.02$ Å		
	d_{x} Å	d_{m} Å	θ	d_{x} Å	d_{m} Å	θ	d_{x} Å	d_{m} Å	θ	d_{x} Å	d_{m} Å	θ	d_{x} Å	d_{m} Å	θ	d_{x} Å	d_{m} Å	θ
1	2	3	4	2	3	4	2	3	4	2	3	4	2	3	4	2	3	4
211	3,206	3,211	13°51′	3,198	3,202	13°55′	3,185	3,185	14°00′	3,173	3,173	14°03′	3,159	3,160	14°06′	3,149	3,151	14°09′
112	3,024	3,040	14°41′	3,016	3,024	14°45′	3,004	3,004	14°51′	2,991	2,992	14°55′	2,981	2,985	14°57′	2,970	2,970	15°02′
202	2,668	2,674	16°45′	2,661	2,662	16°49′	2,651	2,651	16°49′	2,640	2,641	16°58′	2,630	2,633	17°01′	2,621	2,621	17°06′
221	2,636	2,635	17°00′	2,629	2,636	17°00′	2,619	2,619	17°06′	2,609	2,609	17°10′	2,597	2,597	17°16′	2,590	2,590	17°18′
301	2,504	2,504	17°55′	2,498	2,505	17°55′	2,488	2,488	18°02′	2,479	2,479	18°06′	2,467	2,467	18°12′	2,460	2,460	18°15′
311	2,390	2,390	18°48′	2,384	2,381	18°53′	2,375	2,375	18°56′	2,366	2,366	19°00′	2,355	2,355	19°06′	2,348	2,348	19°09′
312	2,069	2,068	21°52′	2,062	2,063	21°56′	2,055	2,055	22°01′	2,047	2,047	22°07′	2,038	2,039	22°12′	2,032	2,032	22°17′
123	1,985	1,984	22°51′	1,980	1,979	22°55′	1,972	1,972	23°00′	1,964	1,964	23°06′	1,957	1,959	23°10′	1,949	1,950	23°16′
303	1,779	1,784	25°36′	1,774	1,774	25°45′	1,767	1,767	25°51′	1,760	1,760	25°58′	1,753	1,755	26°03′	1,747	1,747	26°10′
313	1,737	1,736	26°21′	1,732	1,732	26°25′	1,725	1,725	26°32′	1,718	1,719	26°38′	1,712	1,713	26°44′	1,706	1,706	26°51′
214	1,600	1,599	28°49′	1,595	1,595	28°54′	1,589	1,589	29°01′	1,582	1,582	29°09′	1,577	1,579	29°13′	1,571	1,571	29°22′
530	1,375	1,376	34°04′	1,372	1,372	34°10′	1,367	1,367	34°19′	1,362	1,362	34°28′	1,355	1,355	34°40′	1,351	1,351	34°47′
371	1,042	1,040	47°49′	1,039	1,039	47°53′	1,035	1,035	48°08′	1,031	1,031	48°23′	1,026	1,026	48°42′	1,024	1,024	48°49′

Table 1.2

	$InTl_{0.7}Ga_{0.3}Se_2$			$InTl_{0.65}Ga_{0.35}Se_2$			$InTl_{0.6}Ga_{0.4}Se_2$				$InTl_{0.55}Ga_{0.45}Se_2$			$InTl_{0.5}Ga_{0.5}Se_2$		
	$a = 7.85$, $c = 6.99$ Å			$a = 7.82$, $c = 6.97$ Å			$a = 7,78$, $c = 6.94$ Å				$a = 6,48$, $c = 6.87$ Å			$a = 6,46$, $c = 6.85$ Å		
hkl	$d_{эк}$ Å	$d_{теор}$ Å	θ	$d_{эк}$ Å	$d_{теор}$ Å	θ	$d_{эк}$ Å	$d_{теор}$ Å	θ	hkl	$d_{эк}$ Å	$d_{теор}$ Å	θ	$d_{эк}$ Å	$d_{теор}$ Å	θ
1	2	3	4	2	3	4	2	3	4	1	2	3	4	2	3	4
211	3,137	3,137	14°13′	3,125	3,126	14°16′	3,110	3,110	14°21′	200	3,240	3,240	13°45′	3,230	3,230	13°48′
112	2,958	2,958	15°06′	2,948	2,948	15°09′	2,935	2,935	15°13′	210	2,898	2,898	15°25′	2,889	2,889	15°28′
202	2,610	2,611	17°10′	2,602	2,601	17°14′	2,589	2,590	17°18′	211	2,670	2,670	16°46′	2,662	2,662	16°49′
221	2,580	2,580	17°22′	2,570	2,570	17°18′	2,557	2,557	17°32′	222	1,906	1,906	23°51′	1,900	1,900	23°55′
301	2,451	2,451	18°19′	2,442	2,441	18°24′	2,429	2,429	18°30′	302	1,828	1,828	24°56′	1,823	1,823	25°00′
311	2,339	2,339	19°14′	2,331	2,331	19°18′	2,319	2,319	19°24′	312	1,760	1,760	25°58′	1,755	1,755	26°03′
312	2,024	2,024	22°22′	2,017	2,017	22°26′	2,007	2,007	22°34′	004	1,718	1,717	26°40′	1,713	1,713	26°44′
123	1,941	1,942	23°22′	1,935	1,935	23°28′	1,926	1,926	23°35′	400	1,620	1,620	28°24′	1,615	1,615	28°30′
303	1,740	1,740	26°17′	1,734	1,734	26°23′	1,726	1,726	26°31′	322	1,592	1,592	28°57′	1,588	1,588	29°02′
313	1,699	1,699	26°58′	1,693	1,693	27°04′	1,685	1,685	27°13′	204	1,517	1,517	30°32′	1,513	1,513	30°39′
214	1,564	1,564	29°31′	1,560	1,560	29°36′	1,553	1,553	29°45′	214	1,478	1,477	31°19′	1,473	1,473	31°33′
530	1,346	1,346	34°55′	1,341	1,341	35°04′	1,334	1,334	35°18′	420	1,449	1,449	32°08′	1,444	1,444	32°15′
371	1,020	1,020	49°05′	1,016	1,016	49°21′	1,011	1,011	49°40′	332	1,396	1,396	33°30′	1,391	1,391	33°39′
-	-	-	-	-	-	-	-	-	-	005	1,374	1,374	34°07′	1,370	1,370	34°14′
-	-	-	-	-	-	-	-	-	-	500	1,296	1,296	36°30′	1,292	1,292	36°39′
-	-	-	-	-	-	-	-	-	-	510	1,271	1,271	37°19′	1,267	1,267	37°28′
-	-	-	-	-	-	-	-	-	-	215	1,242	1,241	38°24′	1,238	1,238	38°30′

Table 2.1

Interfacial distances (on Å), indexes on melt roentgen grams of $InTl_{1-x}Ga_xTe_2$ system

$TlIn_2GaSe_4$				$TlIn_2GaTe_4$				$Tl_{0.8}InGa_{0.2}Te_2$				$Tl_{0.7}InGa_{0.3}Te_2$			
$a=6{,}46$, $c=6.85$ Å				$a=6.60$, $c=7.22$ Å				$a=8.38$, $c=7.14$ Å				$a=8{,}31$, $c=7.12$ Å			
hkl	$d_{эк}$ Å	$d_{изм}$ Å	θ	*hkl*	$d_{эк}$ Å	$d_{изм}$ Å	θ	*hkl*	$d_{эк}$ Å	$d_{изм}$ Å	θ	*hkl*	$d_{эк}$ Å	$d_{изм}$ Å	θ
1	2	3	4	1	2	3	4	1	2	3	4	1	2	3	4
200	3,226	3,230	13°50′	200	3,228	3,300	13°49′	012	3,283	3,281	13°35′	210	3,823	3,816	11°38′
210	2,863	2,889	15°37′	210	2,948	2,952	15°09′	003	2,385	2,380	18°52′	302	2,148	2,146	21°02′
211	2,664	2,662	16°50′	211	2,738	2,732	16°21′	312	2,118	2,120	21°21′	401	1,978	1,974	22°56′
222	1,906	1,900	23°51′	300	2,225	2,200	20°16′	331	1,890	1,893	24°04′	420	1,871	1,878	24°20′
302	1,832	1,823	24°53′	310	2,135	2,139	21°10′	114	1,702	1,708	26°56′	402	1,788	1,794	25°32′
312	1,759	1,754	25°59′	113	2,081	2,087	21°45′	403	1,570	1,567	29°24′	114	1,696	1,704	27°02′
004	1,706	1,712	26°52′	203	1,941	1,944	23°24′	441	1,441	1,442	32°21′	520	1,549	1,543	29°51′
400	1,615	1,615	28°31′	213	1,866	1,865	24°24′	105	1,396	1,407	33°31′	441	1,414	1,439	33°02′
322	1,583	1,588	29°08′	321	1,767	1,774	25°24′	305	1,256	1,270	37°52′	600	1,390	1,385	33°41′
204	1,513	1,513	30°38′	104	1,738	1,741	26°37′	443	1,238	1,252	38°31′	630	1,242	1,239	38°22′
214	1,474	1,473	31°32′	400	1,647	1,650	27°55′	542	1,215	1,222	39°23′	533	1,216	1,222	39°21′
420	1,433	1,444	32°33′	331	1,523	1,521	30°25′	700	1,180	1,190	40°48′	720	1,134	1,144	42°50′
332	1,388	1,391	33°44′	402	1,488	1,501	31°12′	623	1,150	1,152	42°06′	425	1,129	1,130	43°04′
005	1,366	1,370	34°21′	421	1,442	1,446	32°19′	216	1,127	1,134	43°10′	731	1,079	1,079	45°36′
500	1,282	1,292	36°58′	105	1,400	1,411	33°25′	515	1,073	1,075	45°56′	515	1,070	1,072	46°06′
510	1,268	1,267	37°27′	422	1,368	1,366	34°18′	517	1,070	1,065	46°06′	800	1,036	1,039	48°05′
215	1,234	1,238	38°40′	502	1,230	1,240	35°25′	800	1,040	1,041	47°48′	426	1,000	1,000	50°26′
440	1,148	1,142	42°11′	600	1,084	1,100	48°12′	734	0,931	0,933	55°54′	661	0,969	0,970	52°42′
441	1,127	1,126	43°09′	-	-	-	-	931	0,871	0,871	62°16′	900	0,913	0,923	57°36′
116	1,106	1,108	44°11′	-	-	-	-	636	0,855	0,859	64°22′	911	0,893	0,910	59°41′
425	0,992	0,994	50°58′	-	-	-	-	313	0,840	0,845	66°36′	931	0,869	0,869	62°31′

Table 2.2

$Tl_{0,6}InGa_{0,4}Te_2$				$Tl_{0,2}InGa_{0,8}Te_2$				$Tl_{0,45}InGa_{0,55}Te_2$				$Tl_{0,55}InGa_{0,45}Te_2$			
$a=6,62$, $c=7.23$ Å				$a=8.20$, $c=7.10$ Å				$a=7.27$, $c=7.11$ Å				$a=6,61$, $c=7.22$ Å			
hkl	$d_\perp$ Å	$d_{\text{изм}}$ Å	θ	hkl	$d_\perp$ Å	$d_{\text{изм}}$ Å	θ	hkl	$d_\perp$ Å	$d_{\text{изм}}$ Å	θ	hkl	$d_\perp$ Å	$d_{\text{изм}}$ Å	θ
1	2	3	4	1	2	3	4	1	2	3	4	1	2	3	4
212	2,287	2,290	19°42'	103	2,269	2,269	19°51'	311	2,179	2,187	20°36'	113	2,148	2,140	21°02'
222	1,961	1,965	23°09'	312	2,100	2,100	21°09'	302	2,006	2,002	22°39'	302	1,877	1,881	24°15'
321	1,783	1,780	25°37'	400	2,055	2,055	22°37'	401	1,770	1,761	25°49'	104	1,745	1,741	26°13'
204	1,588	1,586	29°03'	322	1,890	1,890	24°03'	114	1,709	1,680	26°49'	330	1,557	1,558	29°41'
421	1,441	1,450	32°21'	332	1,708	1,708	26°21'	331	1,664	1,666	27°36'	005	1,440	1,444	32°22'
324	1,289	1,288	36°44'	403	1,550	1,550	29°44'	403	1,450	1,442	32°07'	206	1,129	1,131	43°04'
225	1,233	1,230	38°42'	522	1,397	1,397	33°42'	215	1,306	1,303	36°11'	611	1,082	1,087	45°26'
305	1,213	1,209	39°28'	631	1,203	1,203	39°28'	531	1,229	1,228	38°51'	540	1,079	1,075	45°36'
513	1,144	1,143	42°22'	405	1,163	1,163	41°22'	325	1,159	1,162	41°42'	405	1,033	1,032	48°27'
523	1,096	1,095	44°42'	505	1,069	1,069	46°42'	405	1,123	1,120	43°21'	603	0,997	1,002	50°39'
443	1,051	1,053	47°13'	326	1,032	1,032	48°13'	720	1,004	0,999	50°10'	217	0,969	0,974	52°42'
117	1,013	1,009	49°33'	625	0,930	0,930	55°33'	217	0,978	0,970	52°01'	710	0,936	0,935	55°27'
316	0,991	1,004	51°04'	427	0,883	0,883	60°04'	426	0,956	0,958	53°45'	553	0,872	0,871	62°08'
701	0,944	0,938	54°45'	626	0,868	0,868	62°45'	731	0,952	0,946	54°04'	526	0,854	0,859	64°31'
621	0,922	0,917	56°44'	932	0,839	0,839	66°44'	650	0,935	0,931	55°32'	800	0,840	0,826	66°36'
407	0,878	0,876	61°24'	941	0,827	0,827	68°24'	800	0,911	0,909	57°48'	-	-	-	-
526	0,861	0,861	63°33'	-	-	-	-	108	0,885	0,882	60°35'	-	-	-	-
228	0,846	0,843	65°40'	-	-	-	-	832	0,825	0,828	69°08'	-	-	-	-
-	-	-	-	-	-	-	-	-	-	-	-	-	-	-	-
-	-	-	-	-	-	-	-	-	-	-	-	-	-	-	-

The results of roentgenographical investigation of the melts of $InTl_{1-x}Ga_xSe_2$ systems are given in table 1.

In fig.2 the dependence of lattice parameters of the melts $InTl_{1-x}Ga_xSe_2$ on composition is presented.

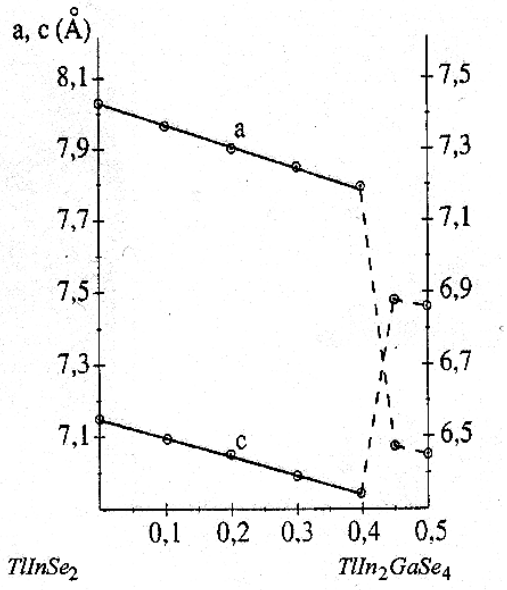

Fig.2. The dependence of parameters of elementary cells of the melts of $InTl_{1-x}Ga_xSe_2$ system on composition.

As it is followed from the fig.2 the parameters of elementary cells "*a*" and "*c*" orderly decrease at the partial replacement of thallium atoms by Ga atoms. The change of cell parameters is explained by the difference of interacting atom radiuses. The parameters of elementary cells of new phase $TlIn_2GaSe_4$ and solid solutions on its base significantly differ from lattice parameters of initial compounds and solid solutions on their base. This proves about the creation of new quadrantal phase in the given system. The change of lattice parameters in solubility regions takes place on the additivity law and essential inclinations from Vegard law doesn't observed in the investigated concentration interval.

As it was shown in [2] in $TlInTe_2$-$InGaTe_2$ system the big region of solubility is observed. That's why the lattice parameters of obtained solid solutions had been defined by us with the aim of the provement state diagram of this system. The experimental data, necessary for the definition of lattice parameters were based on difractograms. It is revealed the lattice parameters decrease to the side of $InGaTe_2$ compound in region 55-100 mol.% $InGaTe_2$. Such order change of lattice parameters is typically through the solubility region. Exactly, lattice parameters are increased from $InGaTe_2$ and $TlInTe_2$ compounds (fig.3).

The lattice parameters in region 52-70 mol.% $InGaTe_2$ strongly differ from the regions 0-20 mol.% $InGaTe_2$ and 55-100 mol.% $InGaTe_2$. Probably, in this region the solid solutions are created on the base of new phase. The decrease of parameter lattice on additivity law is the reason of the replacement of thallium atoms by small Ga atoms in the plane of structure base.

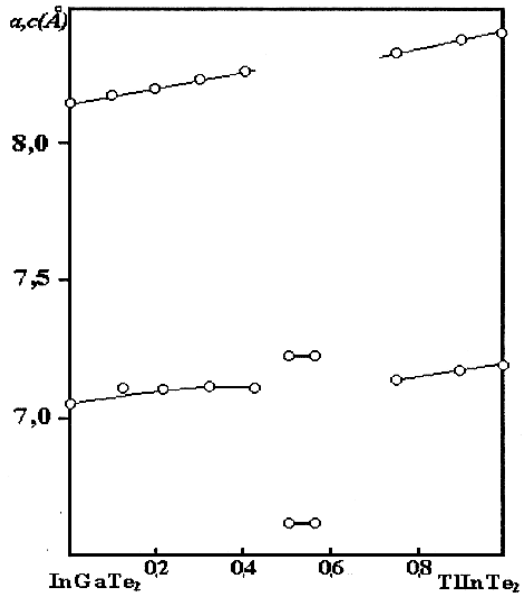

Fig.3. The dependence of lattice parameters on the composition of melts of $InTl_{1-x}Ga_xTe_2$ system.

The results of roentgenogaphic investigations of the melts $TlInTe_2$-$InGaTe_2$ are given in the table 2.

As we already mentioned, the melts $InGaTe_2$ with $TlInTe_2$ also as compounds $InGaTe_2$ and $TlInTe_2$ are crystallized in tetragonal lattice. That's why the superstructure lines don't appear on difractograms in solubility region. The absence of superstructure lines proves that all investigated melts of solid solutions in order and disorder states also as compounds $InGaTe_2$ and $TlInTe_2$ crystallize in the same syngony.

The lines, character for the $TlGaTe_2$ compound appear in solubility region on the base of $TlInTe_2$ (0-20 mol.%) $TlGaTe_2$ and continue to appear till the melt $Tl_{0,7}InGa_{0,3}Te_2$. The additional lines for the melts, consisting 60,55,50 mol/% $TlInTe_2$ appear in solubility region on the base of new phase. These results give us the foundation to prove in the rightness of state diagram of $TlInTe_2$-$InGaTe_2$ system.

The new compounds $TlIn_2GaSe_4$ (Te_4) revealed in $TlInTe_2$-$InGaTe_2$ systems are carried out by roentgen phase investigations.

The experimental necessary material for the calculation of $TlIn_2GaSe_4$ and $TlIn_2GaTe_4$ lattice parameters was consist from crystallograms also. On the base of the carried out investigation it is revealed that these phases crystallize in tetragonal syngony and have the following periods of elementary cells a=6,46Å; c=6,85Å correspondingly.

Thus, compounds $TlIn_2GaSe_4$ and $TlIn_2GaTe_4$ crystallize in tetragonal syngony as well as initial ones. But lattice parameters significantly differ from the parameters of double and triple analogues of TlSe. Probably, this is connected with the new reconstruction of component atoms.

[1] *E.M. Godjaev, Sh.M. Guseynov, M.M. Dadashev.* Diagramma sostoyaniya sistemi $TlInSe_2$-$InGaSe_2$. Fizicheskaya ximiya, 1974, t.48, №10, s.2615-2618.

[2] *E.M. Godjaev, M.G. Gamidov.* Fiziko-khimicheskie i rentgenograficheskie issledovaniya sistemi $TlInTe_2$-$InGaTe_2$. Fizicheskaya ximiya, 1975, t.49, №9, s.2458-2460.

E.Ə. Allahyarov

$TlInC_2^{VI} - InGaC_2^{VI}$ ƏRİNTİLƏR SİSTEMİNİN RENTGENOQRAFİK TƏDQİQİ

Rentgenoqrafik tədqiqatlar yolu ilə $TlInC_2^{VI} - InGaC_2^{VI}$ ərintilər sisteminin elementar özəklərinin parametrləri təyin olunmuşdur.

Э.А. Аллахяров

РЕНТГЕНОГРАФИЧЕСКИЕ ИССЛЕДОВАНИЯ СПЛАВОВ СИСТЕМ $TlInC_2^{VI} - InGaC_2^{VI}$

Рентгенографическими исследованиями определены параметры элементарных ячеек сплавов систем $TlInC_2^{VI} - InGaC_2^{VI}$.

Received: 14.06.06

SAMARİUM NADİR TORPAQ ELEMENTİ İLƏ AŞQARLANMIŞ Se-As ŞÜŞƏVARİ HALKOGENİD YARIMKEÇİRİCİ SİSTEMİNİN OPTİK BURAXMA SPEKTRİ

A.İ. İSAYEV, S.İ. MEHDİYEVA, N.Z. CƏLİLOV, R.İ. ƏLƏKBƏROV
AMEA Fizika İnstitutu, Az-1143, Bakı, H. Cavid. pr., 33

İşdə samarium nadir torpaq elementi ilə aşqarlanmış $Se_{95}As_5$ şüşəvari halkogenid yarımkeçirici (ŞHY) sisteminin nazik təbəqələrinin buraxma spektrləri tədqiq olunmuşdur. Müəyyən olunmuşdur ki, $Se_{95}As_5$ sisteminə az miqdarda (0, 001-0,005 at%) Sm-un əlavə olunması T-buraxma əmsalının qiymətini azaldır, aşqarın konsentrasiyasının sonrakı artımı isə (0,005-1 at%) spektrin 1-1,6 eV intervalında buraxma əmsalının artmasına səbəb olur. T-nin qiymətinin azalması ŞHY-də yüksək koordinasiya ədədinə malik mikrooblastların, artması isə bu oblastlar arasındakı əlaqənin yaranması ilə izah olunmuşdur.

Son zamanlar lifli-optik qurğular üçün perspektivli material sayılan nadir torpaq elementlərinin (NTE) aşqarları daxil edilən şüşəvari halkogenid yarimkecirici maddələrin optik xassələrinin öyrənilməsi sahəsində bir sıra tədqiqat işləri aparılmışdır [1-4].

Digər tərəfdən ŞHY maddələrin holoqrafiya və mikroelektronikada, fotolitoqrafiyada geniş istifadə olunması ilə əlaqədar olaraq bu maddələrdə fotoinduksiya nəticəsində yaranan quruluş dəyişmələrinin öyrənilməsinə xüsusi yer verilmişdir [5-8]. Qeyd edək ki, tərkibində NTE-nin ionları olan ŞHY maddələr spektrin yaxın infraqırmızı diapazonunda işləyən iş telekommunikasiya qurğularının işıqötürücüsünün hazırlanması üçün istifadə olunur [9-10]. Təqdim olunan işin əsas məqsədi samarium aşqar atomlarının $Se_{95}As_5$ sisteminin optik buraxma spektrinə təsirinin tədqiqindən ibarətdir. Tədqiqat üçün $Se_{95}As_5$ tərkibinin seçilməsi onun strukturuna və elektron xassələrinə görə daha stabil olması və enlizolaqlılığı ilə bağlıdır [9].

Təcrübənin metodikası və nümunələrin hazırlanması

Sm aşqarlı $Se_{95}As_5$ tərkibinin sintezi 900°C-dən yuxarı temperaturda 10^{-6} mm.cv.st-na qədər vakuumlu kvars ampulalarda fırlanan sobada aparılmış və söndürülmüş soba rejimində soyutmaqla yerinə yetirilmişdir.Tədqiq olunan maddənin nazik təbəqələri 10^{-6} mm.cv.st. təzyiqli vakuumda termik uçurma üsulu ilə alınmışdır. Ölçmələr 0,5mkm÷2mm qalınlıqlı nümunələrdə ikişüalı spektroskopiya metodu ilə aparılmışdır.

Nəticələr və onların izahı

Şəkil 1,a,b-də müxtəlif miqdarda Sm-la aşqarlanmış $Se_{95}As_5$ sisteminin optik buraxma spektri göstərilmiş, həmin spektrə əsasən α - optik udulma əmsalının qiymətləri hesablanmışdır. Optik buraxma əmsalının düşən fotonun enerjisindən asılılığının 1,6 ÷2 eV intervalından (Urbax qaydasına tabe olan hissəsindən) təyin olunmuş α-udulma əmsalının qiymətlərindən istifadə etməklə

$$\alpha = \alpha_0 \cdot \exp[-(E_g - h\nu)] / E_0 \qquad (1)$$

(1) düsturundan E_0 –xarakteristik enerjinin qiymətləri təyin olunmuşdur. Qeyd edək ki, E_0- xaratkeristik enerji şüşəvari matrisdə atomlararası məsafənin ortakvadratik kənaraçıxmaları haqda məlumat əldə etməyə imkan verir [11].

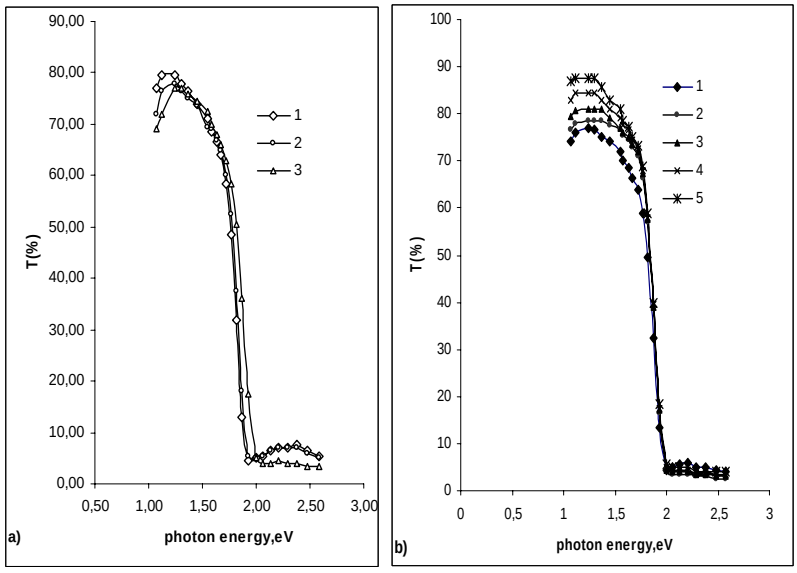

Şəkil 1. Samarium nadir torpaq elementi ilə aşqarlanmış $Se_{95}As_5$ şüşəvari halkogenid yarımkeçirici sisteminin optik buraxma spektri a) -1- $Se_{95}As_5$, 2- $Se_{95}As_5$ +0,001at%Sm, 3- $Se_{95}As_5$ +0,005 at%Sm. b) -1- $Se_{95}As_5$+0,01 at%Sm, 2- $Se_{95}As_5$+0,1 at%Sm, 3- $Se_{95}As_5$+0,3 at%Sm ,4- $Se_{95}As_5$+0,6 at%Sm, 5- $Se_{95}As_5$+1at%Sm.

Şəkil-1a,b dən göründüyü kimi $T(h\nu)$ asılılığında enerjinin yaxın infraqırmızı oblastında buraxma əmsalının qiyməti Sm aşqarının miqdarının (0,001÷0,005 at%) artması ilə azalır. Aşqarın miqdarının sonrakı artımı (0,005÷1 at%) isə buraxma əmsalının artmasına səbəb olur.

(1) düsturundan təyin olunan E_0 xaratkeristik enerjinin qiymətlərinin Sm aşqarı atomlarının miqdarından asılılığı Şəkil 2,a-da təsvir olunmuşdur.

Qeyri kristallik maddələr üçün aşqar ionlarının xaotik paylanması ilə əlaqədar olan qeyri bircins sahələrin yaranması ideyasına əsasən E_0 xarakteristik enerji üçün aşağıdakı düstur alınmışdır [11]

$$E_0 = 2{,}2 \cdot W_B (N_t \cdot a^3{}_B)^{2/5} \qquad (2)$$

Burada $W_B = e^2/2\varepsilon \cdot a_B$, a_B – Bor radiusu , ε -dielektrik nüfuzluğu, N_t yüklü defektlərin effektiv konsentrasiyasıdır. ε=6,58 [12] qəbul edərək (2) düsturuna görə yüklü defektlərin N_t- konsentrasiyası hesablanmış və alınmış nəticələr şəkil 2b-də təsvir olunmuşdur. Şəkil 2a və şəkil 2b-dən göründüyü kimi həm xarakteristik enerjinin, həm də yüklü defektlərin konsentrasiyasının qiymətləri aşqar atomlarının 0,005 at% -nə kimi artır, aşqarın miqdarının sonrakı artımı isə E_0 və N_t-nin azalmasına səbəb olur.

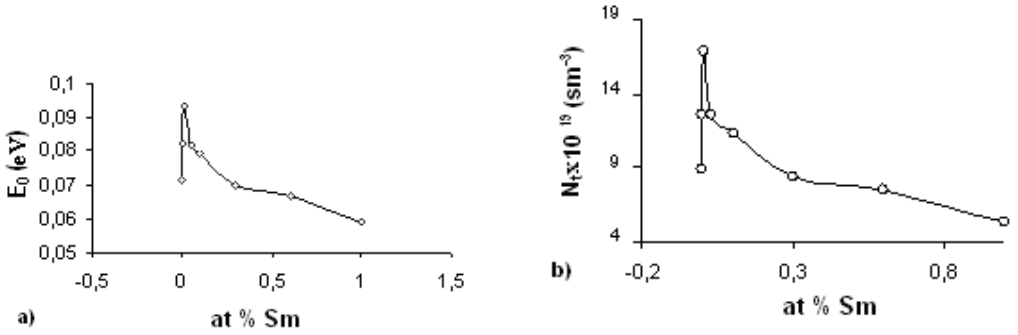

Şəkil.2. $Se_{95}As_5$ şüşəvari halkogenid yarimkeçirici sistemində xarakteristik enerjinin (a) və lokallaşmış halların konsentrasiyasının samarium aşqarının miqdarından asılılığı (b).

ŞHY-maddələrə müxtəlif modifikatorlar daxil etdikdə yüksək koordinasiya ədədli mikrooblastların formalaşması baş verir, bu halda müxtəlif oblastlar arasında potensial baryerlər yaranır ki, onların hündürlüyü yüklü mərkəzlərlə müəyyən olunur.

$Se_{95}As_5$ sistemində Sm atomlarının özlərini Sm^{+3} ionları şəklində aparmalarını və kiçik miqdarlarda əsasən yüksək koordinasiya ədədli oblastlarda toplandıqlarını fərz etsək, onda, quruluşun nizamsızlığı və qeyri-bircinsliyi artmalı, buraxma əmsalı azalmalı və onun əksinə olaraq E_0 - xarakteristik enerji artmalıdır. Həqiqətən də bu fakt aşqarın miqdarı 0,005 at% -nə qədər olduqda Şəkil 1a,b və şəkil 2a,b-də öz əksini tapmışdır. Lakin nisbətən böyük konsentrasiyalarda (0,005÷ 1 at%) aşqar atomları bütün matris boyunca paylanaraq kimyəvi aktivlikləri sayəsində selen zəncirlərinə cəzb olunaraq, nizamsız torun yaranması ilə struktur dəyişməsinə səbəb olur ki, bu da öz növbəsində müxtəlif mikrooblastlar arasında rabitələr yaradır. Digər tərəfdən yüklü defektlər modelinə görə Sm^{+3} ionlarının mövcudluğu məxsusi yüklü defektlərin konsentrasiyasının dəyişməsinə səbəb olmalıdır: Yəni D^+ -mərkəzlər azalmalı, D - mərkəzlər isə artmalıdır. Göstərilən faktorların birgə təsiri böyük konsentrasiyalarda xaratkeristik enerjinin azalmasına və optik buraxma əmsalının artmasına səbəb olur.

[1] *Zakery, S.R. Eliott.* Optical Properties and Applications of Chalcogenide Glasses: A Review // J. Non-Cryst. Solids, 2003. v .330. p. 1 -12.

[2] *M.S. Iovn, S.D. Shutov and A.M. Andriesh*. Chalcogenide Vitreous Semiconductors doped with metals: Properties and Applications // Moldavian Journal of the Physical Sciences, №1, 2002. p. 84-85.

[3] *T. Feuchter, E.K. Mwarahia, J. Wang, L. Reekie and S.I. Wilkinson*. Photon Technol. Lett. 4, 542 (1992).

[4] *R. Brinkman, W. Sohler and H. Suche.* Electron Lett. 27. 415 (1991).

[5] *V.M. Lyubin.* J. Non-Cryst. Sol. 1987. v. 97-98, p.47.

[6] *V.M. Lyubin, T. Tada, M. Klebanov, N.N. Smirnova, A.V. Kolobov, K. Tahaka.* Mater.Lett.1997.v.30, p.79.

[7] *K.K. Shwarts.* The physics of optical recording. Berlin: Springer, 1993.

[8] *A.M. Andriesh.* Glass physics and Chemistry. 1998. v.32. p. 970.

[9] *A.I. Isayev, L.P. Kazakova, E.A. Lebedov, S.I. Mekhtiyeva, I.I. Yatlinko* "Preparation way of the chalcogenide vitreous semiconductors on the basis of Se-As" (in Russian) A.C.-№ 1512015. Moscow, (1989).

[10] *Y.G. KLyava*. PSS (in Russian), 27, 1350, (1985).

[11] *V.L. Bonch-Bruevich.* UPS (in Russian), 140,583 (1983).

[12] *Z.U. Borisov.* "Chalcogenide vitreous semiconductors" (in Russian), L., 344 (1983).

А.И. Исаев, С.И. Мехтиева, Н.З. Джалилов, Р.И. Алекперов

СПЕКТР ОПТИЧЕСКОГО ПРОПУСКАНИЯ ХСП СИСТЕМЫ Se-As, ЛЕГИРОВАННОЙ РЕДКОЗЕМЕЛЬНЫМ ЭЛЕМЕНТОМ САМАРИЕМ

В работе исследованы спектры пропускания ХСП пленок $Se_{95}As_5$ легированных редкоземельным элементом самарием.

Установлено, что при малых концентрациях примеси (0,001-0,005 ат.%) значение коэффициента пропускания *T*

уменьшается, а при увеличении концентрации примеси (0,005-1 ат.%) значение *T* увеличивается в области спектра 1-1,6 eV. Уменьшение значения коэффициента пропускания в ХСП пленках объясняется образованием микрообластей с высоким значением координационного числа, а рост - образованием связей между этими областями.

A.I. Isayev, S.I. Mehtiyeva, N.Z. Jalilov, R.I. Alekperov

OPTICAL TRANSMISSION SPECTRUM OF HGS SYSTEMS Se-As, DOPED BY RARE-EARTH ELEMENT SAMARIUM

The transmission spectrums of HGS films $Se_{95}As_5$ doped by rare-earth element samarium are investigated. İt is established, that the value of the transmission coefficient *T* decreases for the low impurity concentrations (0,001-0,005 at.%) but *T* increases when impurity concentration increases (0,005-1 at.%) in the spectrum region 1-1,6eV. The decrease of the transmission coefficient in HGS films is explained by the formation of microregions with high value of coordination number, and the increase of one is explained by the band formation between of these regions.

Received: 17.09.06

ISSN 1028-8546

2006, Cild XII, 3

Fizika

Azərbaycan Milli Elmlər Akademiyası
Fizika-Riyaziyyat və Texnika Elmləri Bölməsi
Fizika İnstitutu

MÜNDƏRİCAT

(Ardıı var)

СОДЕРЖАНИЕ

(Ardıı var)

CONTENTS